ON THE APPLICATION OF ACTIVE OPEN-LOOP AND CLOSED-LOOP CONTROLS ON A CIRCULAR CYLINDER IN THE PRESENCE AND ABSENCE OF A FREE SURFACE

GINA S. REID

On the application of active open-loop and closed-loop controls on a circular cylinder in the presence and absence of a free surface

by

Gina S. Reid

A thesis submitted in partial fulfillment
of the requirements for the degree of
Masters of Science (Mathematics)

School of Graduate Studies
Memorial University of Newfoundland
St. John's, Newfoundland and Labrador

August 2010

Abstract

This thesis focuses on the application of active open-loop and closed-loop controls on a circular cylinder in the presence and absence of a free surface. The numerical simulations are presented for two-dimensional, uniform, flow of a viscous incompressible fluid past a circular cylinder subject to forced (i) transverse or streamwise oscillations, or (ii) combined streamwise and transverse oscillations, which to the author's knowledge has not previously been studied. The goal of this thesis is to analyze in detail the effects of these three types of cylinder oscillations, and the inclusion of a free-surface on the vortex shedding modes in the near wake region, fluid forces acting on the cylinder as well as pressure distribution around the cylinder.

The numerical method of the study is based on the finite-volume discretization of the special integral form of two-dimensional continuity and unsteady Navier-Stokes equations (when a solid body is present) based on a two-fluid model. The numerical simulations are conducted at a Reynolds number of $R = 200$, for the Froude numbers $Fr \approx 0.0$, $Fr = 0.2$ and 0.4, at three different cylinder submergence depths, $h = 0.25$, 0.5 and 0.75. The flow characteristics are examined for a maximum oscillation amplitude $A = 0.13$, and forcing cylinder oscillation frequency-to-natural vortex shedding frequency ratios $f/f_0 = 1.25, 1.75, 2.25, 2.75$. The numerical simulations are carried out using the computational fluid dynamics code developed by Dr. Kocabiyik's research group at Memorial University.

The results detail the link between the lift force, equivorticity patterns and the pressure fields which was previously uncharted, and paves the way for understanding the application of active flow control mechanisms on coastal and offshore engineering systems.

Acknowledgements

I am indebted to those people who have, for the enitrety of my masters, influenced and supported me during the writing of this thesis.

I especially want to thank my supervisor Dr. Kocabiyik for her superb guidance, patience, and the opportunity she gave to me to work for her.

I would like to thank Dr. Canan Bozkaya for all her support, advice, our inspirational conversations and for being an outstanding role model.

I kindly thank the financial support provided by the School of Graduate Studies.

I am also indebted to the Department of Mathematics and Statistics for the use of their computing resources which were acquired with support from the Canada Foundation of Innovation (CFI), Industrial Research and Innovation Fund (IRIF) of the province of Newfoundland and Labrador and IBM. Sincere thanks also goes to the secreterial staff and the computing support staff.

I would like to thank my friends and colleagues, Beth Liverman, Jared Penney, Satya Kumar, Jason McGraw for their support, interest and valuable discussions.

Finally, I would like to thank my family for their love, patience and support during the course of this degree.

Table of Contents

List of Tables

List of Figures

Nomenclature

$\mathbb{A}$	area open to flow (area aperture)
$\vec{a}$	acceleration of non-inertial frame of reference, $\widehat{\mathrm{X}}$, $(= (a_1, a_2, 0))$
A	forcing amplitude of the recti-linear cylinder oscillation $(= A^*/d)$
C_L	lift coefficient $(= 2L/\rho U^2 d)$
$\widehat{C}_L$	mean lift coefficient
$C_{L,rms}$	RMS lift coefficient
C_D	drag coefficient $(= 2D/\rho U^2 d)$
$\widehat{C}_D$	mean drag coefficient
$C_{D,rms}$	RMS drag coefficient
d	cylinder diameter
D	drag force per unit length
E	total dimensionless mechanical energy
f	forcing frequency of the recti-linear cylinder oscillation $(= df^*/U)$
f_0	natural vortex shedding frequency (i) in the absence of a free surface $(= df_0/U)$; (ii) in the presence of a free surface $(= df^*\|_{fs}/U)$
Fr	Froude number $\left(= U/\sqrt{dg^*}\right)$
$\vec{F^*}$	dimensional external force $(= ({F_1}^*, {F_2}^*, 0))$
$\vec{g}^*$	dimensional gravitational acceleration in inertial frame of reference, X $(= (0, g^*, 0))$

h	depth of cylinder submergence $(= h^*/d)$
Δh	spatial uniform grid step size
$\bar{h}$	height of the fluid at the outflow boundary
$\mathbb{I}$	length of a fluid-body interface open to flow
L	lift force per unit length
$\vec{n}$	outward unit normal vector $(= (n_1, n_2, 0))$
P	fluid property
p	fluid pressure
R	Reynolds number $(= \rho U d/\mu)$
S	control volume boundary
t	time $(= t^* U/d)$
Δt	time step
T	period of forced cylinder oscillation $(= 1/f)$
T_0	period of natural vortex shedding in the absence of a free surface $(= 1/f_0)$
$\vec{u}$	fluid velocity $(= (u, v, 0))$
U	uniform flow velocity
$\bar{u}$	maximum u-velocity of the fluid in the region directly above the cylinder
$\widehat{u}$	average u-velocity of the fluid in the region directly above the cylinder
$\mathbb{V}$	fractional volume open to flow
V	control volume

$V(t)$	material volume
$\mathbb{V}$	volume open to flow (volume aperture)
$\partial V(t)$	material volume boundary
v_j^*	dimensional velocity of an arbitrary time dependent fluid domain $\Omega(t)$
$\vec{\hat{v}}$	velocity of non-inertial frame of reference, $\widehat{\mathrm{X}}$, $(= (v_1, v_2, 0))$
$\vec{x}$	vector of spatial coordinates in inertial frame of reference, X, $(= (x, y, 0))$
X	inertial frame of reference $(= \{\vec{x}^*, t^*\})$
$\widehat{\mathrm{X}}$	non-inertial frame of reference $(= \{\widehat{\vec{x}^*}, \widehat{t^*}\})$
$\widetilde{\mathrm{X}}$	frame of reference which moves with the uniform flow

Greek Symbols

μ	dynamic viscosity of the fluid
ν	kinematic viscosity of the fluid $(= \mu/\rho)$
ρ	fluid density
ω^*	dimensional frequency of the cylinder oscillation $(= 2\pi f^*)$
Ω	arbitrary fluid domain
$\Omega_{i,\ i=1,2}$	computational domain occupied by the fluid
$\partial\Omega$	arbitrary fluid domain boundary
∇	vector differential operator
∇^2	Laplace operator

Superscripts

$*$	dimensional quantity
$\cdot$	differentiation by time

Abbreviations

CFD	computational fluid dynamics
PSD	power spectral density
VOF	volume of fluid
RMS	root mean square

1. Introduction

Combined wave motions and steady currents past ocean structures can induce fluid excitation forces. This causes structural vibrations due to asymmetric vortex shedding, as well as significant decreases in pressure in the rear of the structure when the Reynolds number exceeds a critical value. The failure of the Tacoma Narrows suspension bridge in Washington State in 1940 is a well-known example of the destructive potential of resonant flow state structural vibrations (see Figure 1.1). Control of vortex shedding leads to reduction in the forces acting on the structure and can significantly reduce its vibrations. Since the work of Roshko (1955), many passive and active open-loop control methods have been introduced to control vortex shedding behind a bluff body oscillation, inline with (or transverse to) the incident flow, and rotary oscillation. In the past 15 years, a large amount of research has been conducted on the control of flow over a bluff body using passive, active open-loop, and active closed-loop control methods. Control methods for cases of actuators without power input or feedback sensors (passive control) are easier to implement than the active feedback control method, which requires sensing as well as actuation (Gad-El-Hak (2000) and Choi et al. (2008)).

This thesis focuses on the application of active open-loop and closed-loop controls on a circular cylinder in the presence and absence of a free surface. It examines circular cylinders subject to forced (streamwise or transverse) oscillations (active open-loop), and combined forced streamwise and transverse oscillations (active closed-loop). The primary goal of this research is to understand the physical mechanisms behind the

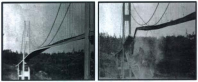

Figure 1.1: The twisting original Tacoma Narrows Bridge which collapsed on November 7, 1940 in the U.S. state of Washington - opened on July 1, 1940 (http://en.structurae.de/structures/data/photos.cfm?ID=s0000074).

response of a cylinder to these forcing mechanisms. This is acheived by examining the effect of forced cylinder oscillation frequency on the near-wake structures, and the pressure distribution and fluid forces at a fixed oscillation amplitude when the cylinder is placed beneath a free surface. The numerical simulations are carried out using the computational fluid dynamics code developed by Dr. S. Kocabiyik's research group at Memorial University of Newfoundland.

A basic schematic that illustrates the physical problem is shown in Figure 1.2. The present model involves two fluid phases in the regions $\mathbf{\Omega_1}$ and $\mathbf{\Omega_2}$ which have densities ρ_1, ρ_2, and kinematic viscosities ν_1, ν_2, respectively. The flow moves from left to right with uniform stream velocity, U, and is assumed to be two-dimensional in the $(x^*, y^*)-$plane. The present model considers uniform, viscous, incompressible flow past an oscillating, horizontal and infinitely long circular cylinder of diameter d that is submerged in region $\mathbf{\Omega_2}$ at a distance h^* below the undisturbed free surface as seen in Figure 1.2. Here g^* is the dimensional acceleration due to gravity, defined by $\overrightarrow{g^*} = (0, g^*, 0)$; A^* is the dimensional amplitude of cylinder oscillation; f^* is the dimensional forcing frequency of an oscillating cylinder; f_0^* is the dimensional natural vortex shedding frequency of a stationary cylinder; and t^* is the dimensional time. The corresponding dimensionless parameters of the physical problem are the maximum oscillation amplitude, $A = A^*/d$; the frequency ratio, f/f_0, with $f = df^*/U$ and $f_0 = df_0^*/U$ being the dimensionless forcing frequency of the cylinder oscillation and natural shedding frequency; the Reynolds number, defined as $R = Ud/\nu_1$ and $R = Ud/\nu_2$ for fluids in $\mathbf{\Omega_1}$ and $\mathbf{\Omega_2}$, respectively; the Froude number, $Fr = U/\sqrt{dg^*}$; and the cylinder submergence depth, $h = h^*/d$. Initially, the cylinder is at rest in the flow. Then, at the dimensionless time $t = Ut^*/d = 0$, the cylinder starts to undergo either (i) forced streamwise or transverse oscillations assigned by $x(t) = A\cos(2\pi ft)$, $y(t) = 0$, or $y(t) = A\cos(2\pi ft)$, $x(t) = 0$, respectively. Or (ii) combined forced streamwise and transverse oscillations assigned by $x(t) = A\cos(2\pi ft)$, $y(t) = A\cos(2\pi ft)$.

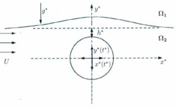

Figure 1.2: Schematic of the problem.

Following the work of Gubanov (2006), it is noted that the dimensionless cylinder velocity, $\vec{U}_{\text{body}}$ at any point $(x, y, 0)$, on the cylinder boundary can be determined by $\vec{U}_{\text{body}} = (\dot{x}, \dot{y}, 0)$.

Uniform flow past a stationary circular cylinder is dependent on the value of the Reynolds number as summarized by Sumer and Fredsøe (1997). Below a Reynolds number of $R \approx 40$, the cylinder wake is stable and thus vortex shedding is not present. The vortices form in the separated layer, but remain attached to the cylinder. As the Reynolds number increases, however, there is a transition from a stable two-dimensional wake to a turbulent three-dimensional wake within $200 < R < 300$. An in-depth analysis of how the characteristics of flow change as the Reynolds number increases from 1 to 100, and the effect on the vorticity created in the wake of the cylinder, can be found in Batchelor (1967). For a Reynolds number of $40 \leq R < 200$, the transition from a stable wake with attached vortices to the cylinder, to the alternate shedding of vortices from either side of the circular cylinder, known as a von Kármán vortex street, occurs. Persistence of these vortices in the wake causes pressure fluctuations and structural vibrations which can severely damage engineering structures. The review paper by Williamson and Govardhan (2004) summarizes the most influential investigations in the past two decades concerned mostly with flow behaviour behind cylindrical bodies.

The shedding of vortices from a circular cylinder lead to unsteady, periodic forces which act on the cylinder. The forces are comprised of the transverse (lift) force, and the streamwise (drag) force. A stationary cylinder is subjected to a lift force with a natural (Strouhal) shedding frequency of f_0, and a drag force equivalent to twice the natural shedding frequency frequency, $2f_0$ (Bishop & Hassan, 1964). An analysis of the relationships between the fluctuating lift force and the influence of the Reynolds number, as well as the fluctuating lift force and near wake flow patterns for flow past a stationary circular cylinder, can be found in the numerical study by Norberg (2003). For a transversely oscillating cylinder, if the forcing frequency, f, of the cylinder approaches the natural shedding frequency, the cylinder will oscillate at the imposed forcing frequency. This phenomenon is called "synchronization" or "lock-on." For a streamwise oscillating cylinder, lock-on occurs when the imposed frequency is twice the natural shedding frequency of the cylinder. The mechanism of vortex shedding, and consequently the fluid forces acting on the cylinder, is greatly affected by the forced oscillations to which a cylinder is subjected: that is, transverse, streamwise, rotational (or a combination of these) oscillations. The majority of numerical and experimental studies carried out for forced tranverse and streamwise oscillations have focused on the flow characteristics of a circular cylinder governed mainly by amplitude and frequency of the oscillation. Literature related to the study of flow characteristics of a cylinder subjected to transverse oscillations can be found in Ongoren and Rockwell (1988), Williamson and Roshko (1988), Blackburn and Henderson (1999), Anagnostopoulos (2000) and Pham et al. (2010). Fundamental literature related to flow characteristics of a cylinder subjected to streamwise oscillations can be found in Cetiner and Rockwell (2001a), Cetiner and Rockwell (2001b), Al-Mdallal et al. (2007) and Kim et al. (2009). Little information has been published on cylinders forced to undergo combined transverse and streamwise oscillations (see Li et al. (2009), Leong and Wei (2008), Dahl et al. (2006), Jauvtis and Williamson (2004), and Jeon and Gharib (2001)).

As mentioned previously, the main goal of this research is to understand the physcial mechanisms behind the response of a cylinder wake to forcing mechanicms (for three types of forced oscillatory motion) when a cylinder is in the presense of a free surface. Relatively few studies have been carried out on free surface problems concerning the effect of time-dependent streamwise (see Cetiner and Rockwell (2001b), Mironova (2008)) or transverse cylinder oscillations (see Gubanov (2006)) on the vortex shedding process. Cetiner and Rockwell (2001b), considered the vortex shedding modes near the fundamental lock-on region and the resulting fluid forces at $R = 917, 2075$; $Fr = 0.07, 0.158$; $A = 0.96$; $f/f_0 = 0.44, 1.0$; and $h = 0.06, 0.19, 11.23$. The experiments were conducted for over a hundred cylinder oscillation cycles and it was observed that for certain cases the flow is locked-on over several cycles of cylinder oscillation. Subsequently, the transition to the non-locked state occurs. Cetiner and Rockwell show that in the event a finite gap exists between the cylinder and the free surface ($h = 0.19$), jet-like flow through the gap act to destabilize such locked-on states by inducing a negative vortex from the cylinder surface. It was also demonstrated that localized distortions of the free surface appear due to vortical structures shed from both the cylinder and the free surface. Mironova (2008), considered uniform two-dimensional free surface flow simulations of forced streamwise oscillations of a circular cylinder. The numerical simulations were conducted at $R = 200$, $A = 0.13$, and $f/f_0 = 1.0, 2.0, 3.0, 4.0$ for three different cylinder submergence depths, $h = 0.25$, 0.5 and 0.75, and the Froude numbers $Fr \approx 0.0$, $Fr = 0.2$ and 0.4. Mironova's work demonstrated that it is possible to generate distinctly different patterns of the vortex formation than that of classical vortex shedding modes, provided that the cylinder is located sufficiently close to the free surface and the Froude number is high. For the limiting case $Fr \approx 0.0$, three basic quasi-locked-on or locked-on asymmetric vortex shedding modes were observed. The coalescence between the vortices in the vortex shedding layers appears for the frequency ratios, $f/f_0 = 2.0$ at $h = 0.5$; $f/f_0 = 3.0$ at $h = 0.5, 0.75$ and $f/f_0 = 4.0$ at $h = 0.25, 0.75$. In the numerical work by Gubanov (2006), uniform two-dimensional free surface flow simulations of forced transverse oscillations of a circular cylinder was examined. The simulations were carried out at $R = 200$, for a fixed cylinder submergence depth, $h = 1.25$, displacement amplitudes $A = 0.25$ and $A = 0.5$, frequency ratios $f/f_0 = 0.95, 1.0, 2.0, 3.0, 4.0$. Fluid forces and near wake vorticty patterns were examined to analyze the numerical results and determine if lock-on of vortex shedding occured. It was demonstrated that the inclusion of the free surface at $h = 1.25$ allowed for the formation of non-classical modes. In particular, the formation of these modes occured at $f/f_0 = 2.0, 4.0$ at $A = 0.5$. For small amplitude oscillation, $A = 0.25$, the presence of a free surface had a slight effect on the vortex shedding modes. Coalescence was observed at $A = 0.5, f/f_0 \geq 2.0$ in the presence and absence of a free surface. It was seen at $A = 0.5$, that the inclusion of the free surface seemed to induce period doubling of C_D at $f/f_0 = 0.95, 1.0$ and $f/f_0 = 3.0$. For all cases, the combination of the forced transverse motion and the inclusion of the free surface did not suppress vortex shedding and consequently the occurence of locked-on vortex shedding behaviour.

In this thesis, determination of lock-on regimes is based heavily on the work of Ongoren and Rockwell (1988). They classify lock-on regimes based on the repetition of vortex shedding in the near wake region of a circular cylinder over an integer number of oscillation cycles. The methods to determine lock-on by Anagnostopoulos (2000) and Cetiner and Rockwell (2001a) are employed as well. Anagnostopoulos (2000) numerically investigated a transversely oscillating cylinder subjected to uniform laminar flow at $R = 106$, for the frequency ratio range $0.8 \leq f/f_0 \leq 1.20$, and an oscillation amplitude that was increased to 50% of the cylinder diameter. In his study, the repetition of the lift force for a transversely oscillating cylinder, and correspondingly the existence of a large peak at the forcing frequency in the power spectra of the lift force, was used to determine if lock-on exists. The dominant frequencies at which the lift and drag forces oscillate can be identified from the PSD of lift and drag coefficents. The figures are developed by taking the time dependent lift and drag coefficents and transforming them into the frequency domain using Fourier analysis. The work of Cetiner and Rockwell (2001a) examined the streamwise oscillations of a circular cylinder subject to uniform flow in the absence of a free surface for the Reynolds number and frequency ratio ranges $405 \leq R \leq 2482$ and $0.0 \leq f/f_0 \leq 3.0$, respectively. The work focused on the relationship between the patterns of vortex shedding in the near wake of the cylinder with the fluid forces, and the corresponding Lissajous patterns and spectra. A Lissajous pattern represents the time change of the lift or drag coefficients as a function of cylinder displacement. Highly congruent Lissajous patterns are associated with lock-on of the forcing frequency with the natural shedding frequency of the cylinder. In Chapter 1.2, the link between the direction of the Lissajous patterns of the lift (or drag) force to the transfer of mechanical energy (from cylinder to fluid or fluid to cylinder) is discussed.

The lock-on modes of this work are classified in accordance to the nomenclature defined by Williamson and Roshko (1988). Williamson and Roshko studied the vortex-modes produced as a result of motion of a transversely oscillating cylinder in the

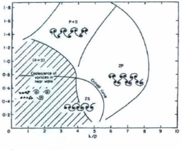

Figure 1.3: A map of the locked-on vortex modes in the wavelength-amplitude plane near the fundamental lock-on region, as observed by Williamson and Roshko (1988). The critical curve marks the transition from one mode of vortex formation to another. The lined area marks where the 'coalescence' type shedding occurs.

absence of a free-surface. They extensively mapped the locked-on vortex modes in the wavelength-amplitude plane at Reynolds numbers and cylinder amplitudes within $300 < R < 1000$ and $0 < A(= A^*/d) \leq 1.8$, respectively, for frequency ratios $f/f_0 \geq 0.3$ (see Figure 1.3). The wavelength ratio is defined as $\lambda/d = UT^*/d$. The common vortex patterns near the fundamental lock-on region ($\lambda/d \approx 5$ *or* $f \approx f_0$) as observed by Williamson and Roshko include the **2S**, **2P** and **P + S** modes. The **2S** mode is commonly referred to as the classical Von Kármán street. It refers to the alternate shedding of two single vortices of opposite rotation from each side of the cylinder within a single vortex shedding cycle, $T_v = kT$, where k is either a fraction or an integer. The **2P** mode refers to the alternate shedding counter-rotating vortex pairs from each side of the cylinder per T_v. The **P + S** mode refers to the shedding of a counter-rotating vortex pair, followed by a single vortex within one cycle. The coalescence phenomenon is the merging of vortices immediately behind the cylinder, or downstream. Coalescence is identifed to have occurred if an uppercase "**C**" is written before the vortex mode. For example, **C(2S)** refers to the alternate shedding of two positive vortices of opposite rotation, where at least one of the shed vortices was formed by the coalesence of vortices.

1.1 Methodology and Governing Equations

This thesis employs the two-fluid flow model used by Mironova (2008). The model desribes the entering of fluids Ω_1 and Ω_2 into the cell inflow boundary with uniform velocity U, which leave the cell via the outflow boundary. Mironova's model is an extension of the single-fluid flow model used by Gubanov (2006). The single-fluid model describes the motion of arbitrarily moving bodies including free surface flows. The model uses a non-boundary fitted grid, which makes passage of the fluid interface through computational cells possible. The governing equations stated in the dimensional form are the continuity and Navier-Stokes equations in a non-inertial frame of reference, expressed as

$$\frac{d\mathbb{V}^*}{dt^*} + \int\limits_{\mathbb{A}^*} (\vec{n} \cdot \vec{u}^*) \, \mathrm{d}S^* = 0, \tag{1.1}$$

$$\frac{d}{dt^*}\int_{\mathbb{V}^*} \vec{u}^*\,\mathrm{d}V^* + \int_{\mathbb{A}^*} (\vec{n}\cdot\vec{u}^*)\vec{u}^*\,\mathrm{d}S^* = -\frac{1}{\rho}\int_{\mathbb{A}^*\cup\mathbb{I}^*} p^*\vec{n}\,\mathrm{d}S^* + \nu\int_{\mathbb{A}^*\cup\mathbb{I}^*} \vec{n}\cdot\nabla\vec{u}^*\,\mathrm{d}S^* + \int_{\mathbb{V}^*}\vec{F}^*\,\mathrm{d}V^* \tag{1.2}$$

The associated boundary conditions of the problem include the no-slip conditions at the cylinder boundary

$$u^* = 0, \quad v^* = 0.$$

The inflow and outflow boundary conditions are defined respectively as,

$$u^* = U - v_1^*, \qquad v^* = -v_2^*;$$

$$\nu\frac{\partial u^*}{\partial x^*} + g^*\bar{h}^* = \frac{p^*}{\rho}, \qquad \frac{\partial v^*}{\partial x^*} = 0,$$

and the free-slip conditions at the top and bottom boundaries of the domain

$$\frac{\partial u^*}{\partial x^*} = 0, \quad v^* = -v_2^*, \tag{1.3}$$

where $\mathbb{V}^*$ and $\mathbb{A}^*$ are the fractional volume and area, respectively, of the computational cell V^*. The dimensional fluid-body interface is defined as $\mathbb{I}^*$; $\vec{u}^*$ is the dimensional velocity; $\vec{n}$ is the outward normal vector to the cell boundary and S^* is the control volume boundary.

Not previously defined dimensionless forms of the parameters found in equations 1.1 and 1.2 are written as

$$u = \frac{u^*}{U}, \quad v = \frac{v^*}{U},$$

$$V = \frac{V^*}{d^2}, \quad S = \frac{S^*}{d}, \quad \mathbb{V} = \frac{\mathbb{V}^*}{d^2}, \quad \mathbb{A} = \frac{\mathbb{A}^*}{d}, \quad \mathbb{I} = \frac{\mathbb{I}^*}{d}.$$

In the two fluid model, the dimensionless fluid pressure is defined as $p/\epsilon = p^*/\rho_2 U^2$, where $\epsilon = \rho_1/\rho_2$ when $\vec{x} \in \Omega_1$, and $\epsilon = 1$ when $\vec{x} \in \Omega_2$. In this thesis, the fluid density and viscoscity ratios are set to $\rho_1/\rho_2 = 1/100$ and $\mu_1/\mu_2 = 1/100$, repectively, which results in a kinematic viscoscity ratio of $\nu_1/\nu_2 = 1$. Hence $\nu_1 = \nu_2$, which can now be referred to ν. The governing equations in dimensionless form are

$$\frac{d\mathbb{V}}{dt} + \int\limits_{\mathbb{A}} (\vec{u} \cdot \vec{n})\, \mathrm{d}S = 0, \tag{1.4}$$

$$\frac{d}{dt} \int\limits_{\mathbb{V}} \vec{u}\, \mathrm{d}V + \int\limits_{\mathbb{A}} (\vec{n} \cdot \vec{u})\vec{u}\, \mathrm{d}S = -\frac{1}{\varepsilon} \int\limits_{\mathbb{A}\cup\mathbb{I}} p\vec{n}\, \mathrm{d}S + \frac{1}{R} \int\limits_{\mathbb{A}\cup\mathbb{I}} \vec{n} \cdot \nabla\vec{u}\, \mathrm{d}S + \int\limits_{\mathbb{V}} \vec{F}\, \mathrm{d}V, \tag{1.5}$$

where the external force, $\vec{F} = (-a_1,\ \frac{1}{Fr^2} - a_2,\ 0)$, is due to the dimensionless gravity force, $\vec{g} = (0,\ 1/Fr^2,\ 0)$, and the dimensionless acceleration of the non-inertial frame of reference, $\vec{a} = (a_1^* d/U^2,\ a_2^* d/U^2,\ 0)$.

It follows that the dimensionless boundary conditions of the problem are the no-slip conditions at the cylinder boundary

$$u = 0, \quad v = 0. \tag{1.6}$$

The inflow boundary condition, and the outflow boundary condition as proposed by Gresho and Sani (1998), are respectively

$$u = U - v_1,\ v = -v_2, \tag{1.7}$$

$$\frac{1}{R}\frac{\partial u}{\partial x} + \frac{\bar{h}}{Fr^2} = p,\ \frac{\partial v}{\partial x} = 0, \tag{1.8}$$

and finally the free-slip conditions at the top and bottom boundaries of the domain are written as

$$\frac{\partial u}{\partial x} = 0, \quad v = -v_2. \tag{1.9}$$

At $t = 0$, that the free-surface is assumed to be undisturbed.

The governing equations are approximated using the finite volume method on a fixed Cartesian grid. Versteeg and Malalasekera (1995) provide an excellent description of the finite volume method. A second-order accurate central difference scheme in space is used in conjunction with a first-order explicit forward Euler scheme to advance the numerical solution in time. A cell merging procedure is used to preserve second-order accuracy of the spatial discretization. The free-surface interface is discretized using a volume-of-fluid (VOF) method proposed by (Hirt & Nichols, 1981). A mass conserving VOF advection method in two-dimensional incompressible flows, as proposed by Aulisa et al. (2003b), is used. For the moving fluid-body interface, the fractional area/volume obstacle representation method proposed by Hirt and Sicilian (1985), and the cut cell method of Gerrits (2001) are used. In this thesis, the numerical simulations were carried out using the CFD code developed by Dr. Kocabiyik's research group at Memorial University. Details of the development, and implementation of the code can be found in Mironova (2008) and Gubanov (2006). The computational code is applied to the model problem of unsteady, laminar, two-dimensional flow of a viscous incompressible fluid past a circular cylinder subject to forced (i) streamwise, (ii) transverse, and (iii) combined streamwise and transverse, oscillations in the presence of a free surface. The unsteady flow calculations are conducted at a fixed Reynolds number of $R = 200$, and cylinder displacement $A = 0.13$, for four frequency ratios, $f/f_0 = 1.25, 1.75, 2.25, 2.75$ at (i) $Fr \approx 0.0, 0.2, 0.4$ at cylinder submergence depths $h = 0.25, 0.5, 0.75$; (ii) $Fr = 0.2$ at $h = 0.5$; and (iii) $Fr = 0.2$ at $h = 0.5$. A comparison of the present results with the reference case $h = \infty$, are included to illustrate the effects cause by the inclusion of a free surface.

1.2 Calculation of Lift and Drag Forces, and Mechanical Energy

The x and y components of the dimensionless force, $\vec{F} = 2\vec{F}^*/(\rho dU)$, exerted by the cylinder on the fluid are the dimensionless drag, C_D, and dimenionless lift, C_L, force coefficients are

$$C_D = C_{D_P} + C_{D_V},\ C_L = C_{L_P} + C_{L_V}, \tag{1.10}$$

respectively, where C_{D_P} and C_{L_P} are the contributions due to the pressure gradient, and C_{D_V} and C_{L_V} are the contributions due to the viscous shear forces. The pressure contributions are

$$C_{D_P} = \int_0^{2\pi} p\cos\theta d\theta,\ C_{L_P} = \int_0^{2\pi} p\sin\theta d\theta$$

$$C_{D_V} = \frac{1}{R}\int_0^{2\pi} \frac{\partial u}{\partial \vec{n}} d\theta,\ C_{L_V} = \frac{1}{R}\int_0^{2\pi} \frac{\partial v}{\partial \vec{n}} d\theta$$

where $\vec{n} = (\cos(\theta), \sin(\theta), 0)$ is the outward unit normal to the cylinder boundary. The fluid forces are analyzed based on the power spectrum density of the lift and drag coefficients and the Lissajous trajectories of the force coefficients. In all figures related to fluid forces that follow, the observed flow regimes in various states (e.g. periodic, quasi-periodic or non-periodic states) are indicated to illustrate the link between the various flow states and the behaviour of the force coefficients. The power spectrum densities and the Lissajous trajectories of the lift and drag coefficients, $C_L(x)$ ($C_L(y)$) and $C_D(x)$ ($C_D(y)$), respectively, are displayed separately in the time intervals corresponding to each of the relevant flow states. The Lissajous curve describes the time change of the lift and drag coefficients as a function of the cylinder displacement, $x(t)$ ($y(t)$). The Lissajous representations of the lift and drag coefficients are also used to demonstrate the mechanism of mechanical energy transfer between the fluid and cylinder, degree of phase-locking or a loss of lock-on, and associated phase shift. For a cylinder undergoing streamwise oscillations, the total dimensionless mechanical energy transfer between the cylinder and the fluid over one period of cylinder oscillation, T, can be defined as

$$E = \int_0^T C_D \dot{x}(t) dt, \tag{1.11}$$

where the overdot indicates differentiation with respect to time (Baranayi (2008)).

The total dimensionless mechanical energy transfer between the cylinder and the fluid over one period of cylinder oscillation, T, for a cylinder undergoing transverse oscillations is defined as

$$E = \int_0^T C_L \dot{y}(t) dt. \tag{1.12}$$

For a cylinder undergoing combined streamwise and transverse oscillations, the total dimensionless mechanical energy transfer between the cylinder and the fluid over one period of cylinder oscillation is defined by the sum of equations 1.11 and 1.12. Thus, it follows that the total dimensionless mechanical energy transfer between the cylinder and fluid, over one period of cylinder oscillation, T, for a cylinder performing transverse-streamwise oscillations can be defined as

$$E = \int_0^T (C_D\dot{x}(t) + C_L\dot{y}(t))dt = E_1 + E_2.$$

The geometrical interpretation of E is the signed area enclosed by the hystersis loops of $C_D(x)$ and $C_L(y)$, where the sign is defined by the direction of the Lisssajous trajectories (Cetiner and Rockwell (2001b)). In all figures that follow, the direction of Lissajous trajectories are indicated by arrows. The energy, E, is negative when the directions of all $C_D(x)$ or $C_L(y)$ traces are counterclockwise, and therefore the energy transfer is from cylinder to fluid. Conversely, the energy is positive, and the transfer of mechanical energy is from the fluid to cylinder when the direction of $C_D(x)$ or $C_L(y)$ is clockwise.

1.3 Code Validation

In this thesis, the present numerical model is validated by conducting numerical simulations for two-dimensional, unsteady, laminar flow past (i) a stationary cylinder in the absence of a free surface; (ii) a cylinder undergoing transverse oscillations in the absence of a free surface, and (iii) a cylinder undergoing forced streamwise oscillations in the absence of a free surface. A validation study for free surface flow past a cylinder is difficult to find. The comparison of the computer flow properties and near wake structures of Reichl et al. (2005) with the present numerical model in the presence of a free surface can be found in Mironova (2008). The results are in good agreement.

A computational grid resolution of 60 cells per diameter is chosen for the current investigation. The mesh has approximately 250 × 190 node points with considerable mesh concentrtion both around the cylinder and in the wake. For this mesh, the distances to upstream, side and outflow boundaries of the computational domain are defined to be $L_1 = 20, L_2 = 30, L_3 = 40$. The discussion of spatial grid resolution is in principle the same as given by Mironova (2008), and the time step $\Delta = 0.005$ used for the evolution of the solution follow exactly those set out in Miranova's discussion. Furthermore, a time-step of $\Delta = 0.005$ and a near wake grid resolution of 60 cells per cylinder diameter is chosen.

1.3.1 Flow past a stationary cylinder in the absence of a free surface

This section presents the results of uniform flow past a stationary cylinder at Reynolds numbers of $R = 550$ and 10^3. The numerical simulations of a stationary cylinder for the present model are compared with numerical results of Li et al. (2004), Ploumhans and Winckelmans (2000),Gubanov (2006) and Al-Mdallal (2004). Near-wake equivorticity patterns at $R = 550$ are compared with numerical results of Li et al. (2004) and Gubanov (2006) in Figure 1.4. Li et al. (2004) employed a kinetic-theory-based lattice Boltzmann method to approximate the problem of flow past a circular cylinder for a Reynolds number of $R = 550$, whereas Gubanov (2006) simulated flow about an oscillating cylinder using a single-fluid model where the governing equations were approximated using the finite volume method. Results are in good agreement as shown in Figure 1.4 for the early time instances of $t = 0.5, 1.5, 2.5$.

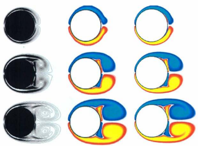

Figure 1.4: Equivorticity patterns for uniform flow past a stationary cylinder in the absence of a free surface at $R = 550$: Li et al. (2004) (left), Gubanov (2006) (middle), present work (right) when $t = 0.5, 1.5, 2.5$ (from top to bottom)

Numerical simulations are also carried out at $R = 1000$ for the case of uniform flow past a stationary cylinder. Figure 1.5 shows good comparison between the present results and the ones obtained by Coutanceau and Pineau (1997) experimentally and the numerical results of Al-Mdallal (2004). It is noted that the numerical method of Al-Mdallal is based on a conjugating Fourier spectral analysis with finite-difference approximations.

Figure 1.6 displays the early time development of the drag coefficent for uniform flow past a stationary cylinder at $R = 550$. It can be seen that the figure shows a good comparison between the present results and the results obtained by Ploumhans and

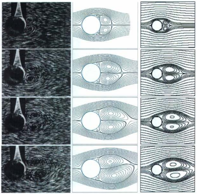

Figure 1.5: Streamline patterns for uniform flow past a stationary cylinder in the absence of a free surface at $R = 10^3$ at the time instances: (a) $t = 4$, (b) $t = 8$, (c) $t = 12$, (d) $t = 16$. Coutanceau and Pineau (1997) (left), Al-Mdallal (2004) (middle), present work (right).

Winckelmans (2000) and Li et al. (2004). Li et al. (2004) implement the lattice-Boltzmann method to solve the problem of impulsively started flow past a circular cylinder for a Reynolds number of $R = 550$. Ploumhans and Winckelmans (2000) use a two-dimensional vortex method based on the vorticity-stream function formulation of the Navier-Stokes equations in combination with the particle strength exchange scheme for diffusion. The value of the drag coefficient at the local maximum (and

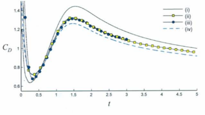

Figure 1.6: The drag coefficient, C_D, for uniform flow past a stationary cylinder in the absence of a free surface at $R = 550$: (i) Gubanov (2006), (ii) Ploumhans and Winckelmans (2000), (iii) Li et al. (2004), (iv) present work.

the local minimum) observed by Gubanov (2006) is higher (lower) than the ones obtained by Ploumhans and Winckelmans (2000), Li et al. (2004) and the present study. This might be due to the use of different boundary conditions: Li et al. (2004) used periodic boundary conditions for the lattice-Boltzmann equations at the upper and lower boundaries of the computational domain, whereas Gubanov (2006) employed inviscid wall conditions. It is noted that the difference between the drag coefficient of Gubanov (2006) and the results in this thesis is about 20%. This could be due to the fact that Gubanov simulated the flow using a single-phase fluid model, whereas the present study employs a two-phase fluid model. In the single-phase flow model, the fluid in Ω_1 is assumed to be much lighter than the fluid in Ω_2. Therefore the fluid in Ω_1 can be neglected, and the governing equations are solved in the region Ω_2 only. Although computational more appealing, the single-phase model is shown to have numerical difficulties which arise due to complexity of the application of boundary conditions at the free surface on the non-boundary-fitted Cartesian grid (Gubanov, 2006).

1.3.2 Flow past a streamwise oscillating cylinder in the absence of a free surface

The numerical simulations are carried out at $R = 855$; $A = 0.13, f/f_0 = 0.5, 1, 2, 3, 4$ by setting the rectilinear oscillatory cylinder displacement to

$$x(t) = A\cos(2\pi f t). \tag{1.13}$$

In Figure 1.7, the present numerical results of the flow development behind a streamwise oscillating cylinder are compared with the numerical results of Al-Mdallal (2004) and the available experimental results obtained by Ongoren and Rockwell (1988). It can be seen that these comparisons are in good agreement.

1.3.3 Flow past a transversely oscillating cylinder in the absence of a free surface

The numerical simulations in the case of a transversely oscillating cylinder were carried out at Reynolds numbers of $R = 200$ and $R = 855$. Figure 1.8 shows the comparison of the present numerical simulations ($R = 200,\ f/f_0 = 0.8,\ A = 0.6$) after setting the rectilinear cylinder displacement to

$$y(t) = -A\cos(2\pi f t), \tag{1.14}$$

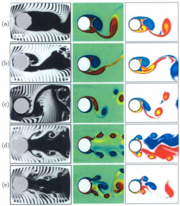

Figure 1.7: Comparison of flow visualization of Ongoren and Rockwell (1988)(left), Al-Mdallal (2004) (middle), and computed present equivorticity lines (right) for a streamwise oscillating cylinder $R = 855, A = 0.13$ at frequency ratios: (a) $f/f_0 = 0.5$; (b) $f/f_0 = 1$; (c) $f/f_0 = 2$; (d) $f/f_0 = 3$; (e) $f/f_0 = .4$.

with numerical results of Meneghini and Bearman (1995) and Gubanov (2006). Meneghini and Bearman simulated flow about an oscillating cylinder using a discrete vortex method. Figure 1.8 shows good agreement between the present equivorticity patterns in the near wake region with both Meneghini and Bearman (1995) and Gubanov (2006).

Figure 1.8: Equivorticity patterns for a transversely oscillating cylinder at $R = 200, A = 0.13$ at frequency ratios $f/f_0 = 0.8$. Meneghini and Bearman (1995) (left), Gubanov (2006) (middle), present work (right).

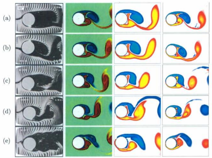

Figure 1.9: Comparison of flow visualization of Ongoren and Rockwell (1988)(left), equivorticity patterns by Al-Mdallal (2004)(mid-left), Gubanov (2006)(mid-right) and present work(right) for uniform flow past a transversely oscillating cylinder at $R = 855, A = 0.13$ at frequency ratios: (a) $f/f_0 = 0.5$; (b) $f/f_0 = 1$; (c) $f/f_0 = 2$; (d) $f/f_0 = 3$; (e) $f/f_0 = 4$.

The numerical simulations of a transversely oscillating cylinder is also carried out at $R = 855$, $A = 0.13$ in the frequency range $0.5 \leq f/f_0 \leq 4.0$. The present equivorticity patterns are compared with the work of Ongoren and Rockwell (1988) and the numerical results of Al-Mdallal (2004) and Gubanov (2006) in Figure 1.9. It can be seen that there is good agreement in the near wake region of the cylinder for $f/f_0 \leq 2$ with all three sets of results.

2. Flow past a streamwise oscillating circular cylinder in the absence of a free surface

This chapter focuses on the results for flow past a circular cylinder subject to forced streamwise oscillations in the absence of a free surface (symbollically represented by $h = \infty$). The numerical simulations are conducted at a Reynolds number of $R = 200$, for a fixed amplitude, $A = 0.13$, in the frequency ratio range, $1.25 \leq f/f_0 \leq 2.75$, which increases by an increment of 0.5.

2.1 Fluid forces and vortex shedding modes

2.1.1 Fluid forces

The time history of the fluctuating lift coefficient, C_L, the PSD of C_L and the Lissajous patterns, $C_L(x)$, are displayed in Figure 2.1. It is evident that for frequency ratio, $f/f_0 = 1.75$, the trace of C_L exhibits a periodic signature every two cycles of cylinder oscillation, $2T$ within $54.83 \leq t \leq 150$. The periodic nature of C_L for this frequency ratio is also suggested by the corresponding Lissajous pattern which displays highly congruent behaviour from cycle to cycle of cylinder oscillation. The C_L traces for frequency ratios, $f/f_0 = 1.25, 2.25, 2.75$, display quasi-periodic signatures every $7T$ for $f/f_0 = 1.25$ within $60.61 \leq t \leq 150$, every $9T$ for $f/f_0 = 2.25$ within $80.81 \leq$

$t \leq 150$, and every $3T$ for $f/f_0 = 2.75$ within $91.83 \leq t \leq 150$. It can be seen that the corresponding Lissajous patterns exhibit congruent behaviour, and that the congruency of these patterns increases as f/f_0 increases from 1.25 to 2.75. It is noted that for each frequency ratio, $f/f_0 = 1.25, 1.75, 2.25, 2.75$, the hysteresis loops of $C_L(x)$ are confined to both the upper and lower half planes. For each frequency ratio, f/f_0, the corresponding spectra of C_L show one dominant peak at f_0. This indicates that C_L oscillates at f_0 for all frequency ratios. It is important to note that the lift coefficients of Figure 2.1 display that there is a transition period for all the frequency ratio cases considered, $f/f_0 = 1.25, 1.75, 2.25, 2.75$, until $t \approx 40, 50, 60, 65$, respectively. Consequently, the intervals $0 \leq t < 60.61$ for $f/f_0 = 1.25$; $0 \leq t < 54.83$ for $f/f_0 = 1.75$; $0 \leq t < 80.81$ for $f/f_0 = 2.25$; and $0 \leq t < 91.83$ for $f/f_0 = 2.75$, respresent the time it takes the flow to settle into the quasi-periodic and periodic states in the near wake region of the cylinder (the transition period).

In Figure 2.2, the time history of the drag coefficient, C_D, the PSD of C_D and the corresponding Lissajous patterns, $C_D(x)$, of C_D are displayed. It is important to note that the Lissajous patterns of C_D, and the PSD of C_D are produced using the same time intervals as those used in C_L, to determine the corresponding effects of C_D traces on flow states. It is evident that the C_D traces display almost periodic signatures every seven periods of cylinder oscillation, $7T$, for $f/f_0 = 1.25$; every period of cylinder oscillation, T, for $f/f_0 = 1.75$; and every nine periods of cylinder oscillation, $9T$, for $f/f_0 = 2.25$. The trace of C_D for $f/f_0 = 2.75$, displays a periodic signature every two periods of cylinder oscillation, $2T$. Thus, the increase of f/f_0 is associated with the stabilization of the fluctuations of C_D. The behaviour of each C_D trace is also suggested by the corresponding Lissajous patterns. The $C_D(x)$ patterns

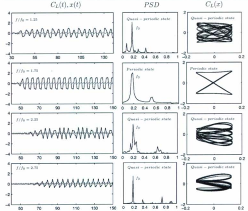

Figure 2.1: The time variation of the lift coefficient, C_L, (black) and the streamwise displacement, $x(t)$, (gray); PSD of C_L; Lissajous patterns of C_L at $R = 200 : A = 0.13, f/f_0 = 1.25, 1.75, 2.25, 2.75$ when $h = \infty$. The Lissajous and PSD plots for $f/f_0 = 1.25, 1.75, 2.25, 2.75$ are obtained for quasi-periodic states in the following time intervals $60.61 \leq t \leq 150, 54.83 \leq t \leq 150, 80.81 \leq t \leq 150, 91.83 \leq t \leq 150$, respectively. The corresponding flow states in the near wake region are indicated for each f/f_0.

display congruent patterns with minimal phase shift for $f/f_0 = 1.25, 1.75, 2.25$, and a highly congruent pattern with little to no phase shift for $f/f_0 = 2.75$, indicating periodic behaviour. It can be seen that the hysteresis loops, for all f/f_0, are mainly

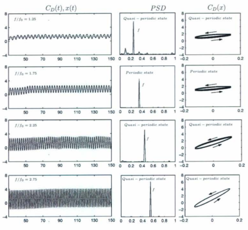

Figure 2.2: The time variation of drag coefficient, C_D, (black) and the streamwise displacement, $x(t)$, (gray); PSD of C_D; Lissajous patterns of C_D at $R = 200 : A = 0.13, f/f_0 = 1.25, 1.75, 2.25, 2.75$, when $h = \infty$. The Lissajous and PSD plots for $f/f_0 = 1.25, 1.75, 2.25, 2.75$ are obtained for quasi-periodic states in the following time intervals $60.61 \le t \le 150, 54.83 \le t \le 150, 80.81 \le t \le 150, 91.83 \le t \le 150$, respectively. The corresponding flow states in the near wake region are indicated for each f/f_0.

confined to the upper half-planes. As f/f_0 increases, there is a shift of the patterns of $C_D(x)$ into the lower half plane. The direction of each $C_D(x)$ is counter-clockwise.

Hence, the mechanical energy transfer is from the cylinder to the fluid. It can also be seen that as f/f_0 increases, the area enclosed by $C_D(x)$ increases. This implies that a higher amount of energy is being transferred from the cylinder to fluid with the increase of f/f_0 from 1.25 to 2.75. For each frequency ratio, f/f_0, the corresponding spectra, PSD, of C_D show one dominant peak at f. This indicates that C_D oscillates at f for all frequency ratios.

2.1.2 Vortex formation modes

Figures 2.3-2.10 display the equivorticity and streamline patterns, and the pressure contours in the near wake of the cylinder when $f/f_0 = 1.25, 1.75, 2.25, 2.75$. The observed flow behaviour is (i) periodic, per $2T$, for $f/f_0 = 1.75$ and (ii) quasi-periodic, per $7T, 9T, 3T$, for $f/f_0 = 1.25, 2.25, 2.75$, respectively.

In Figure 2.3, the equivorticity patterns are displayed for $f/f_0 = 1.25$ over seven periods of cylinder oscillation, $7T$. The vortex shedding mode is the quasi-locked-on $\mathbf{C(10S)}^*$ mode, per $7T$, within $60.61 \leq t \leq 150$ (quasi-periodic state). This is consistent with the behaviour of C_L and C_D at this frequency ratio. The flow is non-periodic for $t < 60.61$. In this mode, five vortices develop and shed on each side of the cylinder over $7T$. Initially, two negative vortices which develop over $0 \leq t \leq T/3$, coalesce at $t = 2T/3$, and then this newly formed vortex sheds into the downstream at $t \approx 5T/3$. Over $2T \leq t \leq 8T/3$, the development of two co-rotating negative vortices is observed in the near wake region. The secondary negative vortex formed in this negative vortex shedding layer detaches at $t \approx 8T/3$ and sheds into the downstream of the cylinder, at $t \approx 3T$. Similarly, over $10T/3 \leq t \leq 4T$, two negative co-rotating vortices develop in the upper shear layer of the cylinder. Then, the secondary vortex becomes detached at $t \approx 4T$ and propogates into the downstream of the cylinder, aided by the development of the positive vortices in the lower vortex shedding layer. Two negative vortices coalesce at $t = 14T/3$ and then the newly formed vortex sheds into the downstream of the cylinder at $t \approx 17T/3$. Finally, in the upper vortex shedding region of the cylinder, the primary negative vortex in the near wake of the cylinder at $t = 17T/3$ continues to develop over $6T \leq t \leq 20T/3$ and is shed downstream of the cylinder at $t \approx 7T$. Meanwhile in the lower vortex shedding region of the cylinder, a positive vortex developed in the previous shedding cycle elongates and becomes weaker and then sheds into the downstream of the cylinder at $t \approx 2T/3$. Subsequently, the newly formed positive vortex formed over $0 \leq t \leq T$ elongates, and then detaches from the positive vortex shedding layer at $t \approx 2T$. On the other hand, at $t = 8T/3$, two positive vortices coalesce to form a single positive vortex which continues to develop over $3T \leq t \leq 10T/3$, and then becomes detached at $t \approx 11T/3$. The positive vortex attached to the cylinder at $t = 4T$ is forced to elongate, over $13T/3 \leq t \leq 14T/3$, due to the interaction with the negative vortex in the upper vortex shedding region, and then sheds into the downstream of the cylinder at $t = 5T$. Finally, a positive vortex developing over $6T \leq t \leq 20T/3$ is subjected to the interaction with the negative vortices in the upper vortex shedding region, and then consequently sheds into the downstream of the cylinder at $t = 7T$. Thus, in the quasi-locked-on $\mathbf{C(10S)}^*$ mode, per $7T$, five vortices alternately develop from each side of the cylinder. In addition, the first two vortices which develop from each side coalesce to form one single vortex followed by a third vortex shed from each side in the first, second and fifth periods.

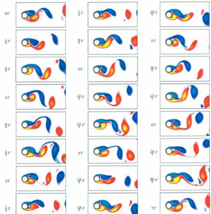

Figure 2.3: The equivorticity patterns over seven periods of cylinder oscillation, $7T$, at $R = 200$: A=0.13, $f/f_0 = 1.25$ when $h = \infty$ [$T \approx 4.04, 60.61 \leq t \leq 88.89$: $(15T, 22T)$]. The quasi-locked-on $\mathbf{C(10S)}^*$ mode, per $7T$, is observed.

Figure 2.4, displays the pressure contours for the aforementioned case of frequency ratio $f/f_0 = 1.25$ over seven periods of cylinder oscillation, $7T$. At $t = 0T$, this figure displays the development of the low pressure region behind the cylinder (near wake region), and the region of high pressure in the stagnation region. At every $t = nT/2$ $(n = 1, 3, 5, 7, 9, 11, 13)$, the high pressure region seems to be confined above and below the low pressure regions, in the downstream of the cylinder. On the other hand, for example at $t = 2T$, synonomous with the shedding of the negative vortex into the upper vortex shedding region, it is evident that the high pressure region has shifted completely to the front of the cylinder and the low pressure region shifts mostly behind the cylinder in the near wake region. The low pressure region in the upper side of the cylinder is also created as a negative vortex is developing at $t = 5T/2$. The high pressure region shifts above and below the low pressure regions, in the downstream of the cylinder, indicating a drastic increase in the concentration of the high pressure region. It is also interesting to note that the structure of the pressure contours in the near wake region at $t = 0, T/2, T, 3T/2$ are almost mirror images of the low pressure regions at $t = 2T$ $(4T, 6T), 5T/2$ $(9T/2, 13T/2), 3T$ $(5T, 7T), 7T/2$ $(11T/2)$, respectively. This indicates the periodic nature of the flow field as expected.

Figure 2.5 displays the equivorticity patterns for $f/f_0 = 1.75$ over two periods of cylinder oscillation, $2T$. The vortex shedding mode is the periodic locked-on **2P** mode, per $2T$, within the interval $19T \leq t \leq 51T$. This is consistent with the C_L, but not with the C_D, behaviour at this frequency ratio. The flow is non-periodic for $t < 19T$. A pair of negative co-rotating vortices develop in the upper vortex shedding region of the cylinder over $0T \leq t \leq 4T/6$, and then sheds into the near wake of the cylinder at $t \approx 5T/6$. On the other hand, a pair of positive co-rotating vortices develop in the lower vortex shedding region of the cylinder over $0 \leq t \leq 10T/6$, and then sheds into the near wake of the cylinder at $t = 11T/6$. No coalescence was observed for this case.

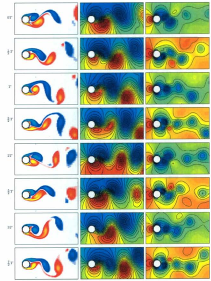

Figure 2.4: The figure caption is given on page 34

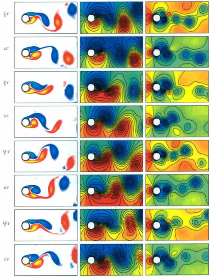

Figure 2.4: The equivorticity patterns (left), streamline patterns (middle) and the pressure contours (right) in the near wake region of the cylinder over seven periods of cylinder oscillation, $7T$, at R = 200: A=0.13, f/f_0 = 1.25 when $h = \infty$ [$T \approx 4.04, 80.80 \leq t \leq 109.08 : (20T, 27T)$]. The quasi-locked-on $\mathbf{C(10S)}^*$ mode, per $7T$, is observed.

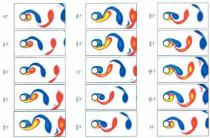

Figure 2.5: The equivorticity patterns over two periods of cylinder oscillation, $2T$, at $R = 200$: A=0.13, $f/f_0 = 1.75$ when $h = \infty$ [$T \approx 2.886, 66.38 \leq t \leq 72.15$: $(23T, 25T)$]. The periodic-locked-on **2P** mode, per $2T$, is observed.

The pressure contours are displayed in the last column of Figure 2.6 for $f/f_0 = 1.75$, over two periods of cylinder oscillation, $2T$. The pressure contours indicate that the high pressure region is associated with the stagnation region. At $t = 0T$, it is evident that the low pressure region develops in the lower side of the cylinder following the development of the positive vortex in the lower vortex shedding layer. At $t = T/2$, as a new negative vortex develops and the negative vortex pair, in the upper region of the cylinder, begins to detach the low pressure region shifts mostly to the upper side of the cylinder, in the near wake region. As the pair is fully shed at $t = T$, it is evident that the low pressure region shifts substantially behind the cylinder, in the near wake. As a new positive vortex develops in the lower vortex shedding layer and as the positive pair of vortices begin to detach at $t = 3T/2$, it can be seen that the region of low pressure mostly shifts from behind the cylinder to the lower side of the cylinder. The concentration of the high pressure region, at this time, increases drastically. Finally, at $t = 2T$, the high pressure concentration decreases and is located near the stagnation region unlike the high pressure region observed at $t = 3T/2$. It is noted that, over $0 \leq t \leq T$, the region of high pressure tends to move in the counterclockwise direction. In general, at $t = nT/2$ $(n = 1, 3)$, the high pressure region is confined above and below the low pressure regions in the downstream of the cylinder.

Figure 2.7 displays the equivorticity patterns over nine periods of cylinder oscillations, $9T$, of the quasi-periodic state when $f/f_0 = 2.25$. The vortex shedding mode is the quasi-locked-on $\mathbf{C(8S)}^*$, per $9T$, within the interval $36T \leq t \leq 66T$. This is consistent with the behaviour of C_L and C_D at this frequency ratio. The flow is non-periodic for $t < 36T$. In this mode, four vortices develop on each side of the cylinder and shed alternately over $9T$. Initially, a negative vortex which has developed over $0 \leq t \leq 2T$, sheds into the upper vortex shedding region of the cylinder at $t \approx 5T/2$. A negative vortex formed by the coalescence of two negative vortices at $t = 3T$, continues to develop over $3T \leq t \leq 4T$, and then it starts to approach another co-rotating negative vortex. These co-rotating vortices coalesce at $t = 9T/2$, and are then shed into the near wake of the cylinder at $t = 5T$. A new negative vortex develops at $t = 5T$, and then coalesces with a second negative vortex at $t = 6T$. This newly formed vortex develops over $6T \leq t \leq 13T/2$, and at $t = 7T$, sheds into the near wake of the cylinder. Similarly, a negative vortex develops over $7T \leq t \leq 15T/2$, and coalesces with a second negative vortex at $t = 8T$, and this newly formed vortex sheds downstream of

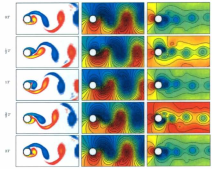

Figure 2.6: The equivorticity patterns (left), streamline patterns (middle) and the pressure contours (right) in the near wake region of the cylinder over two periods of cylinder oscillation, $2T$, at $R = 200$: A=0.13, $f/f_0 = 1.75$ when $h = \infty$ [$T \approx 2.886, 66.38 \leq t \leq 72.15$: $(23T, 25T)$]. The periodic-locked-on **2P** mode, per $2T$, is observed.

the cylinder at $t = 9T$. Meanwhile, in the lower vortex shedding region of the cylinder, a positive vortex develops over $0 \leq t \leq T/2$, and sheds into the lower vortex shedding region of the cylinder at $t = T$. Then, a positive vortex is formed from the coalescence of two positive vortices at $t = 2T$. This vortex continues to develop, and then begins to approach a positive co-rotating vortex at $t \approx 3T$. The positive vortex attached to the positive pair of vortices in the near wake of the cylinder, sheds downstream of the cylinder at $t = 4T$, and the positive pair coalesce at this time. The newly formed positive vortex continues to develop over $9T/2 \leq t \leq 5T$, and at $t = 11T/2$, it

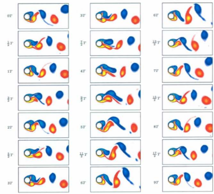

Figure 2.7: The equivorticity patterns over nine periods of cylinder oscillation, $9T$, at $R = 200$: A=0.13, $f/f_0 = 2.25$ when $h = \infty$ [$T \approx 2.245, 80.81 \leq t \leq 107.74$: $(36T, 48T)$]. The quasi-locked-on $\mathbf{C(8S)}^*$ mode, per $9T$, is observed.

coalesces with a primary positive vortex in the near wake of the cylinder. This newly formed positive vortex is subsequently shed into the lower vortex shedding region of the cylinder at $t = 6T$. The primary positive vortex in the near wake of the cylinder continues to develop over $6T \leq t \leq 13T/2$, and at $t = 7T$, coalesces with a second positive vortex in the near wake. This newly formed positive vortex sheds into the downstream of the cylinder at $t \approx 8T$.

The last column of Figure 2.8 displays the pressure contours for the frequency ratio $f/f_0 = 2.25$ over nine periods of cylinder oscillation, $9T$. At $t = 0T$ the high pressure region develops in the stagnation region, and the low pressure region develops behind the cylinder. Similarly to the case $f/f_0 = 1.25$ ($h = \infty$), a large number of vortices are shed into the upper and lower sides of the cylinder. As a result of the multiple shedding of single vortices from the upper and lower regions of the cylinder, the concentrations of high and low pressure regions in the vicinity of the near wake of the cylinder fluctuate dramatically over $9T$. At $t = nT/2$ ($n = 1, 3, 5, 7, 9, 11, 13, 15, 17$) the high pressure region shifts to the above and below the low pressure region in the downstream of the cylinder. On the other hand for example, at $t = T$, synonomous with the development, and the shedding, of a positive vortex in the lower vortex shedding region of the cylinder, it can be seen that the low pressure region shifts substantially downstream of the cylinder, and the high pressure region shifts mostly to the stagnation region. As the positive shed vortex propogates downstream, and the development of a negative vortex in the upper vortex shedding region of the cylinder occurs, it is evident at $t = 3T/2$ that the concentration of the low pressure is in the near wake of the cylinder, and that the high pressure region shifts to the above and below the low pressure region in the downstream of the cylinder. That is, the concentration of the high pressure region dramatically inreases.

For frequency ratio $f/f_0 = 2.75$, the equivorticity patterns in the near wake of the cylinder over three periods of cylinder oscillation, $3T$, are diplayed in Figure 2.9. The shedding of a single negative vortex, and a pair of positive co-rotating vortices

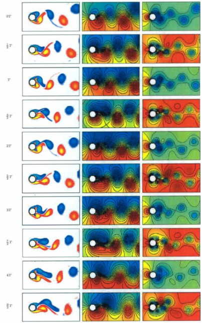

Figure 2.8: The figure caption is given on page 41

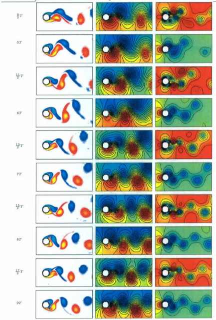

Figure 2.8: The equivorticity patterns (left), streamline patterns (middle) and the pressure contours (right) in the near wake region of the cylinder over nine periods of cylinder oscillation, $9T$, at $R = 200$: A=0.13, $f/f_0 = 2.25$ when $h = \infty$ $[T \approx 2.244, 80.80 \leq t \leq 107.74 : (36T, 48T)]$. The quasi-locked-on $\mathbf{C(8S)}^*$ mode, per $9T$, is observed.

Figure 2.9: The equivorticity patterns over three periods of cylinder oscillation, $3T$, at $R = 200$: A=0.13, $f/f_0 = 2.75$ when $h = \infty$ $[T \approx 1.837, 91.83 \leq t \leq 97.34 : (50T, 53T)]$. The quasi-locked-on $\mathbf{C}(\mathbf{P}+\mathbf{S})^*$ mode, per $3T$, is observed.

occurs within three periods of cylinder oscillation, $3T$. This results in the quasi-lock on $\mathbf{C}(\mathbf{P}+\mathbf{S})^*$ mode, per $3T$, within the interval $50T \leq t \leq 81T$. This is consistent with the behaviour of C_L, but not C_D, at this frequency ratio. The flow is non-periodic for $t < 50T$. At $t = 0$, a pair of positive co-rotating vortices has developed, in the lower vortex shedding region, in the previous shedding cycle. The pair of positive co-rotating vortices detaches at $t \approx T/6$, temporarily, only to re-attach at $t \approx 4T/6$.

Finally, at $t = T$, the pair of positive co-rotating vortices is shed permanently into the near wake of the cylinder. On the other hand, at $t = 7T/6$, the vortex formed from the coalescence of two negative vortices, at $t = 2T/6$, sheds into the upper vortex shedding region of the cylinder. Coalescence of new negative vortices and pairing of positive co-rotating vortices continues to occur, but shedding ceases for the remainder of the period under consideration, $7T/6 \leq t \leq 3T$.

In Figure 2.10, the pressure contours in the near wake region of the cylinder are displayed for the frequency ratio, $f/f_0 = 2.75$ over three periods of cylinder oscillation, $3T$. At $t = 0T$, the high pressure region has developed in the stagnation region of the cylinder, and the low pressure region develops behind the cylinder. At $t = T/2$, the high pressure region extends from the stagnation region of the cylinder to above and below the low pressure region in the downstream of the cylinder. In the near wake, the low pressure region is located in the upper and lower side of the cylinder. Synonmous with the development of a positive vortex and the shedding of a positive vortex pair, at $t = T$, it is evident that the high pressure region shifts back to the stagnation region. The low pressure region shifts substantially behind the cylinder. Once the negative vortex has shed at $t = 7T/6$, (see Figure 9) it can be seen from the pressure distribution displayed at $t = 3T/2$ that the area of high pressure has once again shifted downstream, and that the regions of low pressure have been forced to the immediate upper and lower sides of the cylinder. In connection with the development of a new positive vortex in the near wake of the cylinder, it can be seen that over $2T \leq t \leq 5T/2$, the area of high pressure, now in the stagnation region, moves towards the downstream of the cylinder, and that the area of low pressure shifts to the upper and lower sides of the cylinder from its downstream position. This figure suggest that at $t = nT/2$ ($n = 1, 3, 5$) the high pressure region extends from the stagnation region of the cylinder to above and below the low pressure region in the downstream of the cylinder. It also suggests that at $t = nT/2$, ($n = 1, 3, 5$) that the low pressure regions develop in the upper and lower sides of the cylinder following the simultaneous development of negative and positive vortices in the near wake region at the same time instances.

f/f_0	Vortex shedding mode and flow states	T_v	C_L behaviour ($h = \infty$)	T_v	C_D behaviour ($h = \infty$)	T_v
1.25	**C(10S)*** ($60.61 \le t \le 150$)	$7T$	quasi-periodic ($60.61 \le t \le 150$)	$7T$	quasi-periodic ($60.61 \le t \le 150$)	$7T$
1.75	**2P** ($54.83 \le t \le 150$)	$2T$	periodic ($54.83 \le t \le 150$)	$2T$	quasi-periodic ($54.83 \le t \le 150$)	T
2.25	**C(8S)*** ($80.81 \le t \le 150$)	$9T$	quasi-periodic ($80.81 \le t \le 150$)	$9T$	quasi-periodic ($80.81 \le t \le 150$)	$9T$
2.75	**C(P + S)*** ($91.83 \le t \le 150$)	$3T$	quasi-periodic ($91.83 \le t \le 150$)	$3T$	periodic ($91.83 \le t \le 150$)	$2T$

Table 2.1: Relationship between the behaviour of the lift and drag coefficients and the vortex shedding modes in the absence of a free surface ($h = \infty$) for $f/f_0 = 1.25$ ($60.61 \le t \le 150$), $f/f_0 = 1.75$ ($54.83 \le t \le 150$), $f/f_0 = 2.25$ ($80.81 \le t \le 150$) and $f/f_0 = 2.75$ ($91.83 \le t \le 150$). The superscript "*" denotes quasi-locked-on modes.

In Table 2.1, the relationship between the behaviour of the lift and drag coefficients and the flow states with the indicated vortex-shedding modes for $f/f_0 = 1.25, 1.75, 2.25, 2.75$ are displayed. For the frequency ratios, $f/f_0 = 1.25, 1.75, 2.25, 2.75$ the lock-on modes occur every $7T$, $2T$, $9T$ and $3T$ periods of cylin-

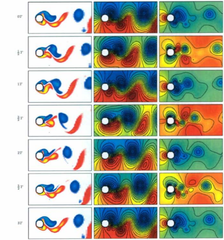

Figure 2.10: The equivorticity patterns (left), streamline patterns (middle) and the pressure contours (right) in the near wake region of the cylinder over three periods of cylinder oscillation, $3T$, at $R = 200$: A=0.13, $f/f_0 = 2.75$ when $h = \infty$ [$T \approx 1.837, 91.83 \leq t \leq 97.34$: $(50T, 53T)$]. The quasi-locked-on $\mathbf{C(P+S)}^*$ mode, per $3T$, is observed.

der oscillation, respectively. Similarly, the traces of C_L for $f/f_0 = 1.25, 1.75, 2.25, 2.75$ displayed repeatable signatures every $7T, 2T, 9T, 3T$, respectively. Thus, the locked-on vortex shedding modes are influenced from the C_L behaviour at each frequency ratio. On the other hand, the traces of C_D for $f/f_0 = 1.25, 1.75, 2.25, 2.75$ displayed almost-repeatable signatures every $7T, T, 9T$ and $2T$, respectively, and thus the locked-on vortex shedding modes and their periods are consistent with the C_D behaviour at only $f/f_0 = 1.25$ and 2.25.

2.2 Summary and Discussion

The pressure contour plots of Figures 2.4-2.10, for $h = \infty$ when $f/f_0 = 1.25, 1.75, 2.25, 2.75$ indicate that at $t = 0T$ (when the cylinder reaches maximum displacement, $x(t) = A$) the high pressure region develops predominantly in the stagnation region of the cylinder for each f/f_0. Conversely, the low pressure regions develop mostly behind, but also in the upper side of the cylinder for $f/f_0 = 1.25, 2.25$ (see Figures 2.4,2.8). Low pressure develops mostly behind, but also in the lower side of the cylinder for $f/f_0 = 1.75, 2.75$ (see Figures 2.6,2.10). In general, the low pressure regions develop in the near wake of the cylinder, where the velocity is highest (formation of new vortices) and hence significantly affect the fluctuating lift forces acting on the circular cylinder. In addition, it can be seen that positive and negative vortices which have shed in the downstream of the cylinder, are represented by the low pressure region (blue contours) for all f/f_0. It is interesting to note that for $f/f_0 = 1.25, 1.75, 2.25, 2.75$ at $h = \infty$, the regions of high pressure surround the regions of low pressure in the downstream of the cylinder at every $t = nT/2$, when n is an odd integer (refer to Figures 2.4, 2.6, 2.8 and 2.10).

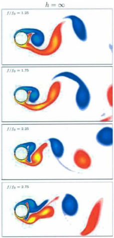

Figure 2.11: The effect of the absence of a free surface, $h = \infty$, and the frequency ratio, f/f_0(=1.25, 1.75, 2.25, 2.75), on the equivorticity patterns at $R = 200$: $A = 0.13$.

The effect of the absence of a free surface $h = \infty$, and the frequency ratio, $f/f_0(= 1.25, 1.75, 2.25, 2.75)$, on the equivorticity patterns in the near wake region is summarized in Figure 2.11. The snapshots are taken at the instant the cylinder reaches maximum displacement, $x(t) = A$. For the periodic/quasi-periodic cases, the snapshots are taken over the time interval in which the flow reaches a periodic/quasi-periodic state. It can be seen at the smaller frequency ratios, $f/f_0 = 1.25, 1.75$, that there is presence of positive vorticity in the upper vortex shedding layer of the cylinder (near wake region). This is the case for $f/f_0 = 2.75$, but in addition there is also negative vorticity in the lower vortex shedding region of the cylinder. The near wake structure of the equivorticty patterns seem to be more skew symmetric (centerline of near wake is directed slightly downward) at $f/f_0 = 1.25, 1.75$. A remarkable difference in the near wake structures is evident in the equivorticity patterns as f/f_0 increases from 1.25 to 2.75. As f/f_0 increases from 1.25 to 2.25 the vortex formation length seems to decrease (by maxiumum of ≈ 46 %).

3. Free surface flow past a streamwise oscillating cylinder $Fr \approx 0.0$

In this Chapter, a viscous incompressible two-fluid model with a streamwise oscillating cylinder beneath a free-slip surface ($Fr \approx 0.0$) is numerically investigated for the cylinder submergence depths $= 0.75, 0.5, 0.25$. In the limiting Froude number case, $Fr \to 0$, the surface becomes a non-deformable free surface (?, ?) and due to pronounced pressure spikes observed in the numerical experiments, the fluid forces cannot be calculated. Thus, only vortex shedding modes are analyzed to determine lock-on modes and their vortex shedding periods, T_v, for non-harmonic oscillations ($f/f_0 = 1.25, 1.75, 2.25, 2.75$) at a Reynolds number of $R = 200$, and a fixed displacement amplitude of $A = 0.13$. The numerical experiments for the Froude number case of $Fr \approx 0.0$, are conducted by setting Fr to 0.03 (or g to 1111) in the computer program, since $Fr = U/\sqrt{dg}$. The resulting flat free-slip surface results are used as the reference case for analyzing the results in Chapters 4 and 5 which examine the Froude number cases of $Fr = 0.2$ and $Fr = 0.4$, respectively.

3.1 Vortex shedding modes at $Fr \approx 0.0$: $h = 0.75$

Figures 3.1-3.5 display the equivorticity patterns for $f/f_0 = 1.25, 1.75, 2.25, 2.75$. The observed flow behaviour is (i) quasi-periodic for $f/f_0 = 1.25, 1.75, 2.25, 2.75$ per $4T, 2T, 2T, 11T$, respectively.

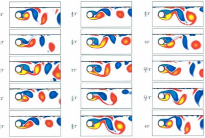

Figure 3.1: The equivorticity patterns over four periods of cylinder oscillation, $4T$, at $R = 200$: $A = 0.13, f/f_0 = 1.25$ when $h = 0.75, Fr \approx 0.0$ [$T \approx 4.04, 56.566 \leq t \leq 72.727$: $(14T, 18T)$]. The quasi-locked-on **6S*** mode, per $4T$, is observed.

For frequency ratio $f/f_0 = 1.25$, the flow exhibits quasi-periodic behaviour every four periods of cylinder oscillation, $4T$, within $10T \leq t \leq 24T$. The flow is non-periodic for $t < 10T$. Figure 3.1 displays the equivorticity patterns for $f/f_0 = 1.25$ over four periods of cylinder oscillation, $4T$, within $14T \leq t \leq 18T$. The vortex shedding mode is the quasi-locked-on **6S*** mode, per $4T$. In this mode, three single vortices are alternately shed from the upper and lower vortex shedding region of the cylinder within $4T$. A negative vortex formed during the previous vortex shedding cycle sheds into the near wake of the cylinder at $t = T/3$. Over $2T/3 \leq t \leq 4T/3$, the development of a second negative vortex is observed in the near wake region. This vortex formed in the upper vortex shedding layer sheds into the downstream of the cylinder, at $t = 5T/3$. Similarly, over $T \leq t \leq 8T/3$, a negative vortex develops in the upper shear layer of the cylinder. Then, this vortex becomes detached shortly after $t = 8T/3$, and finally propogates into the downstream of the cylinder, aided by the development of positive vortices in the lower shedding layer. Meanwhile, a positive vortex formed during the previous vortex shedding cycle detaches over $2T/3 \leq t \leq T$, and then sheds into the downstream of the cylinder. In the lower vortex shedding region of the cylinder, a negative vortex in the near wake of the cylinder develops over $4T/3 \leq t \leq 8T/3$, and then sheds into the downstream of the cylinder at $t \approx 8T/3$. Finally, a positive vortex developing over $3T/2 \leq t \leq 10T/3$ is subject to interaction with the negative vortices in the upper vortex shedding region, and then consequently sheds into the downstream of the cylinder at $t \approx 11T/3$. It is evident that the negative vortex in the upper side of the cylinder, forces the this positive vortex to shed downstream at $t = 11T/3$. Thus, in the quasi-locked-on **6S*** mode, six vortices develop and shed on each side of the cylinder over $4T$. No coalescence was observed in this case.

The behaviour of the flow for $f/f_0 = 1.75$, is quasi-periodic every two periods of cylinder oscillation, $2T$, within $4T \leq t \leq 35T$. The flow is non-periodic for $t < 4T$. In Figure 3.2, the equivorticity patterns over two periods of cylinder oscillation, $2T$, within $10T \leq t \leq 12T$ are displayed for $f/f_0 = 1.75$. The vortex shedding mode is the quasi-locked-on $\mathbf{C(P+S)}^*$ mode, per $2T$, within $4T \leq t \leq 35T$. In this mode, the shedding of single negative vortex and a positive pair of co-rotating vortices occurs within two periods of cylinder oscillation, $2T$. At $t = 0$, a negative vortex formed during the previous vortex shedding cycle continues to develop over $0 \leq t \leq 9T/6$, and then sheds into the upper vortex shedding layer at $t = 10T/6$. Meanwhile, a pair of positive co-rotating vortices has developed in the lower vortex shedding region, in the the previous vortex shedding cycle. This co-rotating positive vortex pair continues to develop over $0 \leq t \leq 4T/6$, and then sheds into the lower vortex shedding region of the cylinder at $t = 5T/6$. Hence, in the quasi-locked-on $\mathbf{C(P+S)}^*$ mode, per $2T$, a single vortex and a pair of co-rotating vortices shed alternately over $2T$. Coalescence is observed for this frequency ratio.

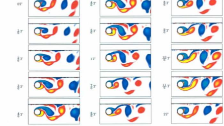

Figure 3.2: The equivorticity patterns over two periods of cylinder oscillation, $2T$, at $R = 200$: A=0.13, $f/f_0 = 1.75$ when $h = 0.75$, $Fr \approx 0.0$ [$T \approx 2.886, 28.860 \leq t \leq 26.936$: $(10T, 12T)$]. The quasi-locked-on $\mathbf{C(P+S)}^*$ mode, per $2T$, is observed.

For frequency ratio $f/f_0 = 2.25$, the flow displays quasi-periodic behaviour every $2T$ within $4T \leq t \leq 27T$, followed by non-periodic behaviour within $27T < t < 32T$, and then quasi-periodic behaviour every $2T$ within $32T \leq t \leq 42T$. Figures 3.3 and 3.4 displays the equivorticity patterns for $f/f_0 = 2.25$ over two periods of cylinder oscillation, $2T$, within $8T \leq t \leq 10T$ and $34T \leq t \leq 36T$, respectively (quasi-periodic states). The observed vortex shedding modes is the quasi-locked on $\mathbf{C(2S)}^*$ mode, per $2T$, within $4T \leq t \leq 27T$ and $32T \leq t \leq 42T$. In this mode, the alternate shedding of a single vortex of opposite rotation from the upper and lower shear layers occurs within two periods of cylinder oscillation, $2T$. In Figure 3.3, a negative vortex formed during the previous vortex shedding cycle continues to develop over $0 \leq t \leq 3T/6$, and coalesces with a second negative vortex at $t = 4T/6$. The resulting negative vortex develops over $4T/6 \leq t \leq 10T/6$, and then subsequently sheds into the upper vortex shedding region of the cylinder at $t = 11T/6$. Meanwhile, a positive vortex formed during the previous vortex shedding cycle continues to develop over $0 \leq t \leq 4T/6$, and then sheds into the near wake region at $t = 5T/6$. It can be seen that the positive and negative vortices which have shed, remain in the mid-wake of the cylinder over $2T$. In Figure 3.4, a negative vortex formed during the previous shedding cycle continues to develop over $0 \leq t \leq 4T/6$, and then subsequently sheds into the upper vortex shedding layer at $t \approx 5T/6$. A positive vortex formed during the previous vortex shedding cycle continues to develop over $0 \leq t \leq 2T/6$ and then coalesces with a positive vortex in the near wake region at $t = 3T/6$. The resulting positive vortex, develops over $4T/6 \leq t \leq 10T/6$, and then sheds into the near wake of the cylinder at $t = 11T/6$. Hence, in the quasi-locked-on $\mathbf{C(2S)}^*$ mode, per $2T$, two vortices are alternately shed within $2T$.

The flow of frequency ratio $f/f_0 = 2.75$, exhibits quasi-periodic behaviour every eleven periods of cylinder oscillation, $11T$, within $9T \leq t \leq 35T$. The flow is non-periodic for $t < 9T$. Figure 3.5, displays the equivorticity patterns for $f/f_0 = 2.75$, over eleven periods of cylinder oscillation, $11T$, within $22T \leq t \leq 33T$. The vortex shedding mode is the quasi-locked-on $\mathbf{C(8S)}^*$ mode, per $11T$, within $9T \leq t \leq 35T$. In this mode, four vortices develop on each side of the cylinder and alternately shed

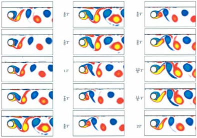

Figure 3.3: The equivorticity patterns over two periods of cylinder oscillation, $2T$, at $R = 200$: A=0.13, $f/f_0 = 2.25$ when $h = 0.75, Fr \approx 0.0$ [$T \approx 2.247, 23.088 \leq t \leq 28.860$: $(8T, 10T)$]. The quasi-locked-on $\mathbf{C(2S)}^*$ mode, per $2T$, is observed.

over $11T$. Initially, a negative vortex which has developed in the previously vortex shedding cycle continues to develop over $T/2 \leq t \leq 2T$, and sheds into the upper vortex shedding region of the cylinder as a secondary vortex at $t \approx 5T/2$. A negative vortex developed over $3T \leq t \leq 7T/2$, coalesces with the primary negative vortex in the near wake of the cylinder at $t \approx 4T$. The resulting negative vortex subsequently sheds into the near wake of the cylinder $t = 5T$. A negative vortex developed over $11T/2 \leq t \leq 7T$, coalesces with a second vortex in the near wake region at $t = 15T/2$. This vortex subsequently sheds into the upper vortex shedding region of the cylinder at $t = 17T/2$. The coalescence of two negative vortices at $t = 9T$ is observed in the upper shear layer. The resulting negative vortex then sheds into the near wake region at $t \approx 11T$. Meanwhile, at $t = 0$, two co-rotating positive vortices are observed in

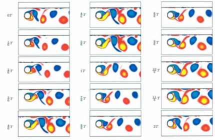

Figure 3.4: The equivorticity patterns over two periods of cylinder oscillation, $2T$, at $R = 200$: A=0.13, $f/f_0 = 2.25$ when $h = 0.75, Fr \approx 0.0$ [$T \approx 2.2447, 76.319 \leq t \leq 80.808$: $(34T, 36T)$]. The quasi-locked-on $\mathbf{C(2S)}^*$ mode, per $2T$, is observed.

the near wake of the cylinder. These vortices subsequently coalesce at $t = T/2$, and then the resulting positive vortex sheds into the lower vortex shedding region of the cylinder at $t = 3T/2$. The positive vortex formed from the coalescence of two positive vortices at $t = 2T$, develops over $2T \leq t \leq 5T/2$ and then approaches another co-rotating positive vortex at $t = 3T$. These three positive co-rotating vortices develop over $3T \leq t \leq 7T/2$, and then they coalesce to form a positive vortex at $t = 4T$. This positive vortex sheds into the downstream of the cylinder at $t = 9T/2$. Similarly, a newly formed positive vortex develops over $5T \leq t \leq 13T/2$, and then fully sheds into the near wake of the cylinder at $t = 7T$. At $t = 8T$, a positive vortex formed by the coalescence of two positive vortices formed continues to develop over $8T \leq t \leq 17T/2$, and then subsequently sheds into the lower vortex shedding region of the cylinder at

$t = 9T$. Thus, in the quasi-locked-on $\mathbf{C(8S)}^*$ mode, per $11T$, four vortices alternately develop from each side of the cylinder. Each vortex that has shed, in this case, was created from coalescence.

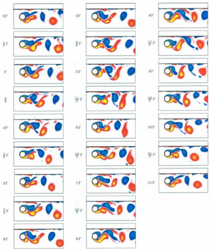

Figure 3.5: The equivorticity patterns over eleven periods of cylinder oscillation, $11T$, at R = 200: A=0.13, $f/f_0 = 2.75$ when $h = 0.75, Fr \approx 0.0$ $[T \approx 1.837, 40.40 \leq t \leq 60.60$: $(22T, 33T)]$. The quasi-locked-on $\mathbf{C(8S)}^*$ mode, per $11T$, is observed.

3.2 Vortex shedding modes at $Fr \approx 0.0$: $h = 0.5$

Figures 3.6-3.9 display the equivorticity patterns in the near wake region of the cylinder for $f/f_0 = 1.25, 1.75, 2.25, 2.75$. The observed flow behaviour is quasi-periodic for $f/f_0 = 1.25, 1.75, 2.25, 2.75$ per $9T, 2T, 2T, 3T$, respectively.

The observed behaviour of the flow for the smallest frequency ratio, $f/f_0 = 1.25$, is quasi-periodic every nine periods of cylinder oscillations, $9T$, within $4T \leq t \leq 24T$. The flow is non-periodic for $t < 4T$. Figure 3.6 displays the equivorticity patterns for $f/f_0 = 1.25$ over nine periods of cylinder oscillations, $9T$, within $13T \leq t \leq 22T$. The observed vortex shedding mode is the quasi-locked-on **14S*** mode, per $9T$, within $4T \leq t \leq 24T$. In this mode, alternate shedding of seven vortices from the upper and lower vortex shedding region of the cylinder, within $9T$ is observed. From this figure, it is evident that the majority of negative vortices shed are secondary vortices which detach from primary negative vortices in the near wake region. The positive vortices which have shed into the lower vortex shedding region, appear to have been aided by the development of negative vortices in the upper vortex shedding layer. Initially, a negative vortex formed during the previous vortex shedding cycle sheds downstream of the cylinder at $t = 3T/2$. Over $3T/2 \leq t \leq 2T$, a second negative vortex develops in the upper shedding layer of the cylinder. This vortex is then subsequently shed into the near wake region of the cylinder at $t = 5T/2$. A negative vortex developed over $3T \leq t \leq 7T/2$, is forced to shed at $t = 4T$ due to the interaction of a developing positive vortex in the lower vortex shedding region of the cylinder. Over $4T \leq t \leq 9T/2$, a negative vortex develops in the upper vortex shedding layer of the cylinder. This negative vortex then sheds downstream of the cylinder at $t = 5T$. The development of a negative vortex occurs over $11T/2 \leq t \leq 6T$, and then this negative vortex subsequently sheds into the upper vortex shedding layer of the cylinder at $t = 13T/2$. Similarly, a negative vortex developed over $13T/2 \leq t \leq 7T$, sheds into the upper vortex shedding region of the cylinder at $t = 15T/2$. Over $8T \leq t \leq 17T/2$, a negative vortex develops in the upper shedding layer of the cylinder. Then, this vortex detaches at $t = 9T$ aided by the development of a positive vortex in the lower side of the cylinder. Meanwhile, a positive vortex developed from the previous vortex shedding cycle sheds into the near wake region at $t = T/2$. The development of a positive vortex in the lower vortex shedding region occurs over $T/2 \leq t \leq 3T/2$, and then this positive vortex sheds into the near wake region as a secondary positive vortex at $t = 2T$. Over $2T \leq t \leq 3T$, a positive vortex develops in the lower shear layer of the cylinder. This positive vortex then sheds downstream of the cylinder at $t = 7T/2$. Subsequently, a positive vortex in the near wake region of the cylinder develops over $7T/2 \leq t \leq 4T$, and is then shed into the lower vortex shedding region at $t = 9T/2$. The newly formed positive vortex formed over $5T \leq t \leq 11T/2$, subsequently sheds into the downstream of the cylinder at $t = 6T$. At the next oscillation period $t = 7T$ a positive vortex, formed over $11T/2 \leq t \leq 13T/2$, sheds into the lower vortex shedding region of the cylinder. Finally, a positive vortex developing over $15T/2 \leq t \leq 17T/2$ is subjected to the interaction with a negative vortex in the upper vortex shedding region, and consequently sheds downstream of the cylinder at $t = 9T$. Hence, in the quasi-locked-on **14S*** mode, per $9T$, seven vortices alternately develop from each side of the cylinder.

In Figure 3.7, the equivorticity patterns over two periods of cylinder oscillation, $2T$, are displayed for $f/f_0 = 1.75$ within $14 \leq t \leq 16T$. The vortex shedding mode for

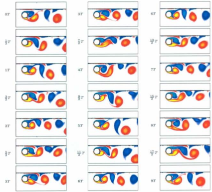

Figure 3.6: The equivorticity patterns over nine periods of cylinder oscillation, $9T$, at $R = 200$: A=0.13, $f/f_0 = 1.25$ when $h = 0.5, Fr \approx 0.0$ [$T \approx 4.04, 52.525 \leq t \leq 89.889$: $(13T, 22T)$]. The quasi-locked-on $\mathbf{14S^*}$ mode, per $9T$, is observed.

this frequency ratio is the quasi-locked-on $\mathbf{C(P+S)^*}$ mode, per $2T$, within $4T \leq t \leq 34T$. The flow exhibits non-periodic behaviour for $t < 4T$. This mode describes the alternate shedding of a negative vortex from the upper vortex shedding region and a pair of positive vortices from the lower vortex shedding region of the cylinder. A negative vortex formed during the previous vortex shedding cycle develops over $0 \leq t \leq 3T/6$, and then coalesces with a second negative vortex at $t = 4T/6$. The resulting negative vortex develops over $5T/6 \leq t \leq T$ and subsequently sheds into the lower vortex shedding layer at $t = 7T/6$. Meanwhile, a pair of positive co-rotating vortices formed during the previous vortex shedding cycle continue to develop over $0 \leq t \leq 4T/6$. This positive vortex pair is then subjected to the interaction of a large negative vortex in the upper vortex shedding layer and as a result, sheds into the lower vortex shedding region of the cylinder at $t = 5T/6$. Hence, in the quasi-locked-on $\mathbf{C(P+S)}^*$ mode, a negative vortex and co-rotating positive vortex pair are alternately shed within $2T$.

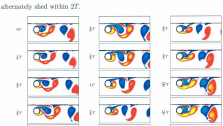

Figure 3.7: The equivorticity patterns over two periods of cylinder oscillation, $2T$, at $R = 200$: $A = 0.13, f/f_0 = 1.75$ when $h = 0.5, Fr \approx 0.0$ [$T \approx 2.886, 40.404 \leq t \leq 46.176$: $(14T, 16T)$]. The quasi-locked-on $\mathbf{C(P+S)}^*$ mode, per $2T$, is observed.

At frequency ratio $f/f_0 = 2.25$, the flow exhibits quasi-periodic behaviour every two periods of cylinder oscillation, $2T$, within $3T \leq t \leq 9T, 15T \leq t \leq 19T, 25T \leq t \leq 31T$ and $37T \leq t \leq 41T$, respectively. A transition into non-periodic behaviour, of the flow, occurs within $9T < t < 15T, 19T < t < 25T, 31T < T < 37T$ and

$41T < t < 45T$. Figure 3.8 displays the equivorticity patterns for $f/f_0 = 2.25$ over two periods of cylinder oscillation, $2T$, within $16T \leq t \leq 18T$. The vortex shedding mode is the quasi-locked-on $\mathbf{C(2S)}^*$ mode, per $2T$, in each time interval the flow displays quasi-periodic behaviour. In this mode, a single vortex develops on each side of the cylinder and alternately sheds over $2T$. A negative vortex formed from the coalescence of two negative vortices in the previous vortex shedding cylinder, continues to develop over $0 \leq t \leq T/6$ and is subsequently shed downstream of the cylinder at $t = 2T/6$. A positive vortex, formed from the coalescence of two positive vortices at $t = 3T/6$, develops over $4T/6 \leq t \leq 10T/6$ and sheds downstream of the cylinder at $t = 11T/6$. Hence, in the quasi-locked-on $\mathbf{C(2S)}^*$ mode, a negative and positive vortex are alternately shed within $2T$.

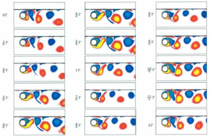

Figure 3.8: The equivorticity patterns over two periods of cylinder oscillation, $2T$, at $R = 200$: $A = 0.13, f/f_0 = 2.25$ when $h = 0.5, Fr \approx 0.0$ [$T \approx 2.247, 35.91 \leq t \leq 40.40$: $(16T, 18T)$]. The quasi-locked-on $\mathbf{C(2S)}^*$ mode, per $2T$, is observed.

At the frequency ratio $f/f_0 = 2.75$, the flow displays quasi-periodic behaviour every three periods of cylinder oscillations, $3T$, within $6T \leq t \leq 54T$. Figure 3.9 displays the equivorticity patterns over three periods of cylinder oscillation, $3T$, for $f/f_0 = 2.75$, within $30T \leq t \leq 33T$. The vortex shedding mode observed is the quasi-locked-on $\mathbf{C(2S)}^*$ mode, per $3T$ within $6T \leq t \leq 54T$. This mode describes the shedding of a single vortex of opposite rotation from the upper and lower vortex shedding regions of the cylinder, within $3T$. In this figure, a co-rotating negative vortex pair formed during the previous vortex shedding cycle continues to develop $0 \leq t \leq 2T/6$, and a third negative vortex begins to co-rotate with the pair at $t = 3T/6$. The three negative vortices co-rotate over $3T/6 \leq t \leq T$, and the tertiary negative vortex (farthest from the near wake of the cylinder) sheds into the upper vortex shedding layer of the cylinder at $t = 7T/6$. It is evident that over this time period, the secondary negative vortex stretches almost parallel to the free-surface. The development and subsequent coalescence of negative vortices occur for the remainder of the vortex shedding cycle, but shedding of negative vortices cease to occur. Meanwhile, a positive vortex developed during the previous vortex shedding cycle develops over $0 \leq t \leq 2T/6$, and then approaches a second positive vortex at $t = 3T/6$. These two positive vortices coalesce at $t = 5T/6$, only to seperate into two positive vortices which co-rotate over $T \leq t \leq 9T/6$. At $t = 10T/6$, the co-rotating positive vortices coalesce a final time and the resulting positive vortex develops over $10T/6 \leq t \leq 11T/6$, and then subsequently sheds into the downstream of the cylinder at $t = 2T$. Hence, the alternate formation and shedding of two vortices within $3T$, results in the quasi-locked-on $\mathbf{C(2S)}^*$ mode, per $3T$.

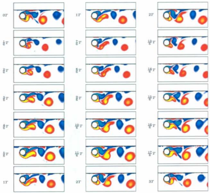

Figure 3.9: The equivorticity patterns over three periods of cylinder oscillation, $3T$, at $R = 200$: A=0.13, $f/f_0 = 2.75$ when $h = 0.5, Fr \approx 0.0$ [$T \approx 1.837, 55.096 \leq t \leq 60.606$: $(30T, 33T)$]. The quasi-locked-on $\mathbf{C(2S)}^*$ mode, per $3T$, is observed.

3.3 Vortex shedding modes at $Fr \approx 0.0 : h = 0.25$

Figures 3.10-3.14 display the equivorticity patterns in the near wake of the cylinder when $f/f_0 = 1.25, 1.75, 2.25, 2.75$. The observed flow behaviour is (i) periodic for $f/f_0 = 1.25, 1.75, 2.75$ per $3T, 2T, 10T$ respectively, and (ii) quasi-periodic for $f/f_0 = 2.25$, per $5T$, respectively.

For $f/f_0 = 1.25$, the flow displays a periodic pattern over three periods of cylinder oscillations, $3T$, within $2T \leq t \leq 20T$. The flow is non-periodic for $t > 20$. In Figure 3.10, the equivorticity patterns are displayed for $f/f_0 = 1.25$ over three periods of cylinder oscillation, $3T$, within $10 \leq t \leq 13T$. The vortex shedding mode is the locked-on **C(4S)** mode, per $3T$, within $2T \leq t \leq 20T$. Figure 3.10, reveals that a negative vortex developed from the previous vortex shedding cycle sheds promptly into the upper vortex shedding layer at $t = T/6$. The development of a negative vortex occurs over $0 \leq t \leq 2T/6$, and at $t = 3T/6$ this negative vortex coalesces with the primary negative vortex in the near wake region of the cylinder. The resulting negative vortex develops over $4T/6 \leq t \leq 11T/6$, and then sheds completely into the upper vortex shedding layer of the cylinder at $t = 2T$. It should be noted that the negative vortices which shed, retain an attachment to the free surface. Meanwhile, a positive vortex formed during the previous vortex shedding cycle develops over $0 \leq t \leq 4T/6$, and then sheds downstream of the cylinder at $t = 5T/6$. Over $T \leq t \leq 8T/6$, a positive vortex develops and then begins to approach a second positive vortex at $t = 9T/6$. The positive vortices co-rotate over $10T/6 \leq t \leq 13T/6$, and then coalesce to form a single positive vortex at $t = 14T/6$. This positive vortex develops over $15T/6 \leq t \leq 17T/6$, and then due to the intense interaction with a negative vortex in the upper vortex shedding layer, the positive vortex is then forced to shed into the downstream of the cylinder at $t = 3T$. Hence, in the locked-on **C(4S)** mode, per $3T$, two vortices alternately develop and shed from each side of the cylinder.

At $f/f_0 = 1.75$, the flow displays periodic behaviour every two periods of cylinder oscillation, $2T$, within $3T \leq t \leq 34T$. The flow is non-periodic for $t < 3T$. Figure 3.11 displays the equivorticity patterns over two periods of cylinder oscillation, $2T$, within

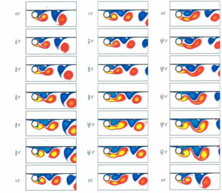

Figure 3.10: The equivorticity patterns over three periods of cylinder oscillation, $3T$, at $R = 200$: A=0.13, $f/f_0 = 1.25$ when $h = 0.25, Fr \approx 0.0$ [$T \approx 4.040, 40.40 \leq t \leq 52.52$: $(10T, 13T)$]. The quasi-locked-on $\mathbf{C(4S)}$ mode, per $3T$, is observed.

$19T \leq t \leq 21T$. The vortex shedding mode observed is the locked-on $\mathbf{C(2S)}$ mode, per $2T$, within $3T \leq t \leq 34T$. In this mode, one vortex develops and alternately shed on each side of the cylinder over $2T$. Initially, a negative vortex formed during the previous vortex shedding cycle sheds into the upper shedding layer of the cylinder at $t = T/6$. The formation of other negative vortices occur in the remainder of the vortex shedding cycle, but these vortices remain attached to the cylinder. In the lower vortex shedding region of the cylinder, a positive vortex develops over $0 \leq t \leq 2T/6$, and then begins to approach the primary positive vortex in the near wake region of the cylinder at $t = 3T/6$. The positive vortices coalesce at $t = 4T/6$, and the resulting positive vortex which develops over $5T/6 \le t \le 9T/6$, sheds downstream of the cylinder at $t \approx 9T/6$.

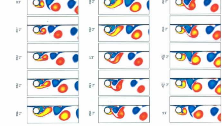

Figure 3.11: The equivorticity patterns over four periods of cylinder oscillation, $2T$, at $R = 200$: A=0.13, $f/f_0 = 1.75$ when $h = 0.25, Fr \approx 0.0$ [$T \approx 2.886, 54.834 \le t \le 60.606$: $(19T, 21T)$]. The quasi-locked-on $\mathbf{C(2S)}$ mode, per $2T$, is observed.

At the frequency ratio $f/f_0 = 2.25$, the flow exhibits quasi-periodic behaviour within $4T \le t \le 23T$ and $26T \le t \le 36T$ and non-periodic behaviour within $23T < t < 26T$, and $t > 36T$. Figures 3.12 and 3.13 display the equivorticity patterns over five periods of cylinder oscillation, $5T$, within $5T \le t \le 10T$ and $26T \le t \le 31T$, respectively for $f/f_0 = 2.25$. The quasi-locked-on $\mathbf{C(4S)}^*$ mode is observed over five periods of cylinder oscillation, $5T$, within $4T \le t \le 23T$ and $26T \le t \le 36T$, respectively. In Figure 3.12, it can be seen that a negative vortex formed during the previous vortex shedding cycle, sheds into the upper vortex sheding layer of the cylinder at $t = T/3$. The shed negative vortex retains an attachment to the free-surface and hence does not shed downstream. This negative vortex begins to approach a negative vortex in the near wake region at $t = 2T/3$. These negative vortices co-rotate over $2T/3 \leq t \leq T$, and at $t = 4T/3$ the co-rotating negative vortices coalesce. The resulting negative vortex sheds into the upper vortex shedding layer at $t \approx 2T$. A negative vortex formed from the coalescence of two negative vortices at $t = 8T/3$ develops over $3T \leq t \leq 11T/3$. This negative vortex is then shed into the upper vortex shedding region of the cylinder at $t = 4T$. Meanwhile, a positive vortex formed during the previous vortex shedding cycle approaches a second co-rotating positive vortex at $t = T/3$. These co-rotating positive vortices coalesces at $t = 2T/3$. The resulting positive vortex develops over $T \leq t \leq 5T/3$, and then begins to co-rotate with a second positive vortex in the near wake region over $2T \leq t \leq 7T/3$. At $t = 8T/3$, the co-rotating positive vortices coalesce and the newly formed positive vortex subsequently sheds into the lower shedding layer of the cylinder at $t = 3T$. A positive vortex develops over $3T \leq t \leq 10T/3$, and then coalesces with a second positive vortex in the near wake region at $t = 11T/3$. The resulting positive vortex develops over $11T/3 \leq t \leq 14T/3$, and then sheds into the lower shedding layer of the cylinder at $t = 5T$.

At frequency ratio $f/f_0 = 2.75$, quasi-periodic flow behaviour over ten periods of cylinder oscillation, $10T$, within $9T \leq t \leq 50T$ is observed. The flow is non-periodic for $t < 9T$. In Figure 3.14, the equivorticity patterns of the flow are displayed over ten periods of cylinder oscillation, $10T$, within $19T \leq t \leq 29T$, for $f/f_0 = 2.75$. The vortex shedding mode is the locked-on **C(6S)** mode, per $10T$. In this mode, three

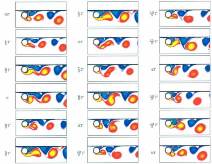

Figure 3.12: The equivorticity patterns over four periods of cylinder oscillation, $5T$, at $R = 200$: A=0.13, $f/f_0 = 2.25$ when $h = 0.25, Fr \approx 0.0$ $[T \approx 2.245, 11.225 \leq t \leq 22.45 : (5T, 10T)]$. The quasi-locked-on $\mathbf{C(4S)}^*$ mode, per $5T$, is observed.

single vortices are alternately shed from the upper and lower vortex shedding region of the cylinder, within $10T$. Initially, a negative vortex formed during the previous vortex shedding cycle sheds downstream of the cylinder at $t \approx T$. The development of a negative vortex occurs over $0 \leq t \leq T/2$, and then this negative vortex approaches the primary negative vortex in the near wake region of the cylinder at $t = T$. Both negative vortices coalesce at $t = 3T/2$, and the resulting negative vortex sheds into the near wake of the cylinder at $t \approx 2T$. The shed negative vortex re-attaches to the secondary negative vortex in the near wake region at $t = 5T/2$, but then sheds completely into the upper vortex shedding layer at $t \approx 9T/2$. A primary negative

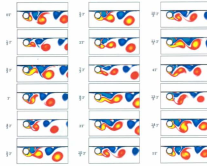

Figure 3.13: The equivorticity patterns over four periods of cylinder oscillation, $5T$, at $R = 200$: A=0.13, $f/f_0 = 2.25$ when $h = 0.25, Fr \approx 0.0$ $[T \approx 2.245, 58.37 \leq t \leq 69.595 : (26T, 31T)]$. The quasi-locked-on $\mathbf{C(4S)}^*$ mode, per $5T$, is observed.

vortex develops over $3T/2 \leq t \leq 5T/2$, and then coalesces with a second negative vortex at $t = 3T$. The resulting negative vortex coalesces with another negative vortex in the near wake region of the cylinder at $t \approx 4T$, and the newly formed negative vortex is then shed into the downstream of the cylinder at $t = 7T$. In the lower vortex shedding region, a positive vortex develops over $0T \leq t \leq T/2$, and then coalesces with a second positive vortex at $t = T$. The resulting positive vortex begins to approach a second positive vortex at $t = 3T/2$, and then these positive vortices coalesce at $t = 5T/2$. The resulting negative vortex detaches from the primary positive vortex in the near wake of the cylinder at $t = 3T$, and then immediately re-attaches

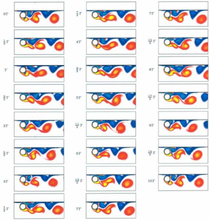

Figure 3.14: The equivorticity patterns over ten periods of cylinder oscillation, $10T$, at $R = 200$: A=0.13, $f/f_0 = 2.75$ when $h = 0.25, Fr \approx 0.0$ $[T \approx 1.837, 34.894 \leq t \leq 53.260 : (19T, 29T)]$. The quasi-locked-on $\mathbf{C(6S)}^*$ mode, per $10T$, is observed.

to the secondary positive vortex in the near wake region of the cylinder at $t = 7T/2$. These positive vortices coalesce at $t = 4T$. The resulting positive vortex develops over $9T/2 \leq t \leq 5T$ and then sheds downstream of the cylinder at $t = 11T/2$. A positive vortex formed from the coalescence of two positive vortices at $t = 7T$, develops over $7T \leq t \leq 17T/2$ and then sheds as a tertiary vortex into the lower vortex shedding region of the cylinder at $t = 9T$. Hence, in the locked-on $\mathbf{C(6S)}$ mode, per $10T$, three vortices develop and shed on each side of the cylinder over $10T$.

3.4 Summary and Discussion

Tables 3.15 summarizes the effect of the free surface presence for the case $Fr \approx 0.0$, $h = 0.75, 0.5, 0.25$ when $f/f_0 = 1.25, 1.75, 2.25, 2.75$ has on vortex shedding modes and their periods, T_v. The majority of the occurring vortex shedding modes are a combination of the classical modes as defined by Williamson and Roshko (1988). Unlike the case $Fr = 0.2$, the presence of the free surface does not lead to the loss of lock-on for $h = 0.25, 0.5, 0.75$. In fact, lock-on modes occur at each f/f_0, for each cylinder submergence depth, h. Table 3.15 shows that the period of vortex shedding is $2T$ for $f/f_0 = 1.75$, regardless of cylinder submergence depth, h. This is also the case for $f/f_0 = 1.75$, in the absence of the free surface. However, it can be seen from this table that with the decrease of h from $h = 0.75, 0.5$ to $h = 0.25$, the vortex shedding modes of $f/f_0 = 1.75$ change from the quasi-locked-on $\mathbf{C(P+S)^*}$ at $h = 0.75, 0.5$ to the locked-on $\mathbf{C(2S)}$ mode at $h = 0.25$. The inclusion of free surface at $h = 0.25, 0.5, 0.75$ for $f/f_0 = 1.75$ also results in the occurence of coalescence in the vortex shedding modes, as oppose to the vortex shedding mode in the absence of the free surface ($h = \infty$). On the other hand, the inclusion of free surface at $h = 0.5, 0.75$ results in the loss of coalescence for the vortex shedding modes of $f/f_0 = 1.25$, as compared to the vortex shedding mode of $h = \infty$. The flow associated with frequency ratio $f/f_0 = 2.25$, exhibits the existence of two states of quasi-periodic behaviour at cylinder submergence depths $h = 0.75, 0.5, 0.25$. The vortex shedding modes occuring for each quasi-periodic state at this f/f_0, are equivalent. Hence, there are no changes in modes synonmous with the change in states for $f/f_0 = 2.25$ at $h = 0.75, 0.5, 0.25$. The commonly observed modes for this case are the classical **C(2S)*** mode, the **C(4S)*** and **C(8S)*** modes. New modes observed for this case are the **C(4S)***, **6S*** and **C(14S)*** modes which are basically the repetition of the classical **C(2S)*** mode two, three and seven times, respectively.

The effect of the cylinder submergence depth, $h(= 0.25, 0.5, 0.75, \infty)$, and the frequency ratio, $f/f_0(= 1.25, 1.75, 2.25, 2.75)$, on the equivorticity patterns in the near wake region are summarized in Figure 3.16. The snapshots are taken at the instant the cylinder reaches maximum displacement, $x(t) = A$. For the periodic/quasi-periodic cases the snapshots are taken over the time interval in which the flow reaches a periodic/quasi-periodic state. It can be seen that there is negligible deformations of the free surface at $h = 0.25, 0.5, 0.75$. That is, the free surface acts as a non-deformable surface irrespective of cylinder submergence depth, h, or frequency ratio, f/f_0, values. It can be seen that the positive vortex structures in the lower shedding layer display significant changes, as opposed to the negative vortex structures, as the cylinder submergence depth decreases from $h = 0.75$ to $h = 0.25$ when compared to the reference case $h = \infty$. At $h = 0.25$, it can be seen that the negative vortex structures in the upper shedding layer of the cylinder interact greatly with the free surface, and as a result experience rapid diffusion across the free surface at this cylinder submergence depth. At each h, the negative vortex structures dominate the near wake region of the cylinder. It is evident that the vortex shedding is skewed symmetric in favor of the positive vortices. As the cylinder submergence depth is reduced from ∞

	$h = 0.75$		$h = 0.5$		$h = 0.25$		$h = \infty$	
f/f_0	Mode	T_v	Mode	T_v	Mode	T_v	Mode	T_v
1.25	**6S*** $(10T \le t \le 24T)$	$4T$	**14S*** $(4T \le t \le 24T)$	$9T$	**C(4S)** $(2T \le t \le 20T)$	$3T$	**C(10S*****)** $(15T \le t \le 37T)$	$7T$
1.75	**C(P + S)*** $(4T \le t \le 35T)$	$2T$	**C(P + S)*** $(4T \le t \le 34T)$	$2T$	**C(2S)** $(3T \le t \le 34T)$	$2T$	**2P** $(19T \le t \le 51T)$	$2T$
2.25	**C(2S)*** $(4T \le t \le 27T)$ $(32T \le t \le 42T)$	$2T$	**C(2S)*** $(3T \le t \le 9T)$ $(15T \le t \le 19T)$ $(25T \le t \le 31T)$ $(37T \le t \le 41T)$	$2T$	**C(4S)*** $(4T \le t \le 23T)$ $(26T \le t \le 36T)$	$5T$	**C(8S)*** $(40T \le t \le 66T)$	$9T$
2.75	**C(8S)*** $(9T \le t \le 35T)$	$11T$	**C(2S)*** $(6T \le t \le 54T)$	$3T$	**C(6S)** $(9T \le t \le 50T)$	$10T$	**C(P + S)*** $(49T \le t \le 81T)$	$3T$

Figure 3.15: The effect of the free surface inclusion at $Fr \approx 0.0, h = 0.75, 0.5$ and the frequency ratio, f/f_0, on vortex shedding modes and their periods, T_v, at $R = 200 : A = 0.13, f/f_0 = 1.25, 1.75, 2.25, 2.75$. The superscript "*" denotes quasi-locked-on modes.

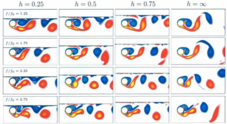

Figure 3.16: The effect of the cylinder submergence depth, h(=0.25, 0.5, 0.75), and the frequency ratio, f/f_0(=1.25, 1.75, 2.25, 2.75), on the equivorticity patterns at $R = 200$: $A = 0.13$, $Fr \approx 0.0$.

to 0.25 the shed vortices downstream of the cylinder become more oval shaped, and their major axes lies almost parallel to the free surface. For all cylinder submergence depths $h = 0.25, 0, 5, 0.75$, the flow behaviour becomes more complicated as f/f_0 increases. It is evident that the behaviour of the near wake region at $h = 0.75$ for each f/f_0 is similar to the reference case $h = \infty$, whereas a noticeable difference occurs for the smaller cylinder submergence depths $h = 0.25, 0.5$ as f/f_0 increases from 1.25 to 2.75. In general, an increase in the frequency ratio, f/f_0, from 1.25 to 2.25 results in the decrease of vortex formation length (maximum length by 40%) for the cylinder submergence depths $h = 0.25, 0.5, 0.75$. In addition, the length of the upper vortex shedding layer increases as f/f_0 increases in the presence of a free surface at $h = 0.25, 0.5, 0.75$.

4. Free surface flow past a streamwise oscillating cylinder at $Fr = 0.2$

In this Chapter, a viscous incompressible two-fluid model with a streamwise oscillating cylinder beneath a free surface is numerically investigated for the Froude number case of $Fr = 0.2$, at the cylinder submergence depths $h = 0.75, 0.5, 0.25$. The numerical simulations are conducted at a fixed Reynolds number of $R = 200$, and displacement amplitude, $A = 0.13$, in the frequency ratio range, $1.25 \leq f/f_0 \leq 2.75$, by an increment of 0.5.

4.1 Fluid forces and vortex shedding modes

4.1.1 Fluid forces at $Fr = 0.2:\ h = 0.75$

In Figure 4.1, the time history of the lift coefficient, C_L, the PSD of C_L and the Lissajous patterns of C_L are displayed. It is evident that for the smallest and largest frequency ratios, $f/f_0 = 1.25$ and $f/f_0 = 2.75$, the C_L traces exhibit non-repeatable signatures. Hence, indicative that a complete loss of phase locking occurs for these frequency ratios. On the other hand, the C_L traces of the frequency ratios $f/f_0 = 1.75$ and $f/f_0 = 2.25$ indicate the transition of the flow from the quasi-periodic state to the non-periodic state. The switchover, for each C_L, is observed at $t \approx 46.2, 42.6$ for the frequency ratios $f/f_0 = 1.75, 2.25$, respectively. The C_L traces for $f/f_0 = 1.75$ and

$f/f_0 = 2.25$ display quasi-periodic signatures every two periods of cylinder oscillation, $2T$, within $0 \le t \le 46.2$ and $0 \le t \le 42.6$, respectively. The quasi-periodicity of the C_L patterns for $f/f_0 = 1.75, 2.25$, is also suggested by the corresponding Lissajous patterns, $C_L(x)$, and hence for both frequency ratios a lock-on between the cylinder motions and the C_L patterns occur. As the switching time is reached for $f/f_0 = 1.75, 2.25$, the traces of C_L become non-persistent, and thus the transition from the quasi-periodic state to the non-periodic state of the near wake occurs. The transition to the non-periodic state is also suggested by the $C_L(x)$ patterns (non-periodic states) which are highly non-congruent. The spectra of C_L, both in the quasi-periodic and non-periodic flow states indicate that C_L oscillates at f_0 when $f/f_0 \le 2.25$. The spectrum of C_L corresponding to $f/f_0 = 2.75$, display a dominant peak at f_0, but also $f + f_0$. Hence, the effect of f_0 weakens as f/f_0 increases from 1.25 to 2.75. At any rate, the dominant peak of each PSD (quasi-periodic and non-periodic states) occurs at f_0, for each f/f_0. Similarly, to the reference case $h = \infty$, it can be seen that the hysteresis loops of $C_L(x)$ are also predominantly contained in both the upper and lower half planes.

In Figure 4.2, the time history of the drag coefficient, C_D, the PSD of C_D, and the Lissajous patterns of C_D is displayed. The traces of C_D for $f/f_0 = 1.25, 2.25, 2.75$ display non-repeatable signatures. The trace of C_D for $f/f_0 = 1.75$ displays an almost periodic signature every $2T$. It is evident that the decrease in repetitiveness of the C_D traces, for $f/f_0 \ge 1.75$, indicates the destabilization of C_D as f/f_0 increases from 1.75 to 2.75. The spectra corresponding to $f/f_0 \le 2.25$, both in the quasi-periodic and non-periodic flow states, indicate that C_D oscillates at the forcing frequency f. The spectrum corresponding to $f/f_0 = 2.75$, however, displays one dominant peak

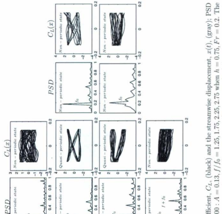

Figure 4.1: The time variation of lift coefficient, C_L, (black) and the streamwise displacement, $x(t)$, (gray); PSD of C_L; Lissajous patterns of C_L at $R = 200 : A = 0.13$, $f/f_0 = 1.25, 1.75, 2.25, 2.75$ when $h = 0.75$, $Fr = 0.2$. The Lissajous and PSD plots for $f/f_0 = 1.75, 2.25$ are obtained for quasi-periodic states in the following time intervals $0 \le t \le 46.2$, $0 \le t \le 42.6$, respectively. The corresponding flow states in the near wake region are indicated for each f/f_0.

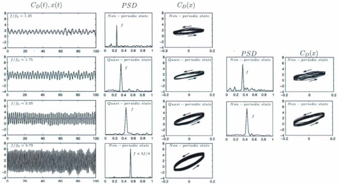

Figure 4.2: The time variation of drag coefficient, C_D, (black) and the streamwise displacement, $x(t)$, (gray); PSD of C_D; Lissajous patterns of C_D at $R = 200 : A = 0.13, f/f_0 = 1.25, 1.75, 2.25, 2.75$ when $h = 0.75, Fr = 0.2$. The Lissajous and PSD plots for $f/f_0 = 1.75, 2.25$ are obtained for quasi-periodic states in the following time intervals $0 \leq t \leq 46.2$, $0 \leq t \leq 42.6$, respectively. The corresponding flow states in the near wake region are indicated for each f/f_0.

at $f + 3f/4$. This is indicative of the effect of f weakening as f/f_0 increases from 1.25 to 2.75. Similarly, to the reference case $h = \infty$, it can be seen that the hysteresis loops for each f/f_0 are also predominantly confined to the upper half planes, and then they slightly shift to the lower half plane as f/f_0 increases from 1.25 to 2.75. At all the considered frequency ratios, f/f_0, the direction of the hysteresis loops are counter-clockwise. This indicates that for each frequency ratio f/f_0, the mechanical energy transfer is from the cylinder to fluid. It is also noted that as f/f_0 increases, the area enclosed by $C_D(x)$ increases and hence the total energy transferred from the cylinder to the fluid increases.

4.1.2 Vortex formation modes at $Fr = 0.2 : h = 0.75$

Figures 4.3-4.8 display the equivorticity and streamline patterns, and pressure contours in the near wake of the cylinder when $f/f_0 = 1.25, 1.75, 2.25$, and 2.75. The observed flow behaviour is (*i*) quasi-periodic per $2T$ for $f/f_0 = 1.75, 2.25$, and (*ii*) non-periodic for $f/f_0 = 1.25, 2.75$.

A series of instantaneous equivorticity plots over twenty periods of cylinder oscillation, $20T$, is plotted in Figure 4.3 for $f/f_0 = 1.25$. This figure shows that the frequency of the vortex shedding is not locked-on to the frequency of the cylinder motion. Coalescence was not observed for this case.

Figure 4.4 displays the equivorticity patterns over two periods of cylinder oscillations, $2T$, for $f/f_0 = 1.75$. The shedding of a single vortex and a pair of positive co-rotating vortices occurs within two periods of cylinder oscillation, $2T$. This results in the

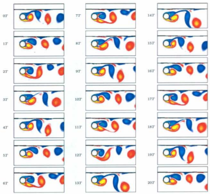

Figure 4.3: The equivorticity patterns over twenty periods of cylinder oscillation, $20T$, at $R = 200$: A=0.13, $f/f_0 = 1.25$ when $h = 0.75, Fr = 0.2$ [$T \approx 4.04, 20.20 \leq t \leq 101.01$: $(5T, 25T)$] (non-periodic state).

quasi-locked-on $\mathbf{C(P+S)^*}$ mode, per $2T$, within $4T \leq t \leq 16T$. This is consistent with the C_L and C_D behaviour at this frequency ratio. The flow is non-periodic for $t > 16T$. At $t = 0T$, a negative vortex formed during the previous vortex shedding cycle continues to develop over $0 \leq t \leq 3T/6$, and at $t = 4T/6$, coalesces with a newly formed negative vortex in the near wake of the cylinder. The resulting negative vortex develops over $4T/6 \leq t \leq 8T/6$, and then sheds into the near wake of the cylinder at $t \approx 9T/6$. Meanwhile, a pair of positive co-rotating vortices developed during the previous vortex shedding cycle continues to develop over $0T \leq t \leq 4T/6$, and then sheds into the near wake of the region at $t \approx 5T/6$. The development of a negative vortex and the development of a pair of co-rotating positive vortices occur, but shedding ceases for the remainder of the period, within $10T/6 \leq t \leq 2T$.

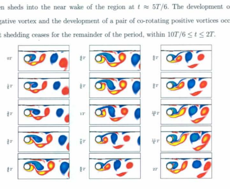

Figure 4.4: The equivorticity patterns over two periods of cylinder oscillation, $2T$, at $R = 200$: A=0.13, $f/f_0 = 1.75$ when $h = 0.75, Fr = 0.2$ [$T \approx 2.886, 23.09 \leq t \leq 28.86$: $(8T, 10T)$]. The quasi-locked-on $\mathbf{C(P+S)^*}$ mode, per $2T$, is observed.

The pressure contours for $f/f_0 = 1.75$ in the near wake region are presented in the last column of Figure 4.5. At $t = 0T$, the high pressure region has developed in the stagnation region and upper left side of the cylinder, and the low pressure region has developed mostly in the upper side, and the downstream of the cylinder. Over $T/4 \leq t \leq 3T/4$, synonomous with the development of a positive vortex in the near wake of the cylinder, the low pressure shifts mostly to the lower side, and downstream, of the cylinder. The high pressure region shifts to the upper side of the cylinder. At $t \approx T$, synonomous with the shedding of a positive vortex pair, it can be seen that the high pressure region shifts mostly back to the stagnation region. The low prssure region remains predominantly downstream and in the lower side of the cylinder. Furthermore over $T \leq t \leq 5T/4$, the high pressure region moves in the counterclockwise direction which ultimately leads to the shifting of the majority of the low pressure to the upper side of the cylinder. As a negative vortex is shed at $t \approx 6T/4$, it is evident that the low pressure region shifts mostly to the upper side of the cylinder. It is also evident at this time, that the concentration of the high pressure region dramatically decreases.

Figure 4.6 displays the equivorticity patterns over two periods of cylinder oscillations, $2T$, for $f/f_0 = 2.25$ within $3T \leq t \leq 5T$. The alternate shedding of a single vortex of opposite rotation from the upper and lower shear layers occurs within two periods of cylinder oscillation, $2T$. This results in the quasi-locked-on $\mathbf{C(2S)}^*$ mode, per $2T$, within $3T \leq t \leq 19T$. This is consistent with the C_L, but not C_D, behaviour at this frequency ratio. The flow becomes non-periodic for $t > 19T$. At $t = 0$, a negative vortex developed in the previous vortex shedding cycle continues to develop over $0T \leq t \leq 2T/6$, and subsequently sheds into the upper vortex shedding region of the cylinder at $t \approx 3T/6$. Meanwhile, a positive vortex formed during the previous vortex shedding cycle coalesces with a newly formed positive vortex at $t = 3T/6$. The resulting positive vortex develops over $3T/6 \leq t \leq 10T/6$, and then sheds downstream of the cylinder at $t = 11T/6$. It can be seen that the positive and negative vortices which have shed, remain in the mid-wake of the cylinder over $2T$.

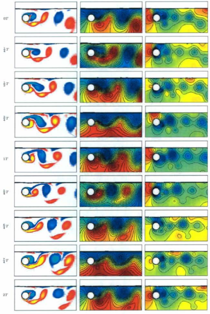

Figure 4.5: The equivorticity patterns (left), streamline patterns (middle) and the pressure contours (right) in the near wake region of the cylinder over two periods of cylinder oscillation, $2T$, at R = 200: A=0.13, f/f_0 = 1.75 when h = 0.75, Fr = 0.2 [$T \approx 2.886, 23.09 \leq t \leq 28.86$: $(8T, 10T)$]. The quasi-locked-on $\mathbf{C(P+S)}^*$ mode, per $2T$, is observed.

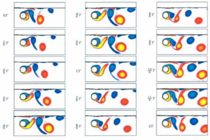

Figure 4.6: The equivorticity patterns over two periods of cylinder oscillation, $2T$, at $R = 200$: $A = 0.13$, $f/f_0 = 2.25$ when $h = 0.75, Fr = 0.2$ $[T \approx 2.2447, 6.734 \leq t \leq 11.224 : (3T, 5T)]$. The quasi-locked-on $\mathbf{C(2S^*)}$ mode, per $2T$, is observed.

In Figure 4.7, the pressure contours of frequency ratio $f/f_0 = 2.25$ are displayed for over two periods of cylinder oscillation, $2T$. At $t = 0T$, this figure displays the development of the the high pressure in the stagnation region of the cylinder, and the low pressure region mainly in the lower side, and downstream of the cylinder (near wake region). At $t = T/2$, synonomous with the development of a new negative vortex in the near wake, and the shedding of another negative vortex, the low pressure region shifts mostly to the upper side of the cylinder. The high pressure region shifts above and below the low pressure regions in the downstream of the cylinder. At $t = 3T/4$, it can be seen that a large positive vortex and a developing negative vortex are situated in the near wake region. In response, the low pressure region is seen to fully enclose the cylinder in the near wake region and most of the downstream of the cylinder. Over

$T \leq t \leq 5T/4$, as a positive vortex starts to detach, and the development of a new negative vortex begins it can be seen that the high pressure region shifts mostly back to the stagnation region of the cylinder and the low pressure region shifts mostly to the upper side of the cylinder and downstream. Synonomous with the development of a positive vortex over $6T/4 \leq t \leq 2T$, the low pressure region shifts mostly to the upper side of the cylinder (at $t = 6T/4$), then downstream (at $t = 7T/4$), and then finally below and downstream of the cylinder (at $t = 2T$.). The high pressure region appears to shift counterclockwise, over this time. It is interesting to note that the structure of the low pressure regions in the near wake of the cylinder at $t = 0, T/4, 3T/4, T$ are almost mirror images of the low pressure regions at $t = T, 5T/4, 7T/4, 2T$. The low pressure regions at $t = T/2$ and $6T/4$, however, are not mirror images of each other in the near wake region (at both time instances the low pressure resides predominantly in the upper side of the cylinder), but are in the downstream of the cylinder.

Figure 4.8, displays a series of instantaneous equivorticty plots over twenty periods of cylinder oscillation for $f/f_0 = 2.75$. This figure displays that the frequency of the vortex shedding is not locked-on to the frequency of the cylinder motion at this particular case (non-periodic state). Coalescence was observed for this case.

At this frequency ratio, $f/f_0 = 2.75$, coalescence of co-rotating vortices is observed in the near wake region of the cylinder. Figure 4.9 displays the coalescence phenomenon for $f/f_0 = 2.75$ over three periods of cylinder oscillation, $3T$. In this figure, at $t = 0T$, a negative vortex "1" and positive vortex "2" have developed from the upper and lower sides of the cylinder, respectively at $t = 0T$. A negative vortex "4" and positive vortex "3" develop from the upper and lower sides of the cylinder over $T/6 \leq t \leq 3T/6$.

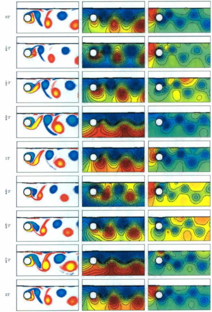

Figure 4.7: The equivorticity patterns (left), streamline patterns (middle) and the pressure contours (right) in the near wake region of the cylinder over two periods of cylinder oscillation, $2T$, at $R = 200$: A=0.13, $f/f_0 = 2.25$ when $h = 0.75, Fr = 0.2$ [$T \approx 2.245, 11.22 \leq t \leq 15.71$: $(5T, 7T)$]. The quasi-locked-on $\mathbf{C(2S)}^*$ mode, per $2T$, is observed.

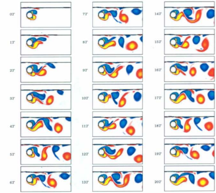

Figure 4.8: The equivorticity patterns over twenty periods of cylinder oscillation, $20T$, at $R = 200$: A=0.13, $f/f_0 = 2.75$ when $h = 0.75, Fr = 0.2$ [$T \approx 1.837, 1.837 \leq t \leq 7.346$: $(1T, 21T)$]. (non-periodic state).

At $t = 4T/6$, the two positive vortices "2" and "3" coalesce to form a single positive vortex "2+3" in the lower shedding layer of the cylinder. A negative vortex "6" and positive vortex "5" develop from the upper and lower sides of the cylinder over $7T/6 \leq t \leq 9T/6$. The two negative vortices "4" and "6" coalesce to form the single negative vortex "4+6" in the upper shedding layer at $t = 10T/6$. Finally, within $3T$, a negative vortex "8" and positive vortex "7" are developed from the upper and lower sides of the cylinder over $13T/6 \leq t \leq 16T/6$. At $t = 17T/6$, the negative vortices "8"

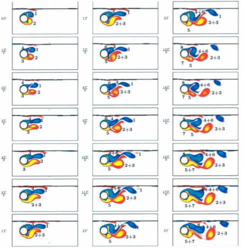

Figure 4.9: Near wake vortex coalescence phenomenon over three periods of cylinder oscillation, $3T$, at $R = 200 : A = 0.13, f/f_0 = 2.75$ when $h = 0.75, Fr = 0.2$ $[T \approx 1.837, 1.837 \leq t \leq 7.346 : (1T, 21T)]$ (non-periodic state).

and "4+6" coalesce to form a single negative vortex "4+6+8" in the upper shedding layer of the cylinder. However, at $t = 3T$, the negative vortex "4+6+8," seperates and the negative vortices "4+6" and "8" begin to co-rotate.

4.1.3 Fluid forces at $Fr = 0.2$: $h = 0.5$

In Figure 4.10, the time variation of the lift coefficient, C_L, the PSD, of C_L and the Lissajous patterns, $C_L(x)$, of C_L are displayed. It is evident that for $f/f_0 = 1.25, 2.75$, the C_L traces exhibit non-repeatable signatures. This observation is also suggested by the corresponding Lissajous patterns of the lift coefficients, $C_L(x)$, in which the patterns display highly non-congruent behaviour. This suggests that there are large phase variations between the fluctuating C_L and the cylinder motion, and hence a loss of lock-on for these frequency ratios. For $f/f_0 = 1.75, 2.25$ the signatures of C_L suggest that the flow exhibits two regimes. The C_L trace of $f/f_0 = 1.75$, indicates the transition of the flow from the quasi-periodic state to the non-periodic state of the near wake. The switchover occurs at $t \approx 16T$. On the other hand, the trace of C_L corresponding to $f/f_0 = 2.25$ suggests that the flow transitions from the non-periodic state to the quasi-periodic state. The switchover occurs at $t \approx 28T$, for this frequency ratio. The C_L trace for $f/f_0 = 1.75$ displays a quasi-periodic signature every two periods of cylinder oscillation, $2T$, within $4T \leq t \leq 16T$. Once the switching time is reached at $t \approx 16T$, the trace displays a non-periodic signature. The C_L trace for $f/f_0 = 2.25$ displays a non-periodic signature for $t < 28T$, but at the switching time of $t \approx 28$ the trace displays a quasi-periodic signature every seven periods of cylinder oscillation, $7T$, within $28T \leq t \leq 42T$. The quasi-periodic behaviour of $f/f_0 = 1.75, 2.25$ within $4T \leq t \leq 16T$ and $28T \leq t \leq 42T$, respectively, indicates a lock-on between the cylinder motions and the C_L patterns. It is evident, that the quasi-periodic behaviour of each frequency ratio is also suggested by the corresponding Lissajous patterns, $C_L(x)$, which exhibit congruent behaviour. It can be seen, however, that for $f/f_0 = 2.25$ the $C_L(x)$ pattern of the quasi-periodic state exhibits less congruent behaviour as compared to the $C_L(x)$ pattern for $f/f_0 = 1.75$ of the quasi-periodic state. This indicates that as f/f_0 increases from 1.25 to 2.25, there is a destabilization of C_L. It should be noted that the justification of the existence of a quasi-periodic state for $f/f_0 = 2.25$ was based on not only a quasi-repeatable signature for C_L, a large peak in the PSD and the quasi-congruent nature of the $C_L(x)$ patterns, but most importantly the repetitiveness of the vortex shedding within $28T \leq t \leq 42T$. The corresponding PSD of C_L for each f/f_0, both in the quasi-periodic and non-periodic flow states, indicate that C_L oscillates predominantly at the natural shedding frequency, f_0. It should be noted however that the an additional large peak at $3f_0$ is present in the PSD of $f/f_0 = 2.75$. This suggests that the effect of f_0 weakens as f/f_0 increases from 1.25 to 2.75. Similarly, to the hysteresis loops of the reference case $h = \infty$, it can be seen that the hysteresis loops of $C_L(x)$ are predominantly confined to both the upper and lower half planes.

In Figure 4.11, the time history of the drag coefficient, C_D, the PSD of C_D and Lissajous patterns, $C_D(x)$, of C_D are displayed. It is evident that the C_D traces for $f/f_0 = 1.25, 2.25$ and 2.75 display non-repeatable signatures. On the other hand, the C_D trace for $f/f_0 = 1.75$ displays an almost repeatable signature every two periods of cylinder oscillation, $2T$. Spectra of C_D suggest that, at $f/f_0 = 1.25, 1.75, 2.25, 2.75$, C_D fluctuates at the forcing frequency, f in both the quasi-periodic and non-periodic flow states. The Lissajous patterns, $C_D(x)$, show that the hysteresis loops are predomineantly confined to the upper half plane. It is also evident that as f/f_0 increase from 1.25 to 2.75, that there is a slight shifting of the hysteresis loops into the lower half plane. This shifting to the lower half plane also occurs for the reference case

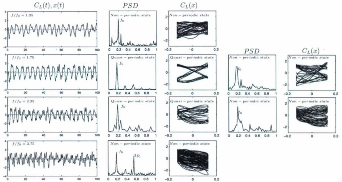

Figure 4.10: The time variation of lift coefficient, C_L, (black) and the streamwise displacement, $x(t)$, (gray); PSD of C_L; Lissajous patterns of C_L at $R = 200 : A = 0.13, f/f_0 = 1.25, 1.75, 2.25, 2.75$ when $h = 0.5, Fr = 0.2$. The Lissajous and PSD plots for $f/f_0 = 1.75, 2.25$ are obtained for quasi-periodic states in the following time intervals $11.54 \leq t \leq 46.18$, $62.851 \leq t \leq 94.276$, respectively. The corresponding flow states in the near wake region are indicated for each f/f_0.

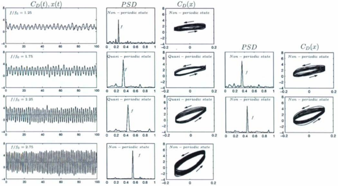

Figure 4.11: The time variation of drag coefficient, C_D, (black) and the streamwise displacement, $x(t)$, (gray); PSD of C_D; Lissajous patterns of C_D at $R = 200 : A = 0.13, f/f_0 = 1.25, 1.75, 2.25, 2.75$ when $h = 0.5, Fr = 0.2$. The Lissajous and PSD plots for $f/f_0 = 1.75, 2.25$ are obtained for quasi-periodic states in the following time intervals $11.54 \leq t \leq 46.18,\ 62.851 \leq t \leq 94.276$, respectively. The corresponding flow states in the near wake region are indicated for each f/f_0.

$h = \infty$ as f/f_0 increases from 1.25 to 2.75, but to a lesser extent. The direction of the hysteresis loops are counter-clockwise, indicating that the mechanical energy transfer is from the cylinder to the fluid. Furthermore, the amount of energy transferred from the cylinder to the fluid increases as f/f_0 increases from 1.25 to 2.75. This is a result of the increase in the area covered by the hysteresis loops of $C_D(x)$ as f/f_0 increases from 1.25 to 2.75.

4.1.4 Vortex formation modes at $Fr = 0.2 : \ h = 0.5$

Figures 4.12-4.17 display the equivorticty and streamline patterns, and pressure contours in the near wake of the cylinder when $f/f_0 = 1.25, 1.75, 2.25, 2.75$. The observed flow behaviour is (i) quasi-periodic per $2T, 7T$, for $f/f_0 = 1.75, 2.25$, respectively and (ii) non-periodic for $f/f_0 = 1.25, 2.75$.

In Figure 4.12, the equivorticity patterns for $f/f_0 = 1.25$ are displayed over twenty periods of cylinder oscillation, $20T$. This figures represents the that the vortex shedding is not locked-on to the frequency of the cylinder motion as this frequency ratio. No coalescence was observed in this figure.

Figure 4.13 displays the equivorticity patterns over two periods of cylinder oscillation, $2T$, for $f/f_0 = 1.75$. The shedding of a single negative vortex, and a pair of positive co-rotating vortices occurs within $2T$. This results in the quasi-locked-on $\mathbf{C(P+S)}^*$ mode, per $2T$, within $4T \leq t \leq 16T$. This is consistent with the behaviour of C_L and C_D for this frequency ratio. The flow is non-periodic for $t > 16T$. At $t = 0$, a negative vortex have developed from the previous vortex shedding cycle continues

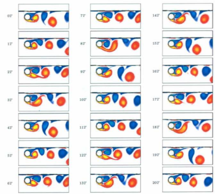

Figure 4.12: The equivorticity patterns over twenty periods of cylinder oscillation, $20T$, at $R = 200$: A=0.13, $f/f_0 = 1.25$ when $h = 0.5, Fr = 0.2$ [$T \approx 4.04, 20.20 \leq t \leq 101.01$: $(5T, 25T)$] (non-periodic state).

to develop over $0T \leq t \leq 3T/6$, and then coalesces with a second negative vortex in the near wake of the cylinder at $t = 4T/6$. This vortex continues to develop over $5T/6 \leq t \leq 7T/6$, and then sheds into the upper vortex shedding layer of the cylinder at $t \approx 8T/6$. Moreover, a pair of positive co-rotating vortices formed during the positive vortex shedding cycle continue to develop over $0T \leq t \leq 5T/6$. This pair is then shed downstream of the cylinder at $t = T$.

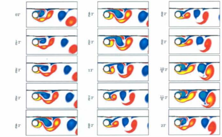

Figure 4.13: The equivorticity patterns over two periods of cylinder oscillation, $2T$, at $R = 200$: A=0.13, $f/f_0 = 1.75$ when $h = 0.5, Fr = 0.2$ $[T \approx 2.886, 11.54 \leq t \leq 17.32 : (4T, 6T)]$. The quasi-locked-on $\mathbf{C(P+S)}^*$ mode, per $2T$, is observed.

The pressure contours of frequency ratio $f/f_0 = 1.75$ are displayed in the last column of Figure 4.14. At $t = 0T$, this figure displays the development of the low pressure region behind and in the upper side of the cylinder and the development of the high pressure region in the stagnation region. At $t = T/2$, the high pressure region extends from the stagnation region of the cylinder to above and below the low pressure region in the downstream of the cylinder. In the near wake, the low pressure region is located mostly in the lower side of the cylinder, but in the upper side and downstream(near wake) as well. Synonomous, with the development of a positive vortex and the shedding of a positive vortex pair, at $t = T$, it is evident that the high pressure region shifts back to the stagnation region. The low pressure region shifts substantially behind the cylinder. Once the negative vortex has shed at $t = 8T/6$, (see Figure 4.13) it can be seen from the pressure distribution displayed at $t = 3T/2$ that the area of high pressure has once again shifted downstream to above and below the low pressure regions. The low pressure shifts mostly to the upper side of the cylinder and remains there for the duration of the cycle. The high pressure region remains predominantly in the stagntaion region of the cylinder, except at $t = T/2, 3T/2$ over the two periods of cylinder oscillation, $2T$. This figure suggests that at $t = T/2, 3T/2$, the high pressure region extends from the stagnation region of the cylinder to above and below the low pressure region in the downstream of the cylinder. The low pressure region, at $t = T/2, 3T/2$, develop in the lower and upper sides of the cylinder, respectively, following the development of positive and negative vortices, in the near wake of the cylinder, at the same time values.

For frequency ratio $f/f_0 = 2.25$, the vortex shedding is more difficult to analyze because of the strong interaction of the cylinder and the shed vortices. The free surface also plays a significant role in the shedding of the vortices because of the close proximity to the cylinder. Figure 4.15 displays the equivorticty patterns for $f/f_0 = 2.25$, over seven periods of cylinder oscillation, $7T$. The vortex shedding mode is the quasi-locked-on $\mathbf{C(6S)}^*$ mode, per $7T$, within $28T \leq t \leq 42T$. In this mode, three vortices develop and alternately shed on each side of the cylinder over $7T$. This is consistent with the behaviour of C_L, but not C_D, at this frequency ratio. The flow is non-periodic for $t < 28T$. Initially, a negative vortex developed in the previous vortex shedding cycle sheds into the upper vortex shedding region of the cylinder at $t = T$. A negative vortex formed from the coalescence of two negative vortices at $t = 5T/3$, continues to develop over $5T/3 \leq t \leq 2T$, and then detaches into the near wake of the cylinder at $t = 7T/3$. This negative vortex, however, approaches a

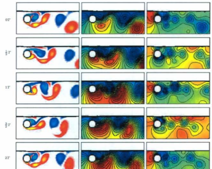

Figure 4.14: The equivorticity patterns (left), streamline patterns (middle) and the pressure contours (right) in the near wake region of the cylinder over two periods of cylinder oscillation, $2T$, at $R = 200$: A=0.13, $f/f_0 = 1.75$ when $h = 0.5, Fr = 0.2$ [$T \approx 2.886, 11.54 \leq t \leq 17.32$: $(4T, 6T)$]. The quasi-locked-on $\mathbf{C(P+S)}^*$ mode, per $2T$, is observed.

co-rotating negative vortex in the near wake of the cylinder at $t = 8T/3$. These two vortices co-rotate over $3T \leq t \leq 10T/3$, and at $t = 11T/3$ the negative vortex pair coalesce to form a negative vortex in the near wake of the cylinder. The resulting negative vortex sheds permanently into the upper vortex shedding layer at $t = 4T$. A negative vortex in the near wake of the cylinder develops over $4T \leq t \leq 13T/3$, and coalesces with a second negative vortex at $t = 14T/3$. This newly formed negative vortex develops over $14T/3 \leq t \leq 5T$, and then sheds into the upper region of the

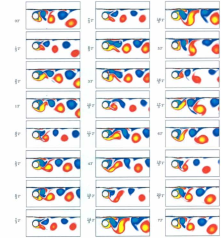

Figure 4.15: The equivorticity patterns over seven periods of cylinder oscillation, $7T$, at $R = 200$: A=0.13, $f/f_0 = 2.25$ when $h = 0.5, Fr = 0.2$ [$T \approx 4.04, 60.61 \leq t \leq 88.89$: $(28T, 35T)$]. The quasi-locked-on $\mathbf{C(6S)}^*$ mode, per $7T$, is observed.

cylinder at $t = 16T/3$. Meanwhile, a positive vortex formed from the coalescence of two positive vortices at $t = 2T/3$ develops over $T \leq t \leq 6T/3$, and then sheds into the near wake of the cylinder at $t = 7T/3$. Furthermore, two positive vortices coalesce in the near wake of the cylinder at $t = 8T/3$. The resulting positive vortex develops over $8T/3 \leq t \leq 10T/3$, and then begins to co-rotate with a second positive vortex over $11T/3 \leq t \leq 13T/3$. At $t = 14T/3$, the pair of co-rotating positive vortices coalesce, and the resulting positive vortex sheds downstream of the cylinder at $t = 5T$. Finally, a positive vortex created from the coalescence of two positive vortices at $t = 17T/3$ develops over $18T/3 \leq t \leq 19T/3$ and then sheds into the downstream of the cylinder at $t = 20T/3$. Hence, in the quasi-locked-on $\mathbf{C(6S)}^*$ mode, per $7T$, three vortices alternately develop and shed from each side of the cylinder.

Figure 4.16 displays the pressure distributions for the frequency ratio $f/f_0 = 2.25$ over seven periods of cylinder oscillation, $7T$. Similarly to the cases $f/f_0 = 1.25$ and 2.25, for $h = \infty$, a large number of vortices are shed into the upper and lower vortex shedding regions of the cylinder. At $t = 0T$, this figure displays the development of the low pressure region in the lower side, and downstream of the cylinder. The region of high pressure develops in the upper left side of the cylinder. At every $t = nT$, $(n = 0, 1, 2, 3, 4, 5, 6, 7)$ the high pressure region is mainly confined to the upper left side of the cylinder and the low pressure region mostly behind the cylinder. At $t = nT/2$ $(n = 0, 1, 2, 3, 4, 5, 6, 7)$, the low pressure region resides predominantly in the upper side of the cylinder, and also the lower side to a lesser extent. The high pressure region is mainly confined above and below the low pressure regions, in the downstream of the cylinder at these times. It can also be seen that the concentration of the high pressure in the near wake of the cylinder is quite low. This is due to the fact that the near wake is dominated by low pressure. For example at $t = 7T/2$, it is evident that as a negative vortex in the upper region of the cylinder is begins to detach, and a new negative vortex is being formed that the low pressure region

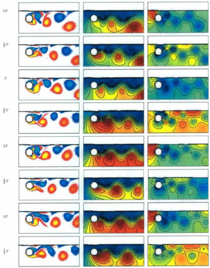

Figure 4.16: The figure caption is given on page 101

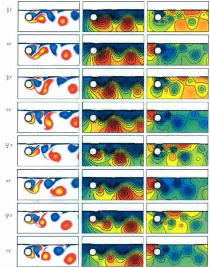

Figure 4.16: The equivorticity patterns (left), streamline patterns (middle) and the pressure contours (right) in the near wake region of the cylinder over seven periods of cylinder oscillation, $7T$, at $R = 200$:A=0.13, $f/f_0 = 2.25$, when $h = 0.5, Fr = 0.2$ $[T \approx 2.245, 62.851 \leq t \leq 78.563 : (28T, 35T)]$. The quasi-locked-on $\mathbf{C(6S)}^*$ mode, per $7T$, is observed.

shifts mostly to the upper side of the cylinder. As the negative vortex is shed at $t = 4T$, it can be seen that the high pressure region shifts back to the upper left side of the cylinder, and that the low pressure region shifts mainly to the upper side, and downstream of the cylinder. The structure of the low pressure pressure contours, in the near wake region, at $t = 0(2T, 5T, 7T)$ are almost a mirror images of the low pressure regions at $t = T(3T, 6T)$. It is noted that the structure of the low pressure regions at $t = 4T$ are not included. On the other hand, the structure of the low pressure regions at $t = T/2$, are nearly replicated by the low pressure regions at $t = nT/2$ $(n = 3, 5, 7, 9, 11, 13)$. The important thing to note, is that the low pressure regions at these times instances all have in common the presence of low pressure predominantly in the upper side of the cylinder. The periodic nature of the flow field around the cylinder is reproduced in the pressure contours.

Figure 4.17 displays the equivorticity patterns over twenty periods of cylinder oscillation, $20T$, for $f/f_0 = 2.75$. At this frequency ratio, the vortex shedding is not locked-on to the frequency of the cylinder oscillation. That is, no locked-on mode occurs for this case. Coalescence of vortices occurs for this case.

4.1.5 Fluid forces at $Fr = 0.2: \ h = 0.25$

In Figure 4.18, the lift coefficient, C_L, the spectra, PSD, and Lissajous patterns, $C_L(x)$, of C_L are displayed. It can be seen that for $f/f_0 = 1.25$, the C_L trace exhibits a non-repeatable signature. Furthermore, the $C_L(x)$ pattern of $f/f_0 = 1.25$ is non-congruent (large phase variations between the fluctuating C_L and the motion of the

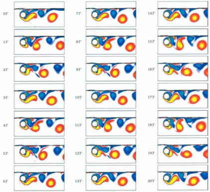

Figure 4.17: The equivorticity patterns over twenty periods of cylinder oscillation, $20T$, at $R = 200$: A=0.13, $f/f_0 = 2.75$ when $h = 0.5, Fr = 0.2$ [$T \approx 1.837, 9.183 \leq t \leq 45.91$: $(5T, 25T)$]. (non-periodic state).

cylinder). On the other hand, the C_L traces for $f/f_0 = 1.75, 2.25, 2.75$ indicate the transition of flow from the quasi-periodic state to the non-periodic state. The switchover for each f/f_0 occurs at $t \approx 13T, 24T, 28T$, respectively. The C_L traces for $f/f_0 = 1.75, 2.25, 2.75$ exhibit a quasi-periodic signature every $2T, 3T, 4T$ within $7T \leq t \leq 13T$, $16T \leq t \leq 24T$ and $12T \leq t \leq 28T$, respectively. The flow elsewhere is non-periodic, for each f/f_0. The quasi-periodic behaviour of C_L at $f/f_0 = 1.75, 2.25, 2.75$ indicates a lock-on between cylinder motion and the C_L pattern. It can be seen that the each corresponding $C_L(x)$ patterns exhibit congruent behaviour at these frequency ratios. It is also evident that the congruency of the $C_L(x)$ patterns increase as f/f_0 increases from 1.75 to 2.75. This implies that there is a reduction in phase variations between the cylinder motion and C_L, and an increase in the stabilization of C_L traces as f/f_0 increases. Similarly to the reference case $h = \infty$, the $C_L(x)$ patterns are confined in both the upper and lower half planes. Spectra of C_L corresponding to the quasi-periodic and non-periodic flow states of $f/f_0 = 1.25, 2.25, 2.75$, indicate that the dominant peak occurs at the forcing frequency, f. On the other hand, the dominant peak occurs at f_0 for $f/f_0 = 1.75$.

Figure 4.19 displays the drag coefficient, C_D, power spectra, PSD, and Lissajous patterns, $C_D(x)$, of C_D. It can be seen that the C_D traces for $f/f_0 = 1.25, 2.25$ display an almost repeatable signatures over $3T$. The C_D trace for $f/f_0 = 1.75$ displays an almost repeatable signature every $2T$. On the other hand, the C_D trace for $f/f_0 = 2.75$ exhibits a non-repeatable signature. The corresponding spectra of C_D both in the quasi-periodic and non-periodic flow states, for each f/f_0, indicate that the dominant peak occurs at f. It can be seen that the corresponding Lissajous patterns, $C_D(x)$, for $f/f_0 > 1.25$ seem to increase in congruency, as f/f_0 increases from 1.75 to 2.75. It is evident that there is an increase in total area covered by $C_D(x)$, as f/f_0 increases from 1.75 to 2.75. It can be seen that the hysteresis loops are mainly confined to the upper half-plane, but that there is a slight shifting into the lower half-plane as f/f_0 increase from 1.25 to 2.75. The direction of each hysteresis loop is counter-clockwise, and thus the mechanical energy transfer is from the cylinder to fluid. The amount of mechanical energy transferred also increases as f/f_0 increases, a result of the increase in total area covered by the hysteresis loops as f/f_0 increases.

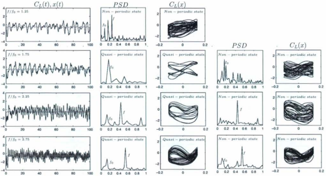

Figure 4.18: The time variation of lift coefficient, C_L, (black) and the streamwise displacement, $x(t)$, (gray); PSD of C_L; Lissajous patterns of C_L at $R = 200 : A = 0.13, f/f_0 = 1.25, 1.75, 2.25, 2.75$, when $h = 0.25, Fr = 0.2$. The Lissajous and PSD plots for $f/f_0 = 1.75, 2.25, 2.75$ are obtained for quasi-periodic states in the following time intervals $20.202 \leq t \leq 37.5180, 35.915 \leq t \leq 53.872$ and $22.039 \leq t \leq 51.423$, respectively. The corresponding flow states in the near wake region are indicated for each f/f_0.

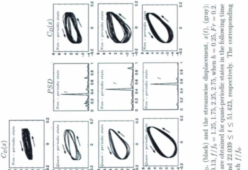

Figure 4.19: The time variation of drag coefficient, C_D, (black) and the streamwise displacement, $x(t)$, (gray); PSD of C_D; Lissajous patterns of C_D at $R = 200$: $A = 0.13$, $f/f_0 = 1.25, 1.75, 2.25, 2.75$, when $h = 0.25$, $Fr = 0.2$. The Lissajous and PSD plots for $f/f_0 = 1.75, 2.25, 2.75$ are obtained for quasi-periodic states in the following time intervals $20.202 \leq t \leq 37.5180$, $35.915 \leq t \leq 53.872$ and $22.039 \leq t \leq 51.423$, respectively. The corresponding flow states in the near wake region are indicated for each f/f_0.

4.1.6 Vortex formation modes at $Fr = 0.2: \; h = 0.25$

In this section the equivorticity, streamline patterns and pressure contours in the near wake of the cylinder when $f/f_0 = 1.25, 1.75, 2.25, 2.75$ are displayed in Figures 4.20-4.26. The observed flow behaviour is (i) non-periodic for $f/f_0 = 1.25$, (ii) quasi-periodic per $2T, 3T, 4T$, for $f/f_0 = 1.75, 2.25, 2.75$, respectively.

It is noted that the equivorticity patterns for a cylinder submergence depth of $h = 0.25$, are much more difficult to analyze as opposed to the cylinder submergence depths at $h = 0.5, 0.75$. In this case, vortices which shed in the upper vortex shedding region of the cylinder, closest to the free surface, have a tendency to re-attach to vortices that are in the near wake region, and hence makes the classification of lock-on modes more complex than higher cylinder submergence depths. In Figure 4.20, the equivorticity patterns for $f/f_0 = 1.25$ are displayed for twenty periods of cylinder oscillation, $20T$. It is evident from this figure and the accompanying lift and Lissajous patterns (see Figure 4.18), that the frequency of the vortex shedding is not locked-on to the frequency of the cylinder oscillation.

Figure 4.21 displays the equivorticity patterns for $f/f_0 = 1.75$ over two periods of cylinder oscillation, $2T$, within $7T \leq t \leq 13T$. The vortex shedding mode is the quasi-locked-on $\mathbf{C(2S)}^*$, per $2T$, within $7T \leq t \leq 13T$. The flow is non-periodic for $t > 13T$. This is consistent with the behaviour of C_L and C_D at this frequency ratio. In this mode, a single vortex develops on each side of the cylinder and alternately shed over $2T$. In the upper vortex shedding region, a negative vortex formed from the coalescence of two vortices at $t = 3T/6$ develops over $4T/6 \leq t \leq 7T/6$, and then

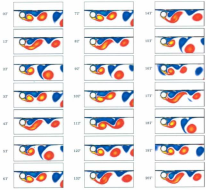

Figure 4.20: The equivorticity patterns over twenty periods of cylinder oscillation, $20T$, at $R = 200$: A=0.13, $f/f_0 = 1.25$ when $h = 0.25, Fr = 0.2$ [$T \approx 4.04, 20.20 \le t \le 101.01$: $(5T, 25T)$] (non-periodic state).

sheds into the upper vortex shedding layer at $t = 8T/6$. In the lower vortex shedding region, a positive vortex formed during the previous shedding cycle continues to develop over $0T \le t \le 3T/6$, and then sheds into the near wake of the cylinder at $t = 4T/6$. Hence, the shedding of a positive vortex followed by the shedding of a negative vortex, within $2T$, results in the quasi-locked-on $\mathbf{C(2S)}^*$ mode, per $2T$.

In Figure 4.22, the pressure contours are displayed for $f/f_0 = 1.75$ over two periods of

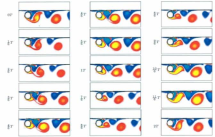

Figure 4.21: The equivorticity patterns over two periods of cylinder oscillation, $2T$, at $R = 200 : A = 0.13, f/f_0 = 1.75$ when $h = 0.25, Fr = 0.2$ $[T \approx 2.886, 23.088 \leq t \leq 28.860 : (8T, 10T)]$. The quasi-locked-on $\mathbf{C(2S)}^*$ mode, per $2T$, is observed.

cylinder oscillation, $2T$. At $t = 0T$, the region of high pressure develops in the upper left side of the cylinder and the low pressure region develops behind the cylinder in the near wake region, and in the lower side of the cylinder. At $t = T/2$, the high pressure region extends from the stagnation region of the cylinder to above and below the low pressure regions in the downstream of the cylinder. In the near wake region, the low pressure is located mostly in the upper side of the cylinder. Synonomous with the shedding of a positive vortex at $t = 4T/6$ (see Figure 4.21) and the development of a negative vortex at $t = 3T/4$, it is evident that the high pressure region moves mostly from the stagnation region to far downstream at this time. This is a result of the movement of the low pressure region to the front, top, bottom, and behind the cylinder in the near wake region. Hence, the near wake region is fully enclosed by low pressure at this time. Once a negative vortex has shed at $t = 8T/6$ (see Figure 4.21) and the development of a new negative, and positive, vortex commences at $t = 6T/4$, it can be seen that the concentration of low pressure increases dramatically in the near wake region of the cylinder. High pressure cannot be detected downstream of the cylinder at this time. However, over $7T/4 \leq t \leq 2T$, the high pressure region (located mostly downstream) shifts mostly to the stagnation region, and upper side of the cylinder. The low pressure region shifts mostly from the front and bottom of the cylinder, to behind the cylinder. The low pressure contours in the near wake of the cylinder are almost the same at the time instances $t = 0T$ and $t = 2T$. Hence, the periodic nature of the flow field around the cylinder is reproduced by the low pressure contours in the near wake of the cylinder.

In Figure 4.23, the equivorticity patterns over three periods of cylinder oscillation, $3T$, are displayed for $f/f_0 = 2.25$. The vortex shedding mode is the quasi-locked-on $\mathbf{C(P+S)}^*$ mode, per $3T$, within $16T \leq t \leq 24T$. The flow is non-periodic for $t > 24T$. This is consistent with the behaviour of C_L and C_D for this frequency ratio. It is evident that a negative vortex formed during the previous vortex shedding, sheds into the near wake of the cylinder at $t = 2T/6$. It can be seen that this negative vortex re-attaches to a negative vortex in the near wake of the cylinder at $t = 4T/6$, detaches again at $t = 7T/6$, attaches to a negative vortex in the near wake region of the cylinder once more at $t = 10T/6$, and then finally detaches at $t = 13T/6$. Hence, the first detachment of this negative vortex at $t = 2T/6$ plays an important role in classifying vortex shedding modes at this small cylinder submergence depth, $h = 0.25$. Meanwhile, a positive vortex develops over $0 \leq t \leq 3T/6$, and then coalesces with a second positive vortex in the near wake region at $t = 4T/6$. This

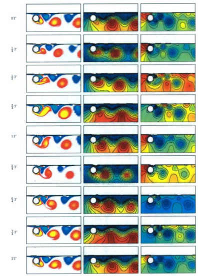

Figure 4.22: The equivorticity patterns (left), streamline patterns (middle) and the pressure contours (right) in the near wake region of the cylinder over four periods of cylinder oscillation, $4T$, at $R = 200$: $A = 0.13, f/f_0 = 1.75$ when $h = 0.25, Fr = 0.2$ $[T \approx 2.886, 23.09 \le t \le 28.86 : (9T, 11T)]$. The quasi-locked-on $\mathbf{C(6S)}^*$ mode, per $2T$, is observed.

positive vortex continues to develop over $5T/6 \leq t \leq 10T/6$, and then begins to co-rotate with a second positive vortex at $t = 11T/6$. The positive vortex pair co-rotate over $12T/6 \leq t \leq 14T/6$ and then shed into the near wake of the cylinder at $t = 15T/6$. Hence, the shedding of a negative vortex followed by the shedding of a positive vortex pair, in which one of these positive vortice is formed from coalescence, results in the quasi-locked-on $\mathbf{C(P+S)}^*$ mode, per $3T$, within $18T \leq t \leq 21T$.

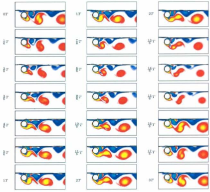

Figure 4.23: The equivorticity patterns over three periods of cylinder oscillation, $3T$, at $R = 200 : A = 0.13, f/f_0 = 2.25$ when $h = 0.25, Fr = 0.2$ $[T \approx 2.2447, 40.40 \leq t \leq 47.14 : (18T, 21T)]$. The quasi-locked-on $\mathbf{C(P+S)}^*$ mode, per $3T$, is observed.

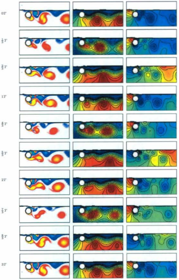

Figure 4.24: The equivorticity patterns (left), streamline patterns (middle) and the pressure contours (right) in the near wake region of the cylinder over three periods of cylinder oscillation, $3T$, at R = 200: A=0.13, f/f_0 = 2.25 when h = 0.25, Fr = 0.2 [$T \approx 2.245, 40.40 \leq t \leq 41.14$: $(18T, 21T)$]. The quasi-locked-on $\mathbf{C}(\mathbf{P}+\mathbf{S})^*$ mode, per $3T$, is observed.

In Figure 4.24, the pressure contours are displayed for $f/f_0 = 2.25$ over two periods of cylinder oscillation, $3T$. At $t = 0T$, this figure shows the development of the high pressure region in the upper left side of the cylinder and the low pressure region in the upper right side and downstream of the cylinder. Synonomous with the shedding of a negative vortex at $t = T/3$, it is evident that the region of low pressure is confined predominantly to the upper and lower sides of the cylinder in the near wake region. The high pressure region is mostly confined to the stagnation region of the cylinder. At $t = nT/3$ ($n = 1, 4, 7$), the low pressure regions are mainly confined to the upper and lower sides, and downstream of the cylinder. The high pressure region, resides in the stagnation region. With the development of new negative and positive vortices at $t = 2T/3$, it can be seen that the low pressure region shifts substantially to the front and lower side of the cylinder. As a result, the high pressure region shifts downstream of the cylinder. At every $t = nT/3$ $(2, 5, 8)$, the high pressure regions seem to be confined to above and below the low pressure regions in the downstream of the cylinder. The low pressure regions in the near wake region, are confined to the front and lower sides of the cylinder at these time instances. Furthermore, synonomous with the shedding of the positive vortex pair at $t = 15T/6$ (see Figure 4.23), and the development of new negative and positive vortices at $t = 8T/3$, as expected, the low pressure region dominates the front, lower side, and downstream of the cylinder. On the other hand, at $t = nT$ ($n = 0, 1, 2, 3$), it can be seen that the low pressure regions are mainly confined to behind the cylinder (near wake region), but also to the upper side of the cylinder. Once again, the high pressure region resides predominantly in the stagnation region of the cylinder. The low pressure contours in the near wake of the cylinder are almost the same at the time instances $t = 0T$ and $t = 3T$. Hence, the periodic nature of the flow field around the cylinder is reproduced by the low pressure contours in the near wake of the cylinder.

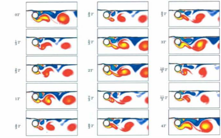

Figure 4.25: The equivorticity patterns over two periods of cylinder oscillation, $2T$, at $R = 200 : A = 0.13, f/f_0 = 2.75$ when $h = 0.25, Fr = 0.2$ $[T \approx 2.2447, 6.734 \leq t \leq 11.224 : (3T, 5T)]$. The quasi-locked-on $\mathbf{C(P+S)}^*$ mode, per $2T$, is observed.

Figure 4.25 exhibits the equivorticity patterns for $f/f_0 = 2.75$ over four periods of cylinder oscillation, $4T$. The vortex shedding mode is the quasi-locked-on $\mathbf{C(P+S)}^*$ mode, per $4T$, within $12T \leq t \leq 28T$. The flow is non-periodic for $t > 28T$. This is consistent with the C_L behaviour at this f/f_0. Initially, a negative vortex sheds near the free surface at $t = T/3$. This negative vortex then re-attaches to a negative vortex in the near wake region of the cylinder at $t = T$, and then sheds once more at $t = 4T/3$. Furthermore, this negative vortex re-attaches to the near wake region at $t = 2T$, and immediately sheds at $t = 7T/3$. It can be seen that this negative vortex attaches to negative vortices in the near wake region of the cylinder at $t = 3T$

and $4T$, respectively, after subsequent detachments from negative vortices in the near wake region of the cylinder. Meanwhile, a pair of positive vortices develops over $0 \leq t \leq T/3$, and then sheds into the lower vortex shedding region of the cylinder at $t = 2T/3$.

Figure 4.26 displays the pressure contours for the frequency ratio $f/f_0 = 2.75$ over four periods of cylinder oscillation, $4T$. At $t = 0T$, the high pressure region has developed in the stagnation region of the cylinder, and the low pressure region has developed mostly behind the cylinder. Synonomous with the shedding of a negative vortex at $t = T/3$ (see Figure 4.25), it is evident from the pressure distributions displayed at $t = T/2$ that the high pressure region shifts below the cylinder, and also above and below the low pressure regions in the downstream of the cylinder. The low pressure has been forced to the immediate upper and lower sides of the cylinder. On the other hand, synonomous with the shedding of a positive vortex into the upper vortex shedding region at $t = 2T/3$ (see Figure 4.25), it can be seen from the pressure distributions at $t = T$ that the high pressure region has shifted mostly back to the stagnation region. The low pressure region has shifted to the front and bottom sides, and downstream, of the cylinder (near wake region). In general, at every $t = nT$ $(n = 0, 1, 2, 3, 4)$ the low pressure region is confined predominantly to the downstream of the cylinder, with the highest concentration of low pressure occurring in the near wake region of the cylinder. On the other hand, at $t = nT/2$ $(n = 1, 3, 5, 7)$, the high pressure region extends from the stagnation region to below the cylinder (near wake region), and above and below the low pressure regions in the downstream of the cylinder. The low pressure contours at $t = 0T$ and $t = 4T$ are nearly replicated in this figure. Hence, the periodic nature of the flow field is reproduced.

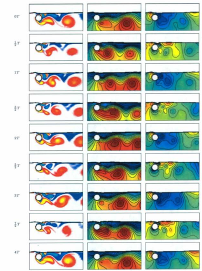

Figure 4.26: The equivorticity patterns (left), streamline patterns (middle) and the pressure contours (right) in the near wake region of the cylinder over four periods of cylinder oscillation, $4T$, at $R = 200$: $A = 0.13, f/f_0 = 2.75$ when $h = 0.25, Fr = 0.2$ $[T \approx 1.837, 25.71 \leq t \leq 33.06 : (14T, 18T)]$. The quasi-locked-on $\mathbf{C(P+S)}^*$ mode, per $4T$, is observed.

4.2 Summary and Discussion

For the case $Fr = 0.2, h = 0.75, 0.5, 0.25$ when $f/f_0 = 1.25, 1.75, 2.25, 2.75$ table 4.1 summarizes the effect the free surface presence has on the vortex shedding modes and their periods, T_v. Table 4.1 shows that non-classical modes occur in the presence of the free surface at $h = 0.5$ for $f/f_0 = 2.25$ and in the absence of the free surface ($h = \infty$) for $f/f_0 = 1.25, 2.25$. The new non-classical vortex shedding modes are formed from multiples of the classical $\mathbf{C(2S)}^*$ mode (see Williamson and Roshko (1988)) and include the $\mathbf{C(10S)}^*$, $\mathbf{C(8S)}^*$ and $\mathbf{C(6S)}^*$ modes, where 10, 8 and 6 refers to the total number of vortices shed from the cylinder within the respective periods, T_v, of vortex shedding. It can be seen that the inclusion of the free surface results in the loss lock-on for the smallest frequency ratio, $f/f_0 = 1.25$, at $h = 0.75, 0.5, 0.25$ and the largest frequency ratio, $f/f_0 = 2.75$, at $h = 0.75, 0.5$. On the other hand, lock-on modes occur at $f/f_0 = 1.75, 2.25$, regardless of cylinder submergence depth. It is interesting to note that regardless of cylinder submergence depth, h, the vortex shedding period for $f/f_0 = 1.75$ is two periods of cylinder oscillation, $2T$. However, as h decreases from ∞ to 0.25 at $f/f_0 = 1.75$, the lock-on modes, unlike the vortex shedding periods, change. However at the highest frequency ratio, $f/f_0 = 2.75$, the quasi-locked-on $\mathbf{C(P+S)}^*$ mode occurs at both $h = \infty$ and $h = 0.25$. It is evident from Table 4.1 that the commonly observed mode is $\mathbf{C(P+S)}^*$.

Tables 4.2 display the mean lift, $\widehat{C_L}$, and mean drag coefficients, $\widehat{C_D}$, for $f/f_0 = 1.25, 1.75, 2.25, 2.75$, respectively. It is evident that as h decreases from ∞ to 0.25, the $\widehat{C_L}$ values switch from positive values (for $h = \infty, 0.75$) to negative values ($h = 0.5, 0.25$). In the presence of a free surface, it can be seen that the $\widehat{C_L}$ values vary

	$h=\infty$		$h=0.75$		$h=0.5$		$h=0.25$	
f/f_0	Mode	T_v	Mode	T_v	Mode	T_v	Mode	T_v
1.25	$\mathbf{C(10S)}^*$	$7T$	non-locked	-	non-locked	-	non-locked	-
1.75	**2P**	$2T$	$\mathbf{C(P+S)}^*$	$2T$	$\mathbf{C(P+S)}^*$	$2T$	$\mathbf{C(2S)}^*$	$2T$
2.25	$\mathbf{C(8S)}^*$	$9T$	$\mathbf{C(2S)}^*$	$2T$	$\mathbf{C(6S)}^*$	$7T$	$\mathbf{C(P+S)}^*$	$3T$
2.75	$\mathbf{C(P+S)}^*$	$3T$	non-locked	-	non-locked	-	$\mathbf{C(P+S)}^*$	$4T$

Table 4.1: The effect of the free surface inclusion on vortex shedding modes and their periods, T_v, for the case $Fr = 0.2$ when $h = 0.25, 0.5, 0.75, \infty$ at $R = 200$: $A = 0.13, f/f_0 = 1.25, 1.75, 2.25, 2.75$. The superscript "*" denotes quasi-locked-on modes.

within the range $-0.6131 \leq \widehat{C_L} \leq 0.1826$. As f/f_0 increases from 1.25 to 2.75, it can be seen that the $\widehat{C_L}$ values decrease for $h = 0.25, h = 0.5$ (except $f/f_0 = 1.75$) and $h = \infty$ (except $f/f_0 = 2.75$). In contrast, for $h = 0.75$ the $\widehat{C_L}$ values increase as f/f_0 increases, except at $f/f_0 = 2.75$. Finally, it is evident that the absolute values of $\widehat{C_L}$ show that the magnitude of $\widehat{C_L}$ values for $h = \infty$ are much less than the $\widehat{C_L}$ values obtained in the presence of a free surface. Furthermore, as h decreases from 0.75 to 0.25, it is evident that the magnitude of $\widehat{C_L}$ values increase. The greatest increase in magnitude observed in $\widehat{C_L}$ values is by a factor of 0.3244. The mean drag coefficient values, $\widehat{C_D}$, do not show as much fluctuation as the values of the mean lift coefficient, $\widehat{C_L}$. Each $\widehat{C_D}$ value is positive and vary within the range $1.2235 \leq \widehat{C_D} \leq 1.7630$. There are no overwhelming differences in the magnitudes of the $\widehat{C_D}$ values in the presence of a free surface $h = 0.75, 0.5, 0.25$, as compared to those in the absence of a free surface, $h = \infty$. The maximum increases in $\widehat{C_D}$ values is by a factor of 1.44.

	$\widehat{C_L}$				$\widehat{C_D}$			
f/f_0	$h=\infty$	$h=0.75$	$h=0.5$	$h=0.25$	$h=\infty$	$h=0.75$	$h=0.5$	$h=0.25$
1.25	0.0055	0.1183	−0.03714	−0.4756	1.2467	1.5212	1.5640	1.6486
1.75	0.0044	0.1566	−0.0330	−0.5428	1.4023	1.6752	1.7630	1.67649
2.25	0.0007	0.1826	−0.04748	−0.56279	1.2610	1.7029	1.7020	1.6331
2.75	0.0130	0.1346	−0.10166	−0.6131	1.2235	1.6362	1.70417	1.60959

Table 4.2: The effect of the free surface inclusion on the mean lift, $\widehat{C_L}$, and drag, $\widehat{C_D}$, coefficients for the case $Fr = 0.2$ when $h = 0.25, 0.5, 0.75, \infty$ at $R = 200 : A = 0.13, f/f_0 = 1.25, 1.75, 2.25, 2.75$.

	$C_{L,rms}$				$C_{D,rms}$			
f/f_0	$h=\infty$	$h=0.75$	$h=0.5$	$h=0.25$	$h=\infty$	$h=0.75$	$h=0.5$	$h=0.25$
1.25	0.4926	0.7966	0.7803	0.8431	1.3157	1.6156	1.6886	1.9001
1.75	0.7401	1.0815	1.0612	0.9838	1.5951	1.8802	2.0452	2.3049
2.25	0.4205	0.9149	0.8558	1.0851	1.7617	2.1955	2.3842	2.7946
2.75	0.3302	0.7589	0.8468	0.9864	2.2544	2.5887	3.0679	3.5943

Table 4.3: The effect of the free surface inclusion on the RMS lift, $C_{L,rms}$, and drag, $C_{D,rms}$, coefficients for the case $Fr = 0.2$ when $h = 0.25, 0.5, 0.75, \infty$ at $R = 200$: $A = 0.13, f/f_0 = 1.25, 1.75, 2.25, 2.75$.

In Table 4.3, the root mean square (RMS) values of the lift and drag coefficients, $C_{L,rms}$, $C_{D,rms}$, are displayed for cylinder submergence depths $h = 0.75, 0.5, 0.25$, and the reference case $h = \infty$, respectively. In this context, the RMS values are used to measure the varying quantities of the lift, C_L, and drag, C_D, coefficients. The $C_{L,RMS}$ and $C_{D,RMS}$ values are defined respectively, as

$$C_{L,rms} = \sqrt{\frac{1}{n}\sum_{i=1}^{n}(C_{L_i})^2}, \quad C_{D,rms} = \sqrt{\frac{1}{n}\sum_{i=1}^{n}(C_{D_i})^2}.$$

It is evident, that the magnitude of the $C_{L,rms}$ values are much larger in the presence of the free surface, $h = 0.75, 0.5, 0.25$, than the RMS values in the absence of the free surface, $h = \infty$. In general, as h decreases from ∞ to 0.25, the $C_{L,rms}$ values tend to increase, for $f/f_0 = 1.25, 2.25, 2.75$, with the exceptions of $C_{L,rms}$ values of $f/f_0 = 1.25, 2.25$ at $h = 0.5$. The $C_{L,rms}$ values of $f/f_0 = 1.75$ decrease as the cylinder submergence depth decrease from $h = \infty$ to $h = 0.25$, with the exception of $f/f_0 = 1.75$ at $h = \infty$. The greatest increase in magnitude observed for $C_{L,rms}$ values is by a factor of 2.99. Similarly, to the trend exhibited by the $C_{L,rms}$, it can be seen that as the cylinder submergence depth decreases from $h = \infty$ to 0.25, the $C_{D,rms}$ values increase. Furthermore, it is evident that as the frequency ratios, f/f_0, increase from 1.25 to 2.75 the $C_{D,rms}$ values increase for $h = \infty, 0.75, 0.5, 0.25$. The maximum increase observed in $C_{D,rms}$ values is by a factor of 1.59. However, it is interesting to note that the maximum increase for $f/f_0 = 1.25$ and 1.75 is by a factor of 1.44 and $f/f_0 = 2.25$ and 2.75 by a factor of 1.59.

Figures 4.5-4.26, display the pressure contour plots of $h = 0.75, 0.5, 0.25$ when $f/f_0 =$

1.25, 1.75, 2.25, 2.75. The pressure contour plots at $h = 0.75$ when $f/f_0 = 2.25$, $h = 0.5$ when $f/f_0 = 1.75$ and $h = 0.25$ when $f/f_0 = 2.75$ indicate that at $t = 0T$ the high pressure region develops mostly in the stagnation region of the cylinder. The high pressure region at $h = 0.75$ when $f/f_0 = 1.75$, $h = 0.5$ when $f/f_0 = 2.25$, and $h = 0.25$ when $f/f_0 = 1.75, 2.25$, develops in the stagnation region and the upper left side of the cylinder. For $f/f_0 = 1.75$ at $h = 0.75, 0.5$, the low pressure region initially develops in the upper side of the cylinder and downstream. On the other hand at $h = 0.25$ for this frequency ratio, the low pressure regions develops in the lower side of the cylinder and downstream. For $f/f_0 = 2.25$ at $h = 0.75, 0.5$ the low pressure region develops initially in the lower side and downstream of the cylinder. However, at $h = 0.25$ the low pressure region develops in the upper right side and downstream of the cylinder. At $h = 0.25$, the frequency ratio $f/f_0 = 2.75$ initially displays the development of the low pressure region in the upper side of the cylinder and downstream. In general, the low pressure regions develop in the near wake of the cylinder, where the velocity is highest (formation of new vortices) and hence significantly affect the fluctuating lift forces acting on the circular cylinder, Positive and negative vortices which have shed downstream of the cylinder, are represented by the low pressure region (blue contours) for all f/f_0. Another interesting aspect of the low pressure contours of the circular cylinder is that for some cases, mirror images of the structures of low pressure are observed in the near wake region of the cylinder. Specifically at $h = 0.75$ when $f/f_0 = 2.25$, the low pressure regions at $t = 0, T/4, 3T/4, T$ are mirror images of the low pressure contours at $t = T, 5T/4, 7T/4, 2T$ (see Figure 4.6). At $h = 0.5$ when $f/f_0 = 2.25$, the low pressure regions at $t = 0(2T, 5T, 7T)$ are almost mirror images of the low pressure contours at $t = T(3T, 6T)$. On the other hand, for this frequency ratio, the structures of low pressure at $t = T/2$ is nearly a replica of the low pressure regions at $t = nT/2$ ($n = 3, 5, 7, 9, 11, 13$) (see Figure 4.16). It is also interesting to note that for $f/f_0 = 2.75$ at $h = 0.25$, the high pressure region at $t = nT/2$ ($n = 1, 3, 5, 7$) extends from the stagnation region of the cylinder to below the cylinder (near wake region) and above and below the low pressure regions in the downstream of the cylinder (refer to Figure 4.26).

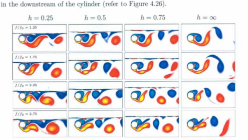

Figure 4.27: The effect of the cylinder submergence depth, h(=0.25, 0.5, 0.75), and the frequency ratio, f/f_0(=1.25, 1.75, 2.25, 2.75), on the equivorticity patterns at $R = 200$: $A = 0.13$, $Fr = 0.2$.

In Figure 4.27, the effect of the cylinder submergence depth, $h(= 0.25, 0.5, 0.75, \infty)$, and the frequency ratio, $f/f_0(= 1.25, 1.75, 2.25, 2.75)$, on the equivorticity patterns in the near wake region are summarized. The snapshots are taken at the instant, $x(t) = A$. For the periodic/quasi-periodic cases the snapshots are taken over the time interval in which the flow reaches a periodic/quasi-periodic state. For non-periodic cases, the commonly appearing equivorticity plots at $x(t) = A$, within the time interval $0 < t \leq 100$, are displayed. It can be seen that the deformations of the free surface become more pronounced as h decreases from ∞ to 0.25, and as f/f_0 increases from 1.25 to 2.75. Similarly to the case $Fr \approx 0.0$, the positive vortex structures in the lower shedding layer display significant changes, as opposed to the negative vortex structures, as the cylinder submergence depth decreases from $h = 0.75$ to $h = 0.25$ when compared to the reference case $h = \infty$. At $h = 0.25$, it can be seen that the negative vortex structures in the upper shedding layer of the cylinder interact greatly with the free surface, and as a result experience rapid diffusion across the free surface at this cylinder submergence depth. The vortex shedding is skewed symmetric in favor of the positive vortices. For each h value, the shed vortices are relatively oval shaped, but as the cylinder submergence depth is reduced from ∞ to 0.25 the major axes of the shed vortices downstream of the cylinder lie more parallel to the free surface. For all cylinder submergence depths $h = 0.25, 0, 5, 0.75$, the flow behaviour becomes more complicated as f/f_0 increases. It is evident that the behaviour of the near wake region at $h = 0.75$ for each f/f_0 is similar to the reference case $h = \infty$, whereas a noticeable difference occurs for the smaller cylinder submergence depths $h = 0.25, 0.5$ as f/f_0 increases from 1.25 to 2.75. In general, an increase in the frequency ratio, f/f_0, from 1.25 to 2.25 results in the decrease of vortex formation length (maximum length by 44%) for the cylinder submergence depths $h = 0.25, 0.5, 0.75$. In addition, the length of the upper vortex shedding layer increases as f/f_0 increases in the presence of a free surface at $h = 0.25, 0.5, 0.75$.

5. Free surface flow past a streamwise oscillating cylinder at $Fr = 0.4$

In this Chapter, a viscous incompressible two-fluid model with a streamwise oscillating cylinder beneath a free surface is numerically investigated for the Froude number case of $Fr = 0.4$, at the cylinder submergence depths $h = 0.75, 0.5, 0.25$. The numerical simulations are conducted at a fixed Reynolds number of $R = 200$, and displacement amplitude, $A = 0.13$, in the frequency ratio range, $1.25 \leq f/f_0 \leq 2.75$, where f/f_0 increases by an increment of 0.5.

5.1 Fluid forces and vortex shedding modes

5.1.1 Fluid forces at $Fr = 0.4$: $h = 0.75$

The time history of the lift coefficient, C_L, the PSD of C_L and the corresponding Lissajous patterns of $C_L, C_L(x)$, are displayed in Figure 5.1. At the smallest and largest frequency ratios $f/f_0 = 1.25, 2.75$, the C_L traces exhibit non-repeatable signatures, and therefore indicate that a complete loss of phase locking occurs. The C_L traces of $f/f_0 = 1.75, 2.25$ suggest that the flow transitions from the quasi-periodic state to the non-periodic state of the near wake. The switchover occurs at $t \approx 12T, 19T$ for $f/f_0 = 1.75, 2.25$, respectively. The C_L traces of frequency ratios $f/f_0 = 1.75$ and 2.25, display quasi-periodic signatures every two periods of cylinder oscillation, $2T$, within $6T \le t \le 12T$ and $4T \le t \le 19T$, respectively (quasi-periodic states). The quasi-periodic nature of the C_L traces for these frequency ratios is also suggested by the corresponding Lissajous patterns which are congruent. It is noted, however, that the congruency of the $C_L(x)$ patterns increase as f/f_0 increases from 1.75 to 2.25. The $C_L(x)$ patterns corresponding to $f/f_0 = 1.25, 2.75$, and to the non-periodic flow states of $f/f_0 = 1.75, 2.25$ are highly non-congruent. It can be seen that the Lissajous patterns of each f/f_0 are confined in both the upper and lower half planes. The spectra of each frequency ratio corresponding to the quasi-periodic and non-periodic flow states, all exhibit one dominant peak at f_0. This indicates that C_L oscillates at the natural shedding frequency, f_0, for all f/f_0.

Figure 5.2, displays the time history of the the drag coefficient, C_D, the PSD of C_D and the corresponding Lissajous patterns of C_D. At the frequency ratios $f/f_0 = 1.25, 2.75$, the C_D traces exhibit non-repeatable signatures. The C_D traces for $f/f_0 = 1.75, 2.25$ display an almost repeatable signature every two periods of cylinder oscillation, $2T$, respectively. It can be seen that the hysteresis loops display congruent behaviour for $f/f_0 = 1.75, 2.25$ in the quasi-periodic states of the flow, and less congruent behaviour for the non-periodic states of the flow for $f/f_0 = 1.75, 2.25$ and $f/f_0 = 1.25, 2.75$. The Lissajous patterns of C_D, $C_D(x)$, display interesting behaviour for this particular case. It is evident that as f/f_0 increases, the angle between the Lissajous patterns and the x-axis increases from zero to $\pi/2$. Similarly to the case $h = \infty$, the direction of each $C_L(x)$ pattern is counter-clockwise. This indicates that the mechanical energy transfer is from the cylinder to the fluid. The associated spectra of $f/f_0 \le 2.25$, all display one dominant peak at the forcing frequency, f for the quasi-periodic and non-periodic states of the flow. The PSD of frequency ratio $f/f_0 = 2.75$, displays two

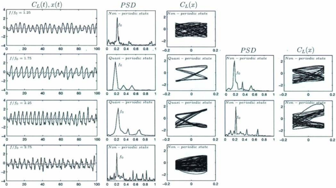

Figure 5.1: The time variation of lift coefficient, C_L, (black) and the streamwise displacement, $x(t)$, (gray); PSD of C_L; Lissajous patterns of C_L at $R = 200 : A = 0.13, f/f_0 = 1.25, 1.75, 2.25, 2.75$ when $h = 0.75, Fr = 0.4$. The Lissajous and PSD plots for $f/f_0 = 1.75, 2.25$ are obtained for quasi-periodic states in the following time intervals $17.316 \leq t \leq 34.6322, 8.98 \leq t \leq 42.65$, respectively. The corresponding flow states in the near wake region are also indicated for each f/f_0.

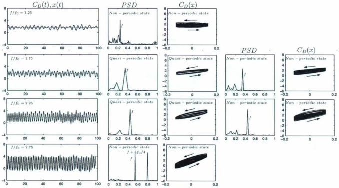

Figure 5.2: The time variation of drag coefficient, C_D, (black) and the streamwise displacement, $x(t)$, (gray); PSD of C_D; Lissajous patterns of C_D at $R = 200 : A = 0.13, f/f_0 = 1.25, 1.75, 2.25, 2.75$ when $h = 0.75, Fr = 0.4$. The Lissajous and PSD plots for $f/f_0 = 1.75, 2.25$ are obtained for quasi-periodic states in the following time intervals $17.316 \leq t \leq 34.6322, 8.98 \leq t \leq 42.65$, respectively. The corresponding flow states in the near wake region are also indicated for each f/f_0.

large peaks at f and $f+5f_0/4$, with the dominant peak occuring at $f+5f_0/4$. Hence, it is evident that the effect of f, on C_D, weakens as f/f_0 increases from 1.25 to 2.75.

5.1.2 Vortex formation modes at $Fr = 0.4:\ h = 0.75$

In this section the equivorticity and streamline patterns and the pressure contours in the near wake of the cylinder when $f/f_0 = 1.25, 1.75, 2.25, 2.75$ are displayed in Figures 5.3- 5.8. The observed flow behaviour is (i) non-periodic for $f/f_0 = 1.25, 2.75$ and (ii) quasi-periodic, per $2T$, for $f/f_0 = 1.75, 2.25$, respectively.

In Figure 5.3, a series of instantaneous equivorticty plots over twenty periods of cylinder oscillation, $20T$, is plotted for $f/f_0 = 1.25$. This figure shows that the frequency of vortex shedding is not locked-on to the frequency of the cylinder motion, for this frequency ratio. Coalescence is not observed in this figure.

Figure 5.4, displays the equivorticity patterns in the near wake of the cylinder over two periods of cylinder oscillations, $2T$, for frequency ratio $f/f_0 = 1.75$. The alternate shedding of a negative vortex from the upper vortex shedding region, and a pair of positive co-rotating vortices from the lower vortex shedding region, occurs within two periods of cylinder oscillation, $2T$. The resulting vortex shedding mode is the quasi-locked-on $\mathbf{C(P+S)}^*$ mode, per $2T$, within $6T \le t \le 12T$. The flow becomes non-periodic for $t > 12T$. This is consistent with the behaviour of C_L and C_D for this frequency ratio. At $t = 0T$, a negative vortex formed during the previous vortex shedding cycle coalesces with a newly formed negative vortex at $t = 4T/6$. The resulting negative vortex continues to develop over $4T/6 \le t \le 10T/6$, and then sheds into the upper vortex shedding region of the cylinder at $t = 11T/6$ aided by the interaction of a positive vortex in the lower vortex shedding region. On the other hand, a pair of positive co-rotating vortices developed in the previous vortex shedding cycle continue to co-rotate over $0T \leq t \leq 5T/6$, and are subsequently shed into the near wake of the region at $t = T$. For the remainder of the period under consideration, $7T/6 \leq t \leq 2T$, a positive pair of co-rotating vortices and a negative vortex develop, but cease to shed.

The pressure contours in the near wake region of the cylinder for $f/f_0 = 1.75$ are presented in the last column of Figure 5.5 over two periods of cylinder oscillation, $2T$. At $t = 0$, the high pressure region develops in the stagnation region of the cylinder, and the region of low pressure develops behind and in the upper side of the cylinder. Synonomous with the development of a positive vortex in the near wake region of the cylinder over $T/4 \leq t \leq 3T/4$, the low pressure region shifts mostly to the lower side of the cylinder. The high pressure region seems to shift in the clockwise direction. As the positive vortex pair is shed at $t = T$, it is evident that the high pressure region shifts mostly back to the stagnation region. The low pressure remains mostly below, and behind the cylinder. In connection with the development of a new negative vortex in the near wake of the cylinder, it can be seen that over $5T/4 \leq t \leq 7T/4$, the region of high pressure shifts in the counterclockwise direction. In the near wake, the low pressure region shifts mostly to the upper side of the cylinder. Once the negative vortex has shed at $t = 11T/6$ (see Figure 5.4), it can be seen from the pressure distributions displayed at $t = 2T$ that the high pressure has shifts back to the stagnation region, and that the region of low pressure shifts to the upper side of the cylinder. Furthermore at $t = 0, T/2, 3T/4, 6T/4, 7T/4$ and $2T$, the high pressure

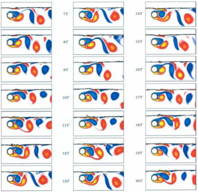

Figure 5.3: The equivorticity patterns over twenty periods of cylinder oscillation, $20T$, at $R = 200$: A=0.13, $f/f_0 = 1.25$ when $h = 0.75, Fr = 0.4$ $[T \approx 4.04, 20.20 \leq t \leq 101.01 : (5T, 25T)]$ (non-periodic state).

region has a significant presence above and below the low pressure regions in the downstream of the cylinder. The pressure contours at time instances $t = 0T$ and $t = 2T$ are nearly identical to each other. Hence, the quasi-periodic nature of the flow is reproduced by the pressure contours.

Figure 5.6 displays the equivorticity patterns in the near wake of the cylinder over two periods of cylinder oscillation, $2T$, for frequency ratio $f/f_0 = 2.25$. This figure displays

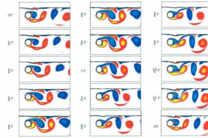

Figure 5.4: The equivorticity patterns over two periods of cylinder oscillation, $2T$, at $R = 200$: A=0.13, $f/f_0 = 1.75$ when $h = 0.75, Fr = 0.4$ $[T \approx 2.886, 23.09 \leq t \leq 28.86 : (8T, 10T)]$. The quasi-locked-on $\mathbf{C(P+S)}^*$ mode, per $2T$, is observed.

the shedding of a positive vortex from the upper vortex shedding region, followed by the shedding of a negative vortex from lower vortex shedding region, within $2T$. The resulting mode the quasi-locked-on $\mathbf{C(2S)}^*$ mode, per $2T$, within $4T \leq t \leq 19T$. The flow is non-periodic for $t > 19T$. This is consistent with the behaviour of C_L and C_D at this frequency ratio. A negative vortex develops over $0T \leq t \leq T/2$ and subsequently coalesces with a second negative vortex in the near wake region of the cylinder at $t = 2T/3$. The resulting negative vortex develops over $4T/6 \leq t \leq 10T/6$ and then detaches from the upper side of the cylinder at $t = 11T/6$. It is evident that this negative vortex is prevented from flowing downstream, until the large positive vortex downstream dissipates. On the other hand, a positive vortex formed during the previous vortex shedding cycle continues to develop over $0T \leq t \leq 2T/3$, and

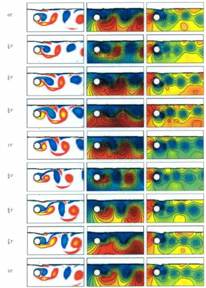

Figure 5.5: The equivorticity patterns, streamline patterns and the pressure distibution in the near wake region of the cylinder over two periods of cylinder oscillation, $2T$, at $R = 200$: A=0.13, $f/f_0 = 1.75$ when $h = 0.75$, $Fr = 0.4$ $[T \approx 2.886, 23.09 \leq t \leq 28.86 : \ (8T, 10T)]$. The quasi-locked-on $\mathbf{C(P+S)}^*$ mode, per $2T$, is observed.

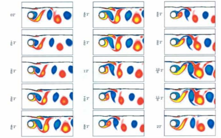

Figure 5.6: The equivorticity patterns over two periods of cylinder oscillation, $2T$, at $R = 200$: A=0.13, $f/f_0 = 2.25$ when $h = 0.75, Fr = 0.4$ [$T \approx 2.237, 13.468 \leq t \leq 17.958$: $(6T, 8T)$]. The quasi-locked-on $\mathbf{C(2S)}^*$ mode, per $2T$, is observed.

subsequently shed into the lower vortex shedding region of the cylinder at $t = 5T/6$. New negative and positive vortices develop over $T \leq t \leq 2T$, but cease to shed.

In Figure 5.7, the pressure contours in the near wake of the cylinder are displayed for $f/f_0 = 2.25$ over two periods of cylinder oscillation, $2T$. At $t = 0$, the high pressure region has developed in the stagnation region of the cylinder, and the low pressure region has developed behind, and in the upper side of, the cylinder. Synonomous with the development of a positive vortex over $T/4 \leq t \leq 3T/4$, it can be seen that the low pressure shifts mostly to the lower side of the cylinder. There is presence of low pressure behind the cylinder, as well. The high pressure region shifts from the stagnation region to above and below the low pressure contours in the downstream

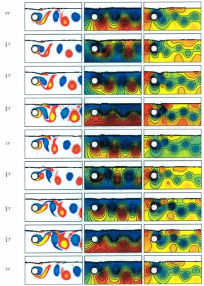

Figure 5.7: The equivorticity patterns, streamline patterns and the pressure distibution in the near wake region of the cylinder over two periods of cylinder oscillation, $2T$, at $R = 200$: A=0.13, $f/f_0 = 2.25$ when $h = 0.75$, $Fr = 0.4$ [$T \approx 2.237, 13.468 \leq t \leq 17.958$: $(6T, 8T)$]. The quasi-locked-on $\mathbf{C(2S)}^*$ mode, per $2T$, is observed.

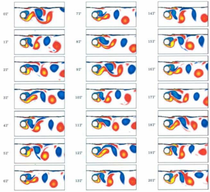

Figure 5.8: The equivorticity patterns over twenty periods of cylinder oscillation, $20T$, at $R = 200$: A=0.13, $f/f_0 = 2.75$ when $h = 0.75, Fr = 0.4$ $[T \approx 1.837, 9.183 \leq t \leq 45.91 : (5T, 25T)]$ (non-periodic state).

of the cylinder at $t = 3T/4$. Once the positive vortex has shed at $t = 5T/6$ (see Figure 5.6), it can be seen from the pressure distributions displayed at $t = T$ that the area of high pressure shifts mostly back to the stagnation region of the cylinder. The regions of low pressure remain mostly in the lower side of the cylinder. In connection with the development of a new negative vortex in the near wake of the cylinder, it can be seen that over $5T/4 \leq t \leq 7T/4$, the area of high pressure shifts counterclockwise. The high pressure region also extends from the stagnation region of the cylinder to above and below the low pressure contours in the downstream of the cylinder. The low pressure region shifts mostly from the lower side of the cylinder to the upper side. Once the negative vortex has shed at $t = 11T/6$ (see Figure 5.6), it can be seen from the pressure distributions displayed at $t = 2T$ that the high pressure region resides predominantly in the stagnation region and the low pressure region mostly to the upper side of the cylinder. The structures of the low pressure contours in the near wake region of the cylinder at $t = 0(2T), T/4, T/2, 3T/4$ are almost mirror images of the low pressure regions in the near wake region of the cylinder at $t = T, 5T/4, 6T/4, 7T/4, 2T$. Therefore, the periodic nature of the flow field around the cylinder is reproduced by the pressure contours.

Figure 5.8 displays the equivorticity patterns for $f/f_0 = 2.75$ over twenty periods of cylinder oscillation, $20T$. This figure displays that the frequency of vortex shedding is not locked-on to the frequency of the cylinder motion, for this frequency ratio. Coalescence is observed at this frequency ratio.

5.1.3 Fluid forces at $Fr = 0.4$: $h = 0.5$

Figure 5.9 displays the time history of the lift coefficient, C_L, the PSD of C_L and the Lissajous patterns, $C_L(x)$. The C_L trace of $f/f_0 = 2.75$, exhibits a non-periodic signature. The traces of the lift coefficient, C_L, display quasi-periodic signatures over $5T$ for $f/f_0 = 1.25$ within $3T \leq t \leq 13T$, and over $2T$ for $f/f_0 = 1.75, 2.25$ within $13T \leq t \leq 19T$, and $4T \leq t \leq 22T$, respectively. At $t \approx 13T, 19T, 22T$, the C_L traces of $f/f_0 = 1.25, 1.75, 2.25$, switch from exhibiting quasi-periodic signatures to non-periodic signatures. The corresponding spectra of C_L display a dominant peak at the natural shedding frequency, f_0, for $f/f_0 = 1.25$; two well defined peaks at f_0 and f for $f/f_0 = 1.75$ and 2.25, respectively; and three well defined peaks at f_0, f and $(5f + 2f_0)/4$ for $f/f_0 = 2.75$. For each frequency ratio it is evident that the dominant peak occurs at f_0. The Lissajous patterns corresponding to $f/f_0 = 1.75$ and $f/f_0 = 2.25$, exhibit congruent patterns which is representative of the quasi-periodic nature of the C_L traces at these frequency ratios. However, non-congruent patterns are observed in the non-periodic flow states of $f/f_0 = 1.25, 1.75, 2.25$ and for $f/f_0 = 2.75$. It is evident that the Lissajous patterns for $f/f_0 = 1.25, 1.75, 2.25$ and 2.75 are confined predominantly to the lower half plane, as opposed to the Lissajous patterns at the reference case, $h = \infty$, which are predominantly confined to both the top and bottom half-planes.

The time history of the drag coefficient, C_D, the PSD of C_D and the Lissajous patterns, $C_D(x)$, of C_D are displayed in Figure 5.10. It can be seen that the C_D trace of $f/f_0 = 1.25$ displays an almost repeatable signature per $5T$. The C_D traces of $f/f_0 = 1.75, 2.25$, display almost repeatable signatures every $2T$. The C_D trace for $f/f_0 = 2.75$ displays a non-repeatable signature. The spectra corresponding to $C_D(x)$ for $f/f_0 \leq 2.25$, all display one dominant peak at the forcing frequency f. Two well defined peaks occur at f and $(5f+2f_0)/4$ for the spectra corresponding to $f/f_0 = 2.75$. Hence, the effect of f weakens as f/f_0 increases from $f/f_0 = 1.25$ to 2.75. Overall, the dominant peak occurs at f for each frequency ratio. It is evident that the corresponding Lissajous patterns, $C_D(x)$, for each frequency ratio display congruent behaviour and that the congruency of each Lissajous pattern increase as f/f_0 increases from 1.25 to 2.75. The hysteresis loops reside predominently in the upper half plane, as opposed to the hysteresis loops of C_L displayed in Figure 5.9. Similarly to the case $Fr = 0.4$ when $h = 0.75$, it can be seen that as f/f_0 increases from 1.25 to 2.75, that the angle between the hysteresis loop and the x-axis increases. The direction of each hysteresis loop is counter-clockwise and therefore the transfer of mechanical energy is from the cylinder to the surrounding fluid.

5.1.4 Vortex formation modes at $Fr = 0.4 : \ h = 0.5$

In Figures 5.11-5.17, the equivorticty and streamline patterns and the pressure contours in the near wake of the cylinder when $f/f_0 = 1.25, 1.75, 2.25, 2.75$ are displayed. The observed flow behaviour is (i) quasi-periodic, per $5T$ for $f/f_0 = 1.25$, and per $2T$ for $f/f_0 = 1.75, 2.25$, respectively and (ii) non-periodic for $f/f_0 = 2.75$.

Figure 5.11 displays the equivorticty patterns over five periods of cylinder oscillations, $5T$, of the quasi-periodic state for $f/f_0 = 1.25$. The vortex shedding mode is the quasi-locked-on $\mathbf{C(8S)}^*$ mode, per $5T$, within $3T \leq t \leq 13T$. The flow is non-periodic for $t > 13T$. This is consistent with the behaviour of C_L and C_D at this frequency ratio. In this mode, four vortices develop on each side of the cylinder and shed alternately over $5T$. Initially, a negative vortex which has developed over $0 \leq t \leq 2T/3$, sheds into the upper vortex shedding region of the cylinder at $t = T$. A negative vortex develops over $4T/3 \leq t \leq 2T$, and then sheds from the upper side of the cylinder at $t = 7T/3$. Furthermore, a negative vortex formed by the coalescence of two negative vortices at $t = 8T/3$ develops over $3T \leq t \leq 10T/3$, and then sheds downstream of the cylinder at $t = 11T/3$. Finally a negative vortex which has developed over

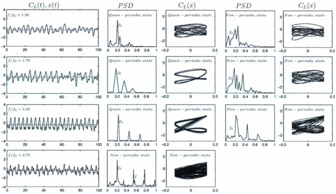

Figure 5.9: The time variation of lift coefficient, C_L, (black) and the streamwise displacement, $x(t)$, (gray); PSD of C_L; Lissajous patterns of C_L at $R = 200 : A = 0.13, f/f_0 = 1.25, 1.75, 2.25, 2.75$ when $h = 0.5, Fr = 0.4$ The Lissajous and PSD plots for $f/f_0 = 1.25, 1.75, 2.25$ are obtained for quasi-periodic states in the following time intervals $3T \leq t \leq 13T, 13T \leq t \leq 19T$, and $4T \leq t \leq 22T$, respectively. The corresponding flow states in the near wake region are indicated for each f/f_0.

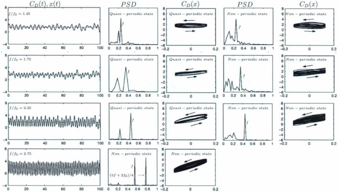

Figure 5.10: The time variation of drag coefficient, C_D, (black) and the streamwise displacement, $x(t)$, (gray); PSD of C_D; Lissajous patterns of C_D at $R = 200 : A = 0.13, f/f_0 = 1.25, 1.75, 2.25, 2.75$ when $h = 0.5, Fr = 0.4$ The Lissajous and PSD plots for $f/f_0 = 1.25, 1.75, 2.25$ are obtained for quasi-periodic states in the following time intervals $3T \leq t \leq 13T, 13T \leq t \leq 19T$, and $4T \leq t \leq 22T$, respectively. The corresponding flow states in the near wake region are indicated for each f/f_0.

$4T \leq t \leq 13T/3$, sheds into the upper vortex shedding layer of the cylinder at $t = 14T/3$. Meanwhile in the lower vortex shedding layer, a positive vortex formed during the previous shedding cycle sheds into the near wake of the cylinder at $t = T/3$. A positive vortex formed from the coalescence of two positive vortices at $t = 2T/3$ develops over $T \leq t \leq 4T/3$, and then sheds downstream of the cylinder at $t = 5T/3$. Next, a positive vortex develops over $2T \leq t \leq 8T/3$, and then sheds from the lower side of the cylinder at $t = 3T$. A primary positive vortex in the near wake of the cylinder develops over $10T/3 \leq t \leq 11T/3$, and then sheds as a secondary vortex into the lower vortex shedding of the cylinder at $t = 4T$.

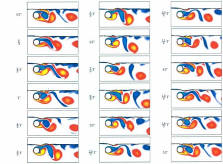

Figure 5.11: The equivorticity patterns over five periods of cylinder oscillation, $5T$, at $R = 200$: $A = 0.13, f/f_0 = 1.25$ when $h = 0.5, Fr = 0.4$ $[T \approx 4.040, 20.20 \leq t \leq 40.40 : (5T, 10T)]$. The quasi-locked-on $\mathbf{C(8S)}^*$ mode, per $5T$, is observed.

In Figure 5.12, the pressure contours are displayed for the frequency ratio $f/f_0 = 1.25$ over five periods of cylinder oscillation, $5T$. At $t = 0$, the high pressure region has developed in the stagnation region, and the low pressure region in the front, upper and lower side of the cylinder. There is significant development of low pressure downstream of the cylinder as well. It can be seen that overall, the concentration of low pressure in the near wake region of the cylinder is very high over the five periods of cylinder oscillation, $5T$. At $t = nT/2$ $(n = 1, 3, 5, 7, 9)$, the high pressure region is mainly confined to the upper left side of the cylinder. At $t = nT$ $(n = 0, 1, 2, 3, 4, 5)$, the concentration of high pressure has dramtically decreased in the upper left side of the cylinder. It is evident, however, that over $5T$ that the high pressure region also extends above and below the low pressure regions in the downstream of the cylinder. With the development of new vortices, it is evident that the low pressure regions favor the side of the cylinder on which the development of these new vortices occur. For example, at $t = T/2$ synonomous with the development of a new negative vortex in the upper side of the cylinder, the region of low pressure shifts mostly to the upper side of the cylinder. That is the concentration of high pressure is greatest in the upper side of the cylinder at this time instance. On the other hand, as a new positive vortex begins to develops at $t = 3T/2$ the low pressure region is seen to shift mostly to the lower side of the cylinder (near wake region). Consequently the concentration of low pressure is greatest in the lower side of the cylinder. The low pressure structures in the near wake region at $t = 0T$ and $t = 5T$ are nearly identical, thus the quasi-periodic nature of the flow is reproduced in this figure.

Figure 5.13 displays the equivorticity patterns for $f/f_0 = 1.75$ over two periods of cylinder oscillations, $2T$, within $15 \leq t \leq 17T$. The vortex shedding mode is the quasi-

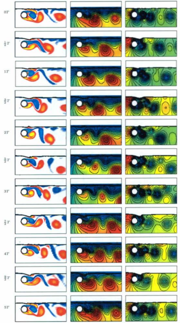

Figure 5.12: The equivorticity patterns(left), streamline patterns (middle) and the pressure contours (right) in the near wake region of the cylinder over five periods of cylinder oscillation, $5T$, at $R = 200$: $A = 0.13, f/f_0 = 1.25$ when $h = 0.5, Fr = 0.4$ $[T \approx 4.040, 20.20 \leq t \leq 40.40 : (5T, 10T)]$. The quasi-locked-on $\mathbf{C(8S)}^*$ mode, per $5T$, is observed.

locked-on $\mathbf{C(2S)}^{*}$ mode, per $2T$, within $13T \leq t \leq 19T$. The flow is non-periodic for $t > 19T$. This is consistent with the behaviour of C_L and C_D at this frequency ratio. This vortex formation mode is the result of the alternate shedding of a single vortex, of opposite rotation, from the upper and lower vortex shedding region of the cylinder over $2T$. A negative vortex formed during the previous vortex shedding cycle develops over $0T \leq t \leq 3T/6$, and then coalesces with a second negative vortex at $t = 4T/6$. The resulting negative vortex develops over $4T/6 \leq t \leq 11T/6$ and then sheds into the upper vortex shedding layer at $t = 2T$. A pair of positive co-rotating vortices formed during the previous vortex shedding cycle, continue to develop over $0T \leq t \leq 2T/6$. A positive vortex, of the vortex pair, coalesces with a newly developed positive vortex in the near wake of the cylinder at $t = 4T/6$. Over $4T/6 \leq t \leq T$, the newly developed positive vortex continues to co-rotate with the secondary positive vortex, but the positive vortices are eventually distanced from each other by the edge of a negative vortex protruding into the lower vortex shedding region. Consequently, the secondary positive vortex furthest from the near wake of the cylinder, sheds downstream of the cylinder at $t = 7T/6$.

For frequency ratio $f/f_0 = 1.75$, the pressure contours are displayed over two periods of cylinder oscillation, $2T$, in Figure 5.14. At $t = 0$, the high pressure develops in the stagnation region and the low pressure region in the upper side and downstream of the cylinder (near wake region). Immediately, is it evident at $t = nT/4$ $(n = 0, 3, 7)$ that the high presure region seems to be confined above and below the low pressure regions in the downstream of the cylinder. The low pressure regions are confined to the upper side of the cylinder and/or behind the cylinder at these time instances. On the other hand, for example at $t = 2T$, synonomous with the shedding of a negative

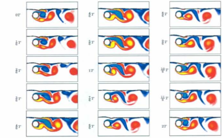

Figure 5.13: The equivorticity patterns over two periods of cylinder oscillation, $2T$, at $R = 200 : A = 0.13, f/f_0 = 1.75$ when $h = 0.5, Fr = 0.4$ [$T \approx 2.886, 43.29 \leq t \leq 49.06$: $(15T, 17T)$]. The quasi-locked-on $\mathbf{C(2S)}^*$ mode, per $2T$, is observed.

vortex into the upper vortex shedding region, it is evident that the high pressure region has shifted completely to the front of the cylinder and that the low pressure region has shifted somewhat behind the cylinder. There is still significant presence of low pressure in the upper side of the cylinder. Synonomous with the development of a positive vortex over $T/4 \leq t \leq T$, the low pressure region shifts mostly behind the cylinder. As the positive vortex is shed at $t = 7T/6$ (see Figure 5.13), the low pressure region is confined to the upper and lower side of the cylinder in the near wake. The high pressure has returned mostly to the stagnation region. The low pressure structures in the near wake region at $t = 0T$ and $t = 2T$ are nearly identical, thus the quasi-periodic nature of the flow field is reproduced in this figure.

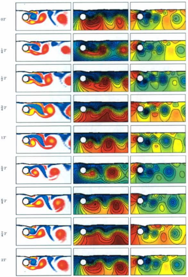

Figure 5.14: The equivorticity patterns, streamline patterns and the pressure distibution in the near wake region of the cylinder over two periods of cylinder oscillation, $2T$, at $R = 200 : A = 0.13, f/f_0 = 1.75$ when $h = 0.5, Fr = 0.4$ $[T \approx 2.886, 43.29 \leq t \leq 49.06 : (15T, 17T)]$. The quasi-locked-on $\mathbf{C(2S)}^*$ mode, per $2T$, is observed.

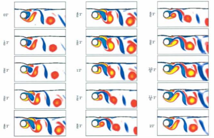

Figure 5.15: The equivorticity patterns over two periods of cylinder oscillation, $2T$, at $R = 200$: $A = 0.13, f/f_0 = 2.25$ when $h = 0.5, Fr = 0.4$ [$T \approx 2.245, 26.93 \le t \le 31.42$: $(12T, 14T)$]. The quasi-locked-on $\mathbf{C(2S)}^*$ mode, per $2T$, is observed.

In Figure 5.15, the equivorticity patterns are displayed for $f/f_0 = 2.25$ over two periods of cylinder oscillation, $2T$. The vortex shedding mode is the quasi-locked-on $\mathbf{C(2S)}^*$ mode, per $2T$, within $4T \le t \le 22T$. The flow is non-periodic for $t > 22T$. This is consistent with the behaviour of C_L and C_D at this frequency ratio. A negative vortex, formed from the coalescence of two negative vortices at $t = T/2$, develops over $2T/3 \le t \le 11T/6$. Then, this negative vortex sheds from the upper side of the cylinder at $t = 2T$. Meanwhile a positive vortex formed during the previous vortex shedding cycle, continues to develop over $0T \le t \le 4T/6$ and subsequently sheds into the near wake of the cylinder at $t = 5T/6$.

Figure 5.16 displays the pressure contours for frequency ratio $f/f_0 = 2.25$ over two

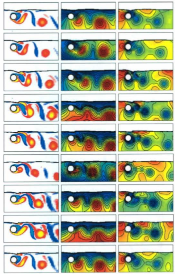

Figure 5.16: The equivorticity patterns, streamline patterns and the pressure distibution in the near wake region of the cylinder over two periods of cylinder oscillation, $2T$, at $R = 200$: $A = 0.13, f/f_0 = 2.25$ when $h = 0.5, Fr = 0.4$ [$T \approx 2.245, 26.93 \leq t \leq 31.42$: $(12T, 14T)$]. The quasi-locked-on $\mathbf{C(2S)}^*$ mode, per $2T$, is observed.

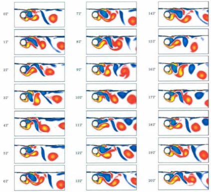

Figure 5.17: The equivorticity patterns over twenty periods of cylinder oscillation, $20T$, at $R = 200$: A=0.13, $f/f_0 = 2.75$ when $h = 0.5, Fr = 0.4$ $[T \approx 1.837, 9.183 \leq t \leq 45.91 : (5T, 25T)]$ (non-periodic state).

periods of cylinder oscillation, $2T$. At $t = 0$, the high pressure region has developed in the stagnation region of the cylinder and the low pressure region has developed in the upper side, and downstream, of the cylinder. Over $0 \leq t \leq 3T/4$ as the positive vortex develops, it is evident that the low pressure region shifts mostly from the upper side of the cylinder to the lower side of the cylinder, and downstream. The high pressure region shifts in a clockwise direction during this time. Synonomous with the development of the negative vortex over $T \leq t \leq 2T$, the low pressure region shifts mostly from the lower side of the cylinder to the upper side. The high pressure region seems to move in a counter-clockwise direction around the left side of the cylinder, at this time. At $t = 0, 5T/4, 7T/4$, it is evident that the presence of the high pressure region is not only high in the stagnation region but above and below the low pressure regions in the downstream of the cylinder as well. The low pressure contours at $t = 0T$ and $t = 2T$ are nearly identical, hence the quasi-periodic nature of the flow field is reproduced in this figure.

Figure 5.17 presents the equivorticity patterns for $f/f_0 = 2.75$ for over twenty periods of cylinder oscillation, $20T$. This figure is presented in accompaniment with the lift and Lissajous patterns and the power density spectrum of frequency ratio $f/f_0 = 2.75$ to conclude that indeed no lock-on mode exists for this case. Coalescence is observed at this frequency ratio.

5.1.5 Fluid forces at $Fr = 0.4:\ h = 0.25$

Figure 5.18 displays the time history of the lift coefficient, C_L, and the PSD and Lissajous patterns, $C_L(x)$, of C_L. It is evident that for the smallest and largest frequency ratios, $f/f_0 = 1.25, 2.75$, the C_L tracess exhibit almost repeatable signatures every four periods of cylinder oscillation, $4T$, within $7T \leq t \leq 14T$ and $19T \leq t \leq 27T$, respectively. The quasi-periodicity of the C_L patterns for $f/f_0 = 1.25, 2.75$ indicate a lock-on between the cylinder motions and the C_L patterns. A complete loss of phase-locking occurs for the frequency ratios $f/f_0 = 1.75$ and 2.25. The traces of both frequency ratios display non-repeatable signatures. The corresponding spectra of $f/f_0 = 1.25, 1.75, 2.25, 2.75$, indicate that the respective C_L traces oscillate at the forcing frequency f. It should be noted however that additional large peaks occur at $2f + 3f_0/2$ and $2f$ for $f/f_0 1.75$ and 2.25, respectively. It is interesting to note that as the cylinder submergence depth decreases from $h \approx \infty$ to 0.25, the effect of the natural shedding frequency, f_0, on C_L decreases, and the effect of the forcing frequency, f, on C_L increases for the case $Fr = 0.4$. Furthermore, the $C_L(x)$ patterns of C_L display somewhat congruent shapes for $f/f_0 = 1.25$ and 2.75, in the quasi-periodic flow states, and less congruent shapes for the non-periodic states of the flow for $f/f_0 = 1.25, 2.75$ and $f/f_0 = 1.75, 2.25$. It is evident that for all f/f_0, the hysteresis loops are largely confined to the lower half plane, as compared to those at the reference case $h = \infty$.

In Figure 5.19, the time history of the drag coefficient, C_D, the PSD of C_D, and the Lissajous patterns of C_D are displayed. Similarly to what was observed in C_L for $f/f_0 = 1.25$, the C_D trace displays almost periodic behaviour every four periods of cylinder oscillation, $4T$. The C_D trace for $f/f_0 = 2.25$ is almost periodic every $3T$ as compared to the non-repeatable signature of the C_L trace. Non persistent patterns of C_D are observed for $f/f_0 = 1.75$ and, in contradiction to what was seen in the C_L trace, $f/f_0 = 2.75$. In all cases the dominant peak occurs at the forcing frequency, f. However, the PSD of $f/f_0 = 1.75$ and 2.25 also display additional large peaks at $2f + 3f_0/2$ and $2f$, respectively. The signatures of $C_D(x)$ are highly congruent for $f/f_0 = 1.25$ and 2.75 for the quasi-periodic states of the flow, and therefore indicate that C_D is phase-locked to the cylinder motion at these frequency ratios. On the other hand, the $C_D(x)$ patterns for $f/f_0 = 1.25, 2.75$ and $f/f_0 = 1.75, 2.25$ for the non-periodic states of the flow display increased phase variations and less congruent

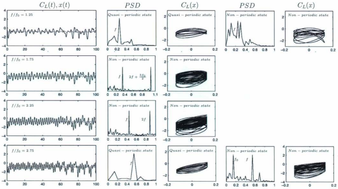

Figure 5.18: The time variation of lift coefficient, C_L, (black) and the streamwise displacement, $x(t)$, (gray); PSD of C_L; Lissajous patterns of C_L at $R = 200 : A = 0.13, f/f_0 = 1.25, 1.75, 2.25, 2.75$ when $h = 0.25, Fr = 0.4$. The Lissajous patterns and PSD plots for $f/f_0 = 1.25, 2.75$ are obtained for quasi-periodic states in the following time intervals $7T \leq t \leq 14T$ and $9T \leq t \leq 27T$, respectively. The corresponding flow states in the near wake region are also indicated for each f/f_0.

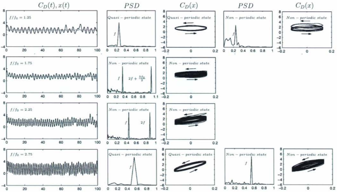

Figure 5.19: The time variation of drag coefficient, C_D, (black) and the streamwise displacement, $x(t)$, (gray); PSD of C_D; Lissajous patterns of C_D at $R = 200 : A = 0.13, f/f_0 = 1.25, 1.75, 2.25, 2.75$ when $h = 0.25, Fr = 0.4$. The Lissajous patterns and PSD plots for $f/f_0 = 1.25, 2.75$ are obtained for quasi-periodic states in the following time intervals $7T \leq t \leq 14T$ and $9T \leq t \leq 27T$, respectively. The corresponding flow states in the near wake region are also indicated for each f/f_0.

shapes. Similarly to the reference case, $h = \infty$, it is evident that the $C_D(x)$ patterns are essentially confined to the upper half plane. The direction of the hysteresis loops for $C_D(x)$ is counter-clockwise and this suggests that the transfer of mechanical energy is from the cylinder to the fluid.

5.1.6 Vortex formation modes at $Fr = 0.4: \ h = 0.25$

In Figures 5.20-5.25 the equivorticity and streamline patterns, and pressure contours in the near wake region of the cylinder when $f/f_0 = 1.25, 1.75, 2.25, 2.75$, are displayed. The observed flow behaviour is (i) quasi-periodic, per $4T$, for $f/f_0 = 1.25, 2.75$ and (ii) non-periodic for $f/f_0 = 1.75, 2.25$.

In Figure 5.20, the equivorticity patterns for $f/f_0 = 1.25$ are displayed over four periods of cylinder oscillation, $4T$. The vortex shedding mode is the quasi-locked-on $\mathbf{C(4S)}^*$ mode, per $4T$, within $7T \leq t \leq 14T$. The flow becomes non-periodic at $t > 17T$. This is consistent with the behaviour of C_L and C_D at this frequency ratio. In the upper vortex shedding region, a negative vortex develops over $0 \leq t \leq T/2$ and then approaches a negative vortex attached to the free surface at $t = 2T/3$. A primary negative vortex develops in the near wake of the cylinder, and as a consequence the negative vortex which has attached to the negative vortex at the free surface detaches over $5T/6 \leq t \leq 7T/6$. This vortex is fully shed into the upper shedding layer at $t = 4T/3$. It is the case that this shed vortex remains in contact with the free surface. Over $4T/3 \leq t \leq 2T$, the secondary negative vortex in the near wake of the cylinder develops. This negative vortex contacts the free surface at $t = 13T/6$

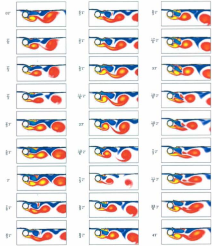

Figure 5.20: The equivorticity patterns over seven periods of cylinder oscillation, $4T$, at $R = 200$: A=0.13, $f/f_0 = 1.25$ when $h = 0.25, Fr = 0.4$ [$T \approx 4.04, 32.32 \leq t \leq 48.48$: $(8T, 12T)$]. The quasi-locked-on $\mathbf{C(4S)}^*$ mode, per $4T$, is observed.

and as a result sheds into the upper vortex shedding layer at $t = 7T/3$. Meanwhile in the lower vortex shedding region, it can be seen that the positive vortex developed in the previous shedding cycle sheds downstream of the cylinder at $t = T/3$. Over

$2T/3 \leq t \leq 4T/3$, two positive vortices co-rotate, and then coalesce at $t = 3T/2$. The resulting positive vortex is then shed into the downstream of the cylinder at $t \approx 2T$.

For $f/f_0 = 1.25$, the pressure contours in the near wake of the cylinder are displayed over four periods of cylinder oscillation, $4T$, in Figure 5.21. At $t = 0$, the low pressure region develops downstream of the cylinder and towards the lower side of the cylinder. The high pressure region develops in the stagnation region of the cylinder. Synonomous with the shedding of a positive vortex at $t = T/3$ (see Figure 5.20), it can be seen that the concentration of low pressure behind the cylinder dramatically decreases. The high pressure region seems to shift counterclockwise. On the other hand, as a positive vortex develops and a secondary positive vortex sheds at $t = 2T$, it can be seen that the region of low pressure shifts mostly behind the cylinder and that the concentration of low pressure increases dramtically. In general, when there are significantly large vortices in the downstream of the cylinder (very near wake) at $t = T, 2T, 3T, 4T$, the concentration of low pressure is high in the downstream of the cylinder at these times. It is interesting to note that the low pressure structures in the near wake of the cylinder, at $t = 0, T/2, T$, are quite similar to images of the low pressure at $t = 2T$ $(4T), 3T/2$ $(5T/2, 7T/2), 3T$. Hence, the periodic nature of the flow field is reproduced for $f/f_0 = 1.25$.

Figure 5.22 and 5.23 display the equivorticity patterns for $f/f_0 = 1.75$ and 2.25, respectively over twenty periods of cylinder oscillation, $20T$. From both Figures, it is evident that the frequency of the vortex shedding is not locked-on to the frequency of the cylinder motion. Coalescence is observed at both frequency ratios.

Figure 5.24 displays the equivorticity patterns of $f/f_0 = 2.75$ over four periods of

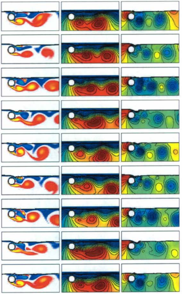

Figure 5.21: The equivorticity patterns, streamline patterns and the pressure distibution in the near wake region of the cylinder over four periods of cylinder oscillation, $4T$, at $R = 200$: A=0.13, $f/f_0 = 1.25$ when $h = 0.25, Fr = 0.4$ [$T \approx 4.04, 32.32 \leq t \leq 48.48$: $(8T, 12T)$]. The quasi-locked-on $\mathbf{C(4S)}^*$ mode, per $4T$, is observed.

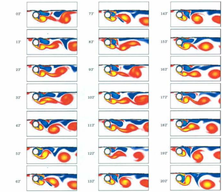

Figure 5.22: The equivorticity patterns over twenty periods of cylinder oscillation, $20T$, at $R = 200$: A=0.13, $f/f_0 = 1.75$ when $h = 0.25, Fr = 0.4$ [$T \approx 2.886, 14.43 \leq t \leq 72.15$: $(5T, 25T)$] (non-periodic state).

cylinder oscillation, $4T$. The vortex shedding mode is the quasi-locked-on $\mathbf{C(2S)}^*$ mode, per $4T$, within $19T \leq t \leq 27T$. The flow is non-periodic for $t > 27T$. This is consistent with C_L behaviour for this frequency ratio. This figure displays the alternate and out-of-phase shedding of one single vortex from both the upper and lower vortex shedding regions of the cylinder. Over $0 \leq t \leq T/3$, a negative vortex formed during the previous vortex shedding cycle continues to develop in the upper shedding layer. At $t = T/2$, this negative vortex attaches to a negative vortex already

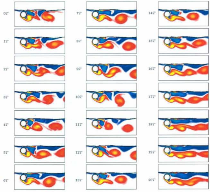

Figure 5.23: The equivorticity patterns over twenty periods of cylinder oscillation, $20T$, at $R = 200$: A=0.13, $f/f_0 = 2.25$ when $h = 0.25, Fr = 0.4$ [$T \approx 2.245, 11.22 \leq t \leq 56.12$: $(5T, 25T)$] (non-periodic state).

attached to the free surface. A new negative vortex begins to develop at this time and starts to co-rotate with the secondary negative vortex in the near wake of the cylinder over $2T/3 \leq t \leq 7T/6$. A third negative vortex forms in the near wake region at $t = 4T/3$ and the three negative vortices co-rotate over $3T/2 \leq t \leq 5T/3$. At $t = 11T/6$, the primary and secondary vortices coalesce in the near wake region. The resulting vortex then co-rotates with the now secondary vortex over $11T/6 \leq t \leq 17T/6$ and at $t = 3T$ this secondary vortex sheds into the upper vortex shedding layer. In the lower

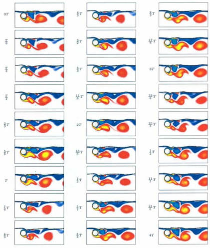

Figure 5.24: The equivorticity patterns over seven periods of cylinder oscillation, $4T$, at $R = 200$: A=0.13, $f/f_0 = 2.75$ when $h = 0.25, Fr = 0.4$ $[T \approx 1.84, 40.40 \leq t \leq 47.75 : (22T, 26T)]$. The quasi-locked-on $\mathbf{C(2S)}^*$ mode, per $4T$, is observed.

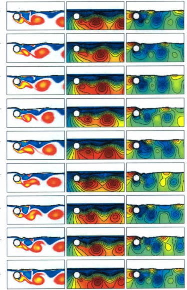

Figure 5.25: The equivorticity patterns, streamline patterns and the pressure distibution in the near wake region of the cylinder over four periods of cylinder oscillation, $4T$, at $R = 200$: A=0.13, $f/f_0 = 2.75$ when $h = 0.25, Fr = 0.4$ [$T \approx 1.84, 40.40 \leq t \leq 47.75$: $(22T, 26T)$]. The quasi-locked-on $\mathbf{C(4S)}^*$ mode, per $4T$, is observed.

vortex shedding layer, it can be seen from that a positive vortex developed from the previous shedding cycle, continues to develop over $0T \leq t \leq T$. This positive vortex sheds from the lower vortex shedding layer of the cylinder at $t = T$.

In the last column of Figure 5.25, the pressure contours are displayed for $f/f_0 = 2.75$ for over four periods of cylinder ocillations, $4T$. The pressure plots indicate that the low pressure region initially develops in the lower side, and downstream of the cylinder. The high pressure region develops in the stagnation region. As a positive vortex develops over $0 \leq t \leq T$, it is evident that at $t = T$, that the low pressure region has mostly shifted to the downstream of the cylinder in the very near wake. At $t = 2T, 3T, 4T$, synonomous with the development of new negative and positive vortices it is evident that the low pressure region shifts mostly behind the cylinder in the near wake as well. It is evident at $t = 0T, T, 2T, 3T, 4T$, that the high pressure region resides mostly in the stagnation region, immediately in front of the cylinder. At $t = T/2, 3T/2, 5T/2, 7T/2$, the high pressure region shifts mostly to the upper left side of the cylinder. The low pressure structures at $t = 0T$ and $t = 4T$ are nearly identical, hence the quasi-periodic nature of the flow field is reproduced at this frequency ratio, $f/f_0 = 2.75$.

5.2 Summary and Discussion

Table 5.1 summarizes the effect free surface inclusion has on the flow regimes, the vortex shedding modes and their periods, T_v, for the case $Fr = 0.4$ at $h = 0.75, 0.5, 0.25$ when $f/f_0 = 1.25, 1.75, 2.25, 2.75$. Table 5.1 displays that for the case $Fr = 0.4$, the presence of the free surface at $h = 0.25$ seems to break up the periodicity of vortex shedding when $f/f_0 = 1.75, 2.25$. Destabilization of the flow also occurs at the cylinder submergence depths $h = 0.75$ when $f/f_0 = 1.25, 2.75$, and at $h = 0.5$ when $f/f_0 = 2.75$, compared to the reference case $h = \infty$. Interesting to note is that the period of the vortex shedding is $2T$ for $f/f_0 = 1.75$, at $h = \infty, 0.75, 0.5$. Similarly, the period of vortex shedding is $2T$ for $f/f_0 = 2.25$ at the larger cylinder submergence depths $h = 0.75, 0.5$. At $f/f_0 = 2.25$, it is evident that the decrease in cylinder submergence depth from $h = 0.75$ to $h = 0.5$, does not result in a switchover in vortex shedding modes. A switchover in vortex shedding modes, however, is observed for $f/f_0 = 1.75$ as $h = 0.75$ decreases to $h = 0.5$. Furthermore, at $h = 0.25$ the period of vortex shedding is $4T$ for both $f/f_0 = 1.25, 2.75$ where quasi-periodic behaviour of the flow is observed. The commonly observed mode for the case $Fr = 0.4$ is the classical $\mathbf{C(2S)}^*$ mode.

	$h = \infty$		$h = 0.75$		$h = 0.5$		$h = 0.25$	
f/f_0	Mode	T_v	Mode	T_v	Mode	T_v	Mode	T_v
1.25	$\mathbf{C(10S)}^*$	$7T$	non-locked	-	$\mathbf{C(8S)}^*$	$5T$	$\mathbf{C(4S)}^*$	$4T$
1.75	$\mathbf{2P}$	$2T$	$\mathbf{C(P+S)}^*$	$2T$	$\mathbf{C(2S)}^*$	$2T$	non-locked	-
2.25	$\mathbf{C(8S)}^*$	$9T$	$\mathbf{C(2S)}^*$	$2T$	$\mathbf{C(2S)}^*$	$2T$	non-locked	-
2.75	$\mathbf{C(P+S)}^*$	$3T$	non-locked	-	non-locked	-	$\mathbf{C(2S)}^*$	$4T$

Table 5.1: The effect of the free surface inclusion on vortex shedding modes and their periods, T_v, for the case $Fr = 0.4$ when $h = 0.25, 0.5, 0.75, \infty$ at $R = 200$: $A = 0.13, f/f_0 = 1.25, 1.75, 2.25, 2.75$. The superscript "*" denotes quasi-locked-on modes.

Table 5.2 displays the values of the mean lift and drag coefficents $\widehat{C_L}$ and $\widehat{C_D}$, for the parameters $Fr = 0.4, R = 200 : A = 0.13, h = 0.75, 0.5, 0.25, \infty$ when $f/f_0 = 1.25, 1.75, 2.25, 2.75$. Upon inspection, it is evident that for $h = 0.75, 0.5, 0.25$ all f/f_0 values of $\widehat{C_L}$ are negative, whereas those in the absence of a free surface, $h = \infty$, are positive. It can be seen that the magnitude of each $\widehat{C_L}$ value, in the presence of a free surface at $h = 0.75, 0.5, 0.25$, are much larger than the $\widehat{C_L}$ values in the absence of a free surface, $h = \infty$. Furthermone, it is evident that $\widehat{C_L}$ varies within the range $-0.8245 \leq \widehat{C_L} \leq -0.1950$ when the free surface is present. Also, as h decreases from 0.75 to 0.25, it can be seen that the values of $\widehat{C_L}$ decrease susbstantially (Q:Can this contribute to the $C_L(x)$ patterns shifting substantially into the lower 1/2 plane). When in the presence of a free surface, the $\widehat{C_L}$ values of each f/f_0 decrease as f/f_0 increases from 1.25 to 2.75, with the exception of $f/f_0 = 1.75, 2.25$ when $h = 0.25$. Analyzing the mean drag coefficient, $\widehat{C_D}$, values it is evident that there is not much fluctuation in these values as h decreases from 0.75 to 0.25. Each $\widehat{C_D}$ values are positive and are confined with the range $1.4477 \leq \widehat{C_D} \leq 1.8790$ when the free surface is present. Similarly to $\widehat{C_L}$, the values of $\widehat{C_D}$ increase as f/f_0 increases from 1.25 to 2.75, with the exception of $f/f_0 = 2.75$ at $h = 0.75, h = 0.5$ and $f/f_0 = 1.25$ at $h = 0.25$.

Table 5.3 displays the RMS values of the lift and drag coefficients, $C_{L,RMS}, C_{D,RMS}$. The RMS values of the lift and drag coefficients are presented for $h = 0.75, 0.5, 0.25$ and compared to the RMS values of the reference case $h = \infty$. It is evident that as the cylinder submergence depth is decreased from ∞ to 0.25, the values of the RMS lift coefficient, $C_{L,RMS}$, increase, with the exception of $f/f_0 = 1.25, 1.75, 2.25$ when $h = 0.5$. Furthermore, it is evident that as f/f_0 increases from 1.25 to 2.75, the

	$\widehat{C_L}$				$\widehat{C_D}$			
f/f_0	$h=\infty$	$h=0.75$	$h=0.5$	$h=0.25$	$h=\infty$	$h=0.75$	$h=0.5$	$h=0.25$
1.25	0.0055	-0.1950	-0.3720	-0.8245	1.2467	1.6301	1.550	1.5405
1.75	0.0044	-0.2039	-0.3918	-0.6676	1.4023	1.636	1.6006	1.4477
2.25	0.0007	-0.2144	-0.4485	-0.8077	1.2610	1.879	1.7336	1.4950
2.75	0.0130	-0.2744	-0.4405	-0.8775	1.2235	1.6796	1.6114	1.5549

Table 5.2: The effect of the free surface inclusion on the mean lift, $\widehat{C_L}$, and drag, $\widehat{C_D}$, coefficients for the case $Fr = 0.4$ when $h = 0.25, 0.5, 0.75, \infty$ at $R = 200$: $A = 0.13, f/f_0 = 1.25, 1.75, 2.25, 2.75$.

	$C_{L,rms}$				$C_{D,rms}$			
f/f_0	$h=\infty$	$h=0.75$	$h=0.5$	$h=0.25$	$h=\infty$	$h=0.75$	$h=0.5$	$h=0.25$
1.25	0.4926	0.6960	0.6282	0.9565	1.3157	1.6781	1.6418	1.6971
1.75	0.7401	0.8353	0.7825	0.8914	1.5951	1.7485	1.7084	1.5783
2.25	0.4205	0.9726	0.9626	1.0387	1.7617	2.165	2.0289	1.7469
2.75	0.3302	0.7166	0.7166	1.0971	2.2544	2.3071	2.1857	2.0534

Table 5.3: The effect of the free surface inclusion on the RMS lift, $C_{L,rms}$, and drag, $C_{D,rms}$, coefficients for the case $Fr = 0.4$ when $h = 0.25, 0.5, 0.75, \infty$ at $R = 200$: $A = 0.13, f/f_0 = 1.25, 1.75, 2.25, 2.75$.

$C_{L,RMS}$ values increase, except for the cases $f/f_0 = 1.75$ when $h = 0.25$; $f/f_0 = 2.75$ when $h = 0.5, 0.75$. The maximum increase observed for $C_{L,RMS}$ values is by a factor of 3.32. From Table 5.3, it is evident that when the cylinder submergence depth increases from 0.25 to 0.75, the RMS values of the drag coefficient, $C_{D,RMS}$ increases for $f/f_0 = 1.75, 2.25.275$. On the other hand, the $C_{D,RMS}$ values tend to decrease, with the exception of $f/f_0 = 1.25$ at $h = 0.75$. Overall, as f/f_0 increases from 1.25 to 2.75, the $C_{D,RMS}$ values increase, with the exception of $f/f_0 = 1.75$ when $h = 0.25$. The maximum increased observed for $C_{D,RMS}$ values is by a factor of 1.29.

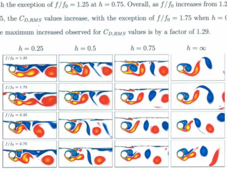

Figure 5.26: The effect of the cylinder submergence depth, h(=0.25, 0.5, 0.75), and the frequency ratio, f/f_0(=1.25, 1.75, 2.25, 2.75), on the equivorticity patterns at $R = 200$: $A = 0.13$, $Fr = 0.4$.

Figures 5.5-5.25, display the pressure contour plots of $h = 0.75, 0.5, 0.25$ when $f/f_0 = 1.25, 1.75, 2.25, 2.75$. The pressure contour plots at $h = 0.25, 0.5, 0.75$ for each f/f_0, periodic/quasi-periodic behaviour is exhibited, display the development of the high pressure region in the stagnation region of the cylinder. For $f/f_0 = 1.75, 2.25$ at

$h = 0.75, 0.5$, the low pressure region develops in the upper side of the cylinder and downstream. For $f/f_0 = 1.25$ at $h = 0.5$ the low pressure region initially develops in the upper, lower, front (closer proximity to near wake than stagnation region) sides, and downstream of the cylinder. On the other hand at $h = 0.25$ for $f/f_0 = 1.25, 2.75$, the low pressure regions develops in the lower side of the cylinder and downstream. In general, the low pressure regions develop in the near wake of the cylinder, where the velocity is highest (formation of new vortices) and hence significantly affect the fluctuating lift forces acting on the circular cylinder. Positive and negative vortices which have shed downstream of the cylinder, are represented by the low pressure region (blue contours) for all f/f_0. Another interesting aspect of the low pressure contours of the circular cylinder is that for some cases, mirror images of the structures of low pressure are observed in the near wake region of the cylinder. Specifically at $h = 0.75$ when $f/f_0 = 2.25$, the low pressure contours in the near wake region of the cylinder at $t = 0(2T), T/4, T/2, 3T/4$ are almost mirror images of the low pressure regions in the near wake region of the cylinder at $t = T, 5T/4, 6T/4, 7T/4, 2T$ (see Figure 5.7). On the other hand, the low pressure structures for $f/f_0 = 1.25$ ($h = 0.25$) at $t = 0, T/2, T$ are similar to images of the low pressure structures at $t = 2T$ $(4T), 3T/2$ $(5T/2.7T/2), 3T$ (see Figure 5.21). An interesting trend observed in this thesis is the presence of the high pressure regions above and below the low pressure contours in the downstream of the cylinder. At $h = 0.75$ when $f/f_0 = 1.75$, the high pressure region has significant presence above and below the low pressure regions in the downstream of the cylinder at $t = 0, T/2, 3T/4, 6T/4, 7T/4, 2T$. Similarly, at $h = 0.5$ when $f/f_0 = 1.75, 2.25$ the high pressure regions extend above and below the low pressure contours in the downstream of the cylinder at $t = 0, 3T/4, 7T/4$ and

$t = 0, 5T/4, 7T/4$, respectively (see Figures 5.14-5.16).

The effect of cylinder submergence depth, $h = 0.25, 0.5, 0.75$, and the frequency ratio, $f/f_0 = 1.25, 1.75, 2.25, 2.75$ on the equivorticity patterns for the case $R = 200, A = 0.13$ when $Fr = 0.4$ is displayed in Figure 5.26. The reference case $h = \infty$ is presented to help demonstrate the changes the vorticity undergoes in the near wake of the cylinder with the inclusion of free surface. All snapshots are taken at the instant the cylinder reaches maximum displacement, $x(t) = A$ and are taken within the time interval the flow reaches a periodic/quasi-periodic state. For non-periodics cases, the snapshots are taken within $0 < t \leq 100$. It is immediately evident that opposed to the case $Fr \approx 0.0$, the free surface undergoes considerable deformation. In comparison to the reference case $h = \infty$, it is evident that as h decreases from 0.75 to 0.25 the near wake structure of the vorticity change considerably. From this figure it is evident that opposed to the cases $Fr \approx 0.0$ and $Fr = 0.2$, that a considerable amount of opposite signed vorticity is present at the free surface and in the flow. This vorticity interferes with the development of negative vorticity in the upper shear layer of the cylinder at $h = 0.75$ at the smallest cylinder submergence depth, and at $h = 0.5, 0.25$ for each f/f_0. At each cylinder submergence depth, h, shed negative vortices seem to be lifted up towards the free surface aided by the propogation of positive vorticity into the upper shedding layer. As a result, these negative vortices dissapate rapidly, and become weak, as they approach the free surface. Hence, the vortex shedding becomes more skew symmetric in favour of the positive vortices as the cylinder submergence depth decreases from ∞ to 0.25. It can be seen that the major axes of the negative vortices downstream of the cylinder tend to lie perpendicular to the free surface for the larger cylinder submergence depths, $h = 0.5, 0.75, \infty$. On the other hand, the major axes of the negative vortices at $h = 0.25$ tend to lie more parallel to the free surface. This is a result of the strong interaction with the free surface and the rapid diffusion of these vortices after contact is made. Both cases also apply to the shed positive vortices in the downstream of the cylinder, except that the positive vortices do not primarily interact with the free surface. In general, the vortex formation length remains consistent as h decreases from ∞ to 0.25, for all f/f_0, except the cases $h = 0.25$ when $f/f_0 = 1.25, 1.75, 2.75$ (maximum increase $\approx$ 23%). On the other hand, the increase in f/f_0 from 1.25 to 2.25 results in a decrease in vortex formation length (maximum by $\approx$ 44%) for the cylinder submergence depths $h = 0.25, 0, 5, 0.75, \infty$.

6. Flow past a transversely ocillating circular cylinder

This Chapter analyzes the results for flow past a transversely oscillating cylinder. The numerical simulations are carried out at a Reynolds number of $R = 200$, at cylinder submergence depths of $h = \infty$ (absence of free-surface) and $h = 0.5$ (presence of free-surface), a displacement amplitude of $A = 0.13$, in the frequency range of $1.25 \leq f/f_0 \leq 2.75$, where f/f_0 increases by increments of 0.5. The results are obtained by analyzing the fluid forces acting on the cylinder and by means of the equivorticity patterns in the near wake of the cylinder. It should be noted that the results obtained for flow past a transversely oscillating cylinder in the absence of a free surface, will be compared to those obtained under the same conditions as above with the exception of the cylinder submergence depth, $h = 0.5$. The goal is to understand the effect free-surface inclusion has on vortex shedding modes and fluid forces acting on the cylinder. The unsteady flow calculations are conducted up to time $t = 100$ when $h = \infty$ and $h = 0.5$, when $Fr = 0.2$.

6.1 Flow past a transversely ocillating circular cylinder in the absence of a free surface

6.1.1 Fluid Forces ($h = \infty$) :

Figure 6.1 displays the time history of the fluctuating lift coefficient, C_L, and the PSD of the lift coefficient. For $f/f_0 = 1.25$ and 1.75, the traces of the lift coefficient display almost repeatable signatures, every $9T$, within $5T \leq t \leq 24T$ and $5T \leq t \leq 34T$, respectively. The trace of C_L for $f/f_0 = 2.25$ displays a quasi-periodic signature every $7T$ within $6T \leq t \leq 43T$. Finally, the trace of C_L for $f/f_0 = 2.75$ displays a quasi-periodic signature every $3T$ within $8T \leq t \leq 54T$. The corresponding spectra of the lift coefficients display peaks at the natural shedding frequency, f_0, and the forcing frequency, f. The dominant peak, however, occurs at f for each f/f_0. It should also be noted that a significant peak occurs at $f + 2f_0$ in the spectrum of $f/f_0 = 2.75$, which is indicative of a decrease in the effect of f on C_L as f/f_0 increases from 1.25 to 2.75.

In Figure 6.2, the time history of the fluctuating drag coefficient, C_D, and the PSD of C_D is displayed. The traces of the drag coefficient display almost repeatable signatures for $f/f_0 = 1.25, 1.75, 2.25, 2.75$, every $9T, 9T, 7T$ and $3T$, respectively. It is evident from Figure 2, that each spectra displays multiple peaks for each frequency ratio. For $f/f_0 = 1.25, 1.75, 2.25, 2.75$, the dominant peak occurs at $f_0/4, 3f_0/4, 5f_0/4$ and $7f_0/4$, respectively. Evidently, an increase of $f_0/2$ is observed from dominant peak to dominant peak as f/f_0 increases from 1.25 to 2.75.

In Figure 6.3, the Lissajous patterns of $C_L, C_L(y)$, and $C_D, C_D(y)$, are displayed. It can be seen that the hysteresis loops associated with $C_L(y)$ are confined to both the upper and lower half-planes for each frequency ratio, $f/f_0 = 1.25, 1.75, 2.25, 2.75$. The Lissajous patterns of C_L display somewhat congruent shapes, but it is evident that there is variations in the phase occurring from cycle to cycle of cylinder oscillation as f/f_0 increases from 1.25 to 2.75. In column (b) of Figure 3, the $C_L(y)$ patterns for $f/f_0 = 1.25, 1.75$ are shown for over two periods of cylinder oscillation, $2T$, to

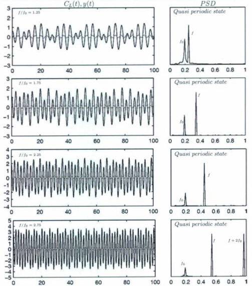

Figure 6.1: The time variation of lift coefficient, C_L, (black) and the transverse displacement, $y(t)$, (gray); PSD of C_L; at $R = 200 : A = 0.13, f/f_0 = 1.25, 1.75, 2.25, 2.75$ when $h = \infty$. The PSD plots for $f/f_0 = 1.25, 1.75, 2.25, 2.75$ are obtained for quasi-periodic states in the following time intervals $5T \le t \le 24T, 5T \le t \le 34T, 6T \le t \le 43T, 8T \le t \le 54T$, respectively. The corresponding flow states in the near wake region are also indicated for each f/f_0.

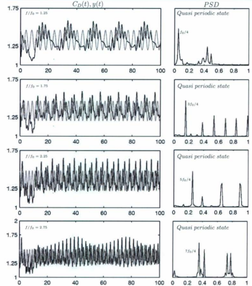

Figure 6.2: The time variation of drag coefficient, C_D, (black) and the transverse displacement, $y(t)$, (gray); PSD of C_D at $R = 200$: $A = 0.13$, $f/f_0 = 1.25, 1.75, 2.25, 2.75$ when $h = \infty$. The PSD plots for $f/f_0 = 1.25, 1.75, 2.25, 2.75$ are obtained for quasi-periodic states in the following time intervals $5T \leq t \leq 24T, 5T \leq t \leq 34T, 6T \leq t \leq 43T, 8T \leq t \leq 54T$, respectively. The corresponding flow states in the near wake region are also indicated for each f/f_0.

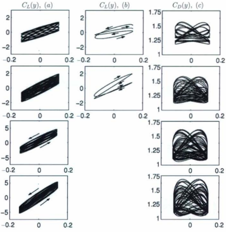

Figure 6.3: Lissajous patterns of $C_L(y), (a), (b)$, and $C_D(y), (c)$, for $R = 200, A = 0.13, h = \infty$, and $f/f_0 = 1.25, 1.75, 2.25, 2.75$. (from top to bottom). The $C_L(y)$ patterns for $f/f_0 = 1.25, 1.75$ in column b are shown for two periods of cylinder oscillation to display the change in mechanical energy transfer between cylinder and fluid. The Lissajous patterns in column (a) and (c) for $f/f_0 = 1.25, 1.75, 2.25, 2.75$ are obtained for quasi-periodic states in the following time intervals $5T \leq t \leq 24T, 5T \leq t \leq 34T, 6T \leq t \leq 43T, 8T \leq t \leq 54T$, respectively.

display the change in the transfer of mechanical energy. The direction of $C_L(y)$, for $f/f_0 = 1.25, 1.75$, changes from a counter-clockwise direction to a clockwise direction. Therefore, in both cases, the mechanical energy is transferred between the cylinder and fluid. The direction of the hystersis loops of $C_L(y)$ for $f/f_0 = 2.25, 2.75$, are counterclockwise, and thus the energy transfer is from the cylinder to the fluid. The hysteresis loops associated with $C_D(y)$ are confined predominantly to the upper half-plane. Also evident, is that the trajectories of $C_D(y)$ display less congruent patterns from one cycle to cycle of cylinder oscillation, as f/f_0 increases from 1.25 to 2.75. This indicates an increase in phase variations between C_D and the cylinder motions, and hence a loss of phase-locking occurs.

6.1.2 Vortex formation modes ($h = \infty$) :

In Figure 6.4, the equivorticity patterns are displayed over nine periods of cylinder oscillations, $9T$ for $f/f_0 = 1.25$. The observed lock-on mode is the quasi-locked-on **14S*** mode, per $9T$, within $5T \leq t \leq 24T$. This is consistent with the behaviour of C_L and C_D at this frequency ratio. The flow is non-periodic for $t < 5T$. In this mode, seven vortices develop and then alternately shed on each side of the cylinder, within $9T$. A negative vortex formed during the previous vortex shedding cycle develops over $0 \leq t \leq T$, and then sheds from the primary negative vortex into the upper shedding layer of the cylinder at $t = 3T/2$. A negative vortex developed over $3T/2 \leq t \leq 2T$ sheds from the upper side of the cylinder at $t = 5T/2$. Over $5T/2 \leq t \leq 4T$, a negative vortex develops, and is then forced to shed downstream due to the interaction with a positive vortex in the lower shedding layer at $t = 9T/2$. Shortly after, a negative vortex is shed from the upper vortex shedding layer at $t = 11T/2$. A negative vortex formed over $11T/2 \leq t \leq 6T$, sheds into the upper vortex shedding layer at $t = 13T/2$. Furthermore, a negative vortex developed over $7T \leq t \leq 15T/2$, sheds downstream of the cylinder at $t = 8T$. Finally, a negative vortex develops over $8T \leq t \leq 17T/2$, and then sheds into the upper vortex shedding layer of the cylinder at $t = 9T$. Meanwhile, a positive vortex developed from the previous vortex shedding cycle sheds from the lower side of the cylinder at $t = T/2$. A positive vortex develops over $T/2 \leq t \leq 3T/2$, and then sheds downstream of the cylinder at $t = 2T$. Over $2T \leq t \leq 3T$, a positive vortex develops and is then shed into the lower vortex layer at $t = 7T/2$. A positive vortex developed over $7T/2 \leq t \leq 4T$, sheds downstream of the cylinder at $t = 5T$. Without delay, a positive vortex is shed from the lower side of the cylinder at $t = 6T$. A positive vortex develops over $6T \leq t \leq 13T/2$ and then detaches from the primary vortex in the near wake of the cylinder at $t = 7T$. Lastly, a positive vortex developed over $15T/2 \leq t \leq 17T/2$, sheds into the lower vortex shedding region of the cylinder at $t = 9T$. Coalescence was not observed in this figure.

Figure 6.5 displays the pressure contours for $f/f_0 = 1.25$, over nine periods of cylinder oscillation, $9T$. Initially, this figure displays the development of high pressure in the lower left area of the stagnation region, and the low pressure region in the upper side and downstream of the cylinder. It is evident, that over $9T$, the high pressure region resides predominently in the stagnation region of the cylinder. The concentration of the high pressure regions also remains relatively consistent over the vortex shedding period, $T_v = 9T$. At $t = nT/2$ $(n = 0, 2, 4, 5, 8, 10, 12, 15, 18)$ the low pressure region is confined mostly to the upper side and downstream of the cylinder (near wake). At $t = nT/2$ $(n = 1, 3, 6, 9, 11, 13, 14, 17)$, the low pressure

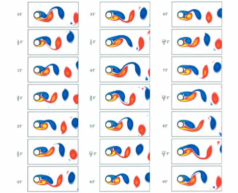

Figure 6.4: The equivorticity patterns over nine periods of cylinder oscillation, $9T$, at $R = 200 : A = 0.13, f/f_0 = 1.25$ when $h = \infty$ $[T \approx 4.04, 52.525 \leq t \leq 89.889 : (13T, 22T)]$. The quasi-locked-on **14S*** mode, per $9T$, is observed.

region is mostly confined to the lower side, and downstream of the cylinder (near wake). At $t = 7T/2, 8T$ the low pressure region is confined predominently to the downstream of the cylinder. For example at $t = 3T/2$, synonomous with the development of the positive vortex in the lower vortex shedding layer, the low pressure region shifts mostly to the lower side and downstream of the cylinder. As the secondary positive vortex detaches, and a new positive vortex is formed, at $t = 2T$, the low pressure region shifts to the upper side of the cylinder. It is evident that the structure of the pressure contours, in the near wake of the cylinder, at $t = 0T$ $(9T), T/2, T, 3T/3, 2T, 5T/2, 3T, 7T/2, 4T, 9T/2$ are almost mirror images of the low pressure regions at $t = 9T/2, 5T, 11T/2, 6T, 13T/2, 7T, 15T/2, 8T, 17T/2$, respectively. Therefore, the pressure contours recreate the periodic nature of the flow field around the cylinder at this frequency ratio.

In Figure 6.6, the equivorticity patterns are displayed for $f/f_0 = 1.75$ over nine periods of cylinder oscillation, $9T$. The observed vortex shedding mode is the quasi-locked-on **10S*** mode, per $9T$, within $5T \leq t \leq 34T$. This is consistent with the behaviour of C_L and C_D at this frequency ratio. A negative vortex formed during the previous vortex shedding cycle develops over $0 \leq t \leq T$, and then sheds from the upper side of the cylinder at $t = 3T/2$. Over $2T \leq t \leq 3T$, a negative vortex develops and then sheds downstream at $t = 7T/2$. A negative vortex developed over $4T \leq t \leq 5T$, sheds as a secondary negative vortex at $t = 11T/2$. Over $6T \leq t \leq 13T/2$, a negative vortex develops and is then shed from the upper side of the cylinder at $t = 7T$. A negative vortex developed over $15T/2 \leq t \leq 17T/2$, sheds into the near wake of the cylinder at $t = 9T$. In the lower vortex shedding region, a secondary positive vortex is shed in the near wake of the cylinder at $t = T$. Over $T \leq t \leq 2T$, a positive vortex develops in the lower side of the cylinder and is then shed downstream of the cylinder at $t = 5T/2$. A positive vortex develops over $3T \leq t \leq 7T/2$, and then seperates from the primary positive vortex in the near wake of the cylinder at $t = 4T$. Furthermore, over $9T/2 \leq t \leq 11T/2$ a positive vortex develops. This vortex is then shed from the lower side of the cylinder at $t = 6T$. A positive vortex develops over $13T/2 \leq t \leq 15T/2$, and then sheds downstream of the cylinder at $t = 8T$. Coalescence was not observed in this figure.

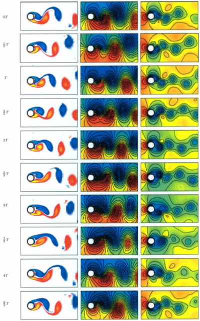

Figure 6.5: The figure caption is given on page 181

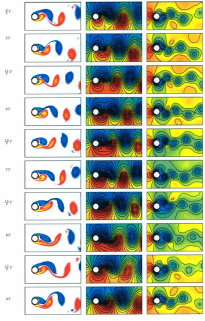

Figure 6.5: The equivorticity patterns(left), streamline patterns(middle) and the pressure contours(right) in the near wake region of the cylinder over nine periods of cylinder oscillation, $9T$, at $R = 200$: A=0.13, $f/f_0 = 1.25$ when $h = \infty$ $[T \approx 4.04, 52.525 \leq t \leq 89.889 : (13T, 22T)]$. The quasi-locked-on **14S*** mode, per $9T$, is observed.

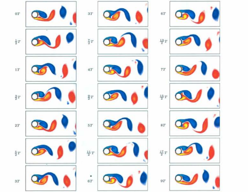

Figure 6.6: The equivorticity patterns over nine periods of cylinder oscillation, $9T$, at $R = 200$: A=0.13, $f/f_0 = 1.75$ when $h = \infty$ [$T \approx 2.886, 37.52 \leq t \leq 63.49$: $(13T, 22T)$]. The quasi-locked-on $\mathbf{10S^*}$ mode, per $9T$, is observed.

In Figure 6.7, the pressure contours are displayed for $f/f_0 = 1.75$ over seven periods of cylinder oscillation, $7T$. At $t = 0T$, this figure displays the development of the low pressure region in the upper side and downstream of the cylinder in the near wake. The development of high pressure occurs in the stagnation region towards the lower side of the cylinder. At $t = nT/2$ ($n = 1, 3, 5, 7, 9, 11, 13, 15, 17$), the high pressure region seems to be confined to the upper area of the stagnation region and moreso above, then below, the low pressure regions in the downstream of the cylinder. At $t = nT/2$ ($n = 0, 2, 4, 6, 8, 10, 12, 14, 16, 18$), the high pressure region seems to be confined to the lower portion of the stagnation region and morese below, than above, the low pressure regions in the downstream of the cylinder. At $t = nT/2$, when n is an even integer, the low pressure region is mostly confined to the upper side and behind the cylinder. At $t = nT/2$, when n is an odd integer, the low pressure region is mostly confined to the lower side and behind the cylinder. Hence, initially the low pressure region shifts from the upper side of the cylinder to the lower side and then back to the upper side, and so on, repeating this cycle until $t = 9T$. It is also interesting to note that similarly to the behaviour of the pressure at $f/f_0 = 1.25$, the structure of the pressure contours at $t = 0T$ $(9T), T/2, T, 3T/3, 2T, 5T/2, 3T, 7T/2, 4T, 9T/2$ are almost mirror images of the low pressure regions at $t = 9T/2, 5T, 11T/2, 6T, 13T/2, 7T, 15T/2, 8T, 17T/2$, respectively. Therefore, the pressure contours recreate the periodic nature of the flow field around the cylinder at this frequency ratio.

Figure 6.8 displays the equivorticity patterns over seven periods of cylinder oscillation, $7T$, for $f/f_0 = 2.25$. The observed mode for this frequency ratio is the quasi-locked-on **6S*** mode, per $7T$, within $6T \le t \le 43T$. In this mode, three vortices develop on each side of the cylinder and shed alternately over $7T$. A negative vortex formed during the previous vortex shedding cycle continues to develop over $0T \le t \le T$ and then sheds downstream of the cylinder at $t \approx 4T/3$. Over $5T/3 \le t \le 11T/3$, the development of a second negative vortex is observed in the near wake region. This vortex subsequently sheds into the downstream of the cylinder at $t \approx 11T/3$. A negative vortex develops over $4T \le t \le 17T/3$ and is shed into the near wake of the cylinder at $t = 6T$. Meanwhile, a positive vortex formed during the previous

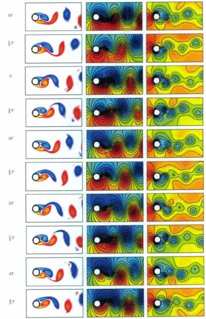

Figure 6.7: The figure caption is given on page 185

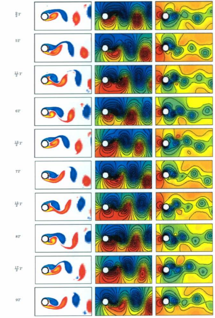

Figure 6.7: The equivorticity patterns(left), streamline patterns(middle) and the pressure contours(right) in the near wake region of the cylinder over nine periods of cylinder oscillation, $9T$, at $R = 200$: A=0.13, $f/f_0 = 1.75$ when $h = \infty$ [$T \approx 2.886, 37.52 \leq t \leq 63.49$: $(13T, 22T)$]. The quasi-locked-on **10S*** mode, per $9T$, is observed.

vortex shedding cycle sheds into the near wake at $t = T/3$. Over $T/3 \leq t \leq 7T/3$, the development of a second positive vortex occurs. This positive vortex is shed from the lower side of the cylinder at $t = 8T/3$. Finally, a positive vortex developing over $10T/3 \leq t \leq 14T/3$ is subject to interaction with a negative vortex in the upper shedding layer and consequently sheds into the downstream of the cylinder at $t = 5T$. Coalescence was not observed in this figure.

In Figure 6.9, the pressure contours of $f/f_0 = 2.25$ are displayed for over seven periods of cylinder oscillation, $7T$. At $t = 0T$, this figure displays the development of the low pressure region in the upper side of the cylinder and downstream (near wake region). The development of high pressure occurs in the stagnation region. At $t = nT/2$ ($n = 1, 3, 5, 7, 9, 11, 13$), the high pressure region is confined mostly to the stagnation region, and moreso above, than below, the low pressure regions in the downstream of the cylinder. Furthermore, the low pressure regions are positioned mostly in the lower side of the cylinder, but also behind the cylinder in the near wake region. At $t = nT/2$ ($n = 0, 2, 4, 6, 8, 10, 12, 14$), the high pressure region seems to be confined to the lower portion of the stagnation region and moreso below, than above, the low pressure regions in the downstream of the cylinder. Furthermore, the low pressure regions are positioned in the upper side of the cylinder, but also behind the cylinder in the near wake region. For example as the negative vortex sheds at $t = T$, the area of high pressure is situated in the lower left portion of the stagnation region and the low pressure is situated in the upper side of the cylinder. As the positive vortex begins to shed over $T \leq t \leq 2T$, the high pressure region shifts cpounter clockwise. At $t = 5T/2$, the high pressure region is positioned in the upper portion of the stagnation region, and the low pressure region in the lower side

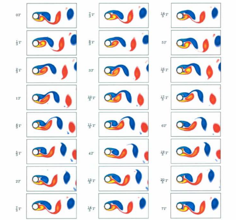

Figure 6.8: The equivorticity patterns over seven periods of cylinder oscillation, $7T$, at $R = 200 : A = 0.13, f/f_0 = 2.25$ when $h = \infty$ $[T \approx 4.04, 60.61 \leq t \leq 88.89 : (15T, 22T)]$. The quasi-locked-on **6S*** mode, per $7T$, is observed.

of the cylinder. It is interesting to note that the structure of the pressure contours at $t = 0T$ $(7T), T/2, T, 3T/3, 2T, 5T/2, 3T$ are almost mirror images of the low pressure regions at $t = 7T/2, 4T, 9T/2, 5T, 11T/2, 6T, 13T/2$, respectively. Therefore, the periodic nature of the flow field are reproduced in the pressure contours.

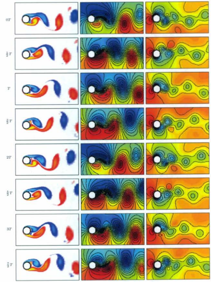

Figure 6.9: The figure caption is given on page 189

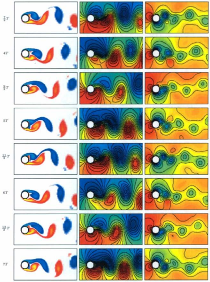

Figure 6.9: The equivorticity patterns(left), streamline patterns(middle) and the pressure contours(right) in the near wake region of the cylinder over seven periods of cylinder oscillation, $7T$, at $R = 200$: A=0.13, $f/f_0 = 2.25$ when $h = \infty$ [$T \approx 2.245, 44.893 \leq t \leq 60.615$: $(20T, 27T)$]. The quasi-locked-on $\mathbf{6S}^*$ mode, per $7T$, is observed.

The equivorticity patterns are displayed for $f/f_0 = 2.75$ over three periods of cylinder oscillations, $3T$, in Figure 6.10. The observed mode for this frequency ratio is the quasi-locked-on $\mathbf{2S}^*$, per $3T$, within $8T \leq t \leq 54T$. This is consistent with the C_L and C_D behaviour at this frequency ratio. The flow is non-periodic for $t < 8T$. This mode describes the alternate shedding of a single vortex from the upper and lower vortex shedding regions of the cylinder within $3T$. At $t = 0$, a negative vortex formed during the previous vortex cycle continues to develop in the upper vortex shedding region over $T/6 \leq t \leq 9T/6$. This negative vortex is then shed from the upper side of the cylinder at $t = 10T/6$. Meanwhile in the lower vortex shedding region, a positive vortex formed during the previous vortex shedding cycle sheds downstream of the cylinder at $t = T/6$.

In Figure 6.11, the pressure distributions in the near wake of the cylinder are displayed for $f/f_0 = 2.75$ over three periods of cylinder oscillation, $3T$. At $t = 0T$, the region of high pressure has developed in the lower left area of the stagnation region. The low pressure region hsa developed in the upper side of the cylinder, following the development of a new negative vortex in the upper vortex layer of the cylinder. It is evident that at $t = nT/2$ $(n = 1, 3, 5)$ the high pressure region resides predominently in the lower left region of the stagnation region, and the low pressure resides in the the lower side of the cylinder. At $t = nT/2$ $(n = 0, 2, 4, 6)$ the high pressure region is mostly confined to the upper left area of the stagnation region, and the low pressure region to the upper side of the cylinder. Synonomous with the shedding and development of a negative vortex at $t = T$, the low pressure shifts from the lower side of the cylinder (at $t = T/2$), to the upper side of the cylinder. As the positive vortex detaches at $t = 5T/2$, the low pressure region moves from the upper

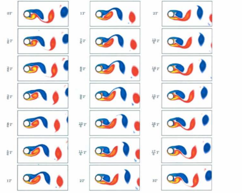

Figure 6.10: The equivorticity patterns over three periods of cylinder oscillation, $3T$, at $R = 200 : A = 0.13, f/f_0 = 2.75$ when $h = \infty$ $[T \approx 1.837, 55.10 \leq t \leq 60.621 : (30T, 33T)]$. The quasi-locked-on $\mathbf{2S^*}$ mode, per $3T$, is observed.

side of the cylinder (at $t = 2T$) to the lower side. The structure of the pressure contours at $t = 0T$ $(3T), T/2, T$ are almost mirror images of the low pressure regions at $t = 3T/2, 2T, 5T/2$, respectively. Therefore, the periodic nature of the flow field are reproduced in the pressure contours.

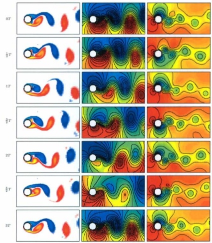

Figure 6.11: The equivorticity patterns, streamline patterns and the pressure distibution in the near wake region of the cylinder over three periods of cylinder oscillation, $3T$, at $R = 200$: A=0.13, $f/f_0 = 2.75$ when $h = \infty$ $[T \approx 1.837, 40.40 \leq t \leq 45.91 : (22T, 25T)]$. The quasi-locked-on $\mathbf{2S}^*$ mode, per $3T$, is observed.

6.2 Fluid forces and vortex shedding modes in the presence of a free surface

6.2.1 Fluid forces at $Fr = 0.2: \ h = 0.5$

The time history of the lift coefficient, C_L, and the spectra of C_L are displayed in Figure 6.12. The C_L trace for $f/f_0 = 2.25$ displays a quasi-periodic signature every $7T$ within $3T \leq t \leq 26T$, followed by a non-periodic signature for $t > 26T$. On the other hand, the C_L trace for $f/f_0 = 2.75$ displays a quasi-periodic signature per $3T$ within $4T \leq t \leq 54T$ ($0T \leq t \leq 4T$, refers to the transition state). The C_L traces for $f/f_0 = 1.25, 1.75$ display non-periodic signatures. The spectrum corresponding to C_L for $f/f_0 = 1.25$, display two peaks at f_0 and f. The spectrum corresponding to the non-periodic state of this frequency ratio, displays a single peak at f. The spectra of $f/f_0 = 1.75$ and $f/f_0 = 2.25$ for the quasi-periodic and non-periodic states of the flow both display a dominant peak at f. Finally, two well defined peaks at f and $f + 3f_0/2$ are observed from the spectrum of $f/f_0 = 2.75$.

Figure 6.13 displays the time history of the drag coefficient, C_D, and the spectra of C_D. It is evident that each C_D trace, corresponding to $f/f_0 = 1.25, 1.75, 2.25, 2.75$, respectively, display non-periodic signatures. The corresponding spectra all display dominant peaks at the forcing frequency, f, with the exception of the spectrum of $f/f_0 = 2.75$ which displays an equally large peak at $f + 3f_0/2$. Hence, once again indicative of the weakened effect of f on C_D.

It is evident that the corresponding Lissajous patterns of $C_L, C_L(y)$, of Figure 6.12 are confined to both the lower and upper half planes. On the other hand, the $C_D(y)$ patterns of Figure 6.13 are confined mostly to the upper half-plane. It is evident that as f/f_0 increase from 1.25 to 2.75, that the total area covered and the congruency of the Lissajous patterns for $C_L(y)$ and $C_D(y)$ increase, and that there is slight shifthing of the patterns into the lower half plane. For $f/f_0 = 1.25$ and $f/f_0 = 1.75$, the mechanical energy transfer occurs between the fluid and cylinder and this is denoted by $\leftrightarrow$. On the other hand, the mechanical energy transfer is from the cylinder to fluid, $' \rightarrow,'$ for $f/f_0 = 2.25$ and 2.75.

6.2.2 Vortex formation modes at $Fr = 0.2: \; h = 0.5$

Figures 6.14-6.19 display the equivorticity and streamline patterns, and pressure contours in the near wake of the cylinder when $f/f_0 = 1.25, 1.75, 2.25$, and 2.75. The observed flow behaviour is (*i*) quasi-periodic per $7T$ for $f/f_0 = 2.25$, and per $3T$ for $f/f_0 = 2.75$ and (*ii*) non-periodic for $f/f_0 = 1.25, 1.75$.

A series of instantaneous equivorticity plots over twenty periods of cylinder oscillation, $20T$, for $f/f_0 = 1.25$ and 1.75 are plotted in Figures 6.14-6.15. Both figure show that the frequency of the vortex shedding is not locked-on to the frequency of the cylinder motion at these frequency ratios. Coalescence was not observed for both frequency ratios.

Figure 6.16 displays the equivorticity patterns over seven periods of cylinder oscillation, $7T$, of the quasi-periodic state when $f/f_0 = 2.25$. The vortex shedding mode is

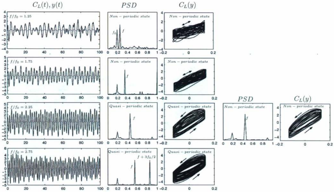

Figure 6.12: The time variation of lift coefficient, C_L, (black) and the transverse displacement, $y(t)$, (gray); PSD of C_L; Lissajous patterns of C_L at $R = 200 : A = 0.13, f/f_0 = 1.25, 1.75, 2.25, 2.75$ when $h = 0.5, Fr = 0.2$. The Lissajous and PSD plots for $f/f_0 = 2.25, 2.75$ are obtained for quasi-periodic states in the following time intervals $3T \leq t \leq 26T$ and $4T \leq t \leq 54T$, respectively. The corresponding flow states in the near wake region are indicated for each f/f_0.

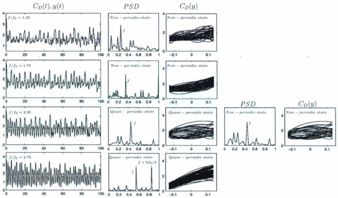

Figure 6.13: The time variation of drag coefficient, C_D, (black) and the transverse displacement, $y(t)$, (gray); PSD of C_D; Lissajous patterns of C_D at $R = 200 : A = 0.13, f/f_0 = 1.25, 1.75, 2.25, 2.75$ when $h = 0.75, Fr = 0.2$. The Lissajous and PSD plots for $f/f_0 = 2.25, 2.75$ are obtained for quasi-periodic states in the following time intervals $3T \leq t \leq 26T$ and $4T \leq t \leq 54T$, respectively. The corresponding flow statess in the near wake region are indicated for each f/f_0.

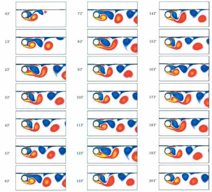

Figure 6.14: The equivorticity patterns over twenty periods of cylinder oscillation, $20T$, at $R = 200$: A=0.13, $f/f_0 = 1.25$ when $h = 0.5, Fr = 0.2$ [$T \approx 4.04, 4.04 \le t \le 84.84$: $(1T, 21T)$] (non-periodic state).

the quasi-locked-on $\mathbf{C(6S)}^*$ mode, per $7T$, within $3T \le t \le 26T$. This is consistent with the C_L behaviour, but not C_D, at this frequency ratio. The flow is non-periodic for $t > 26T$. In this mode, three vortices develop on each side of the cylinder and alternately shed over $7T$. It is also evident from this figure that coalescence of vortices only occurs in the upper shedding layer (only the negative vortices experience coalescence). A negative vortex formed in the previous vortex shedding cycle, coalesces with a second negative vortex at $t = 2T/3$. The resulting negative vortex develops

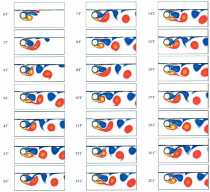

Figure 6.15: The equivorticity patterns over twenty periods of cylinder oscillation, $20T$, at $R = 200$: A=0.13, $f/f_0 = 1.75$ when $h = 0.5, Fr = 0.2$ $[T \approx 2.886, 2.886 \leq t \leq 60.60$: $(1T, 21T)]$ (non-periodic state).

over $T \leq t \leq 4T/3$, and sheds into the upper vortex shedding region at $t \approx 5T/3$. A negative vortex develops over $5T/3 \leq t \leq 7T/3$ and then coalesces with another negative vortex at $t = 8T/3$. This vortex develops over $3T \leq t \leq 10T/3$, and then sheds into the near wake of the cylinder at $t \approx 11T/3$. A negative vortex formed from the coalescence of two negative vortices at $t = 14T/3$, develops over $14T/3 \leq t \leq 5T$. At $t \approx 16T/3$, the negative vortex is seen to approach a second co-rotating negative vortex. These two negative vortices coalesce at $t = 6T$. The resulting negative sheds

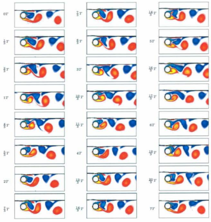

Figure 6.16: The equivorticity patterns over seven periods of cylinder oscillation, $7T$, at $R = 200$: A=0.13, $f/f_0 = 2.25$ when $h = 0.5, Fr = 0.2$ [$T \approx 2.245, 26.93 \le t \le 42.66$: $(12T, 19T)$]. The quasi-locked-on $\mathbf{C(6S)}^*$ mode, per $7T$, is observed.

from the upper side of the cylinder at $t = 20T/3$. Meanwhile, a positive vortex formed during the previous vortex shedding cycle continues to develop over $0T \le t \le 2T/3$. This positive vortex is shed downstream of the cylinder at $t \approx T$. A positive vortex develops over $4T/3 \le t \le 7T/3$, and at $t = 8T/3$ sheds downstream of the cylinder aided by the protrusion of a negative vortex into the lower shedding layer. A positive vortex developed over $8T/3 \leq t \leq 14T/3$, sheds from the lower side of the cylinder at $t \approx 5T$.

In Figure 6.17, the pressure contours in the near wake region of the cylinder are displayed for the frequency ratio $f/f_0 = 2.25$, over seven periods of cylinder oscillation, $7T$. At $t = 0T$, the high pressure region has developed in the stagnation region, and above and below the low pressure regions in the downstream of the cylinder. The low pressure region has developed mostly in the upper side, and downstream of the cylinder. At $t = T/2$, the high pressure region has shifted mostly to the upper side of the cylinder, and the low pressure region has dramatically increased in concentration and has shifted below and downstream of the cylinder. Note that the concentration of high pressure is very low downstream of the cylinder at $t = T/2$. Overall, this figure suggests that at $t = nT/2$ $(n = 1, 3, 5, 7, 9, 11, 13)$ that the low pressure region develops in the lower side, and downstream of the cylinder. The high pressure region has been forced mostly to the upper side of the cylinder in the very near wake. Interesting to note is that at $t = nT/2$ $(n = 2, 4, 6, 8, 10, 12, 14)$, the positioning of the high and low pressure regions are almost mirror images of the positions of the high and low pressure mentioned above. That is, the high pressure region is largely confined to the stagnation region, lower side, and above and below the low pressure regions in the downstream of the cylinder. In return, the low pressure region is forced to the upper side of the cylinder.

In Figure 6.18, the equivorticity patterns for $f/f_0 = 2.75$ are displayed for over three peridos of cylinder oscillation, $3T$. The shedding of two vortices occur within the

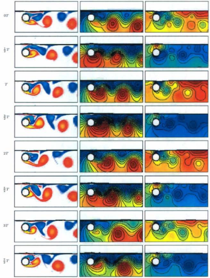

Figure 6.17: The figure caption is given on page 202

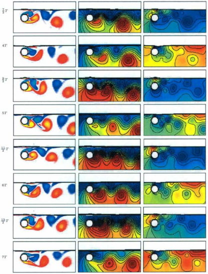

Figure 6.17: The equivorticity patterns (left), streamline patterns (middle) and the pressure contours (right) in the near wake region of the cylinder over seven periods of cylinder oscillation, $7T$, at R = 200: A=0.13, f/f_0 = 2.25 when h = 0.5, Fr = 0.2 $[T \approx 2.245, 38.17 \leq t \leq 53.88 : (17T, 24T)]$. The quasi-locked-on $\mathbf{C(6S)}^*$ mode, per $7T$, is observed.

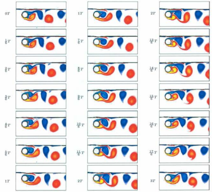

Figure 6.18: The equivorticity patterns over three periods of cylinder oscillation, $3T$, at $R = 200$: A=0.13, $f/f_0 = 2.75$ when $h = 0.5, Fr = 0.2$ [$T \approx 1.837, 91.83 \leq t \leq 97.34$: $(50T, 53T)$]. The quasi-locked-on $\mathbf{2S}^*$ mode, per $3T$, is observed.

three periods of cylinder oscillation, $3T$. This results in the quasi-lock on $\mathbf{2S}^*$ mode, per $3T$, within $4T \leq t \leq 54T$. This is consistent with C_L, but not C_D behaviour, at this frequency ratio. The flow is non-periodic for $t < 4T$. Initally, a negative vortex developed in the previous vortex shedding cycle sheds from the primary negative vortex in the near wake of the cylinder at $t \approx 4T/6$. The primary negative vortex develops over $4T/6 \leq t \leq 3T$, but remains attached to the cylinder. Meanwhile, a positive vortex formed during the previous vortex shedding cycle continues to develop over $0T \leq t \leq 11T/6$, and then sheds downstream of the cylinder at $t = 14T/6$. A positive vortex develops over $15T/5 \leq t \leq 3T$, but remains attached to the cylinder. Coalescence was not observed at this frequency ratio.

Figure 6.19 displays the pressure contours for the frequency ratio $f/f_0 = 2.75$ over three periods of cylinder oscillation, $3T$. At $t = 0T$, the high pressure region has developed in the stagnation region and the upper left side of the cylinder, and the low pressure region in the upper side and downstream of the cylinder. At $t = T/2$, synonomous with the continued development of a negative and positive vortex in the near wake of the cylinder, the low pressure shifts above, below, behind the cylinder (near wake), and in the stagnation region. The high pressure region has been forced downstream. As the negative vortex has shed at $t = 4T/6$ (see Figure 6.18), it can be seen at $t = T$ that the high pressure region has shifted mostly back to the upper left side of the cylinder (in the stagnation region) and the low pressure region mostly to the upper side of the cylinder in the near wake, and very far downstream. Overall, it is evident that at $t = nT/2$ ($n = 0, 2, 4, 6$) that the high pressure region is located in the upper left side of the cylinder (stagnation region) and the low pressure region in the upper side of the cylinder and far downstream. On the other hand, at $t = nT/2$ ($n = 1, 3, 5$) the concentration of the low pressure region is very high in the near wake of the cylinder, and is located above, below, behind and in the stagnation region of the cylinder. The high pressure region is located very far downstream. The structures of the low pressure regions at $t = 0T$ and $t = 3T$ are somewhat similar and thus the quasi-periodic nature of the flow field is reproduced in this figure.

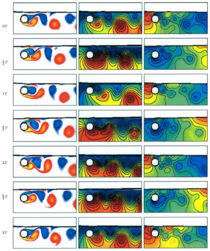

Figure 6.19: The equivorticity patterns (left), streamline patterns (middle) and the pressure contours (right) in the near wake region of the cylinder over three periods of cylinder oscillation, $3T$, at $R = 200$: A=0.13, $f/f_0 = 2.75$ when $h = \infty$ $[T \approx 1.837, 91.83 \leq t \leq 97.34 : (50T, 53T)]$. The quasi-locked-on **2S*** mode, per $3T$, is observed.

6.3 Summary and Discussion

Table 6.1 describes the effect the absence of the free-sufrace ($h = \infty$) and the inclusion of free-sufrace at $h = 0.5$ has on the vortex shedding modes for the transversely oscillating cylinder case when $f/f_0 = 1.25, 1.75, 2.25, 2.75$. It is interesting to note that as f/f_0 increases from 1.25 to 2.75, the number of total vortices shed per vortex shedding period decreases by 4 at each frequency ratio when $h = \infty$. It is evident that coalescence was not observed in the vortex shedding for $h = \infty$. For the free surface inclusion at $h = 0.5$, coalesence was observed for $f/f_0 = 2.25$. Otherwise, no coalesence was observed. It can be seen that the inclusion of the free surface results in the loss of lock-on for $f/f_0 = 1.25$ at $h = 0.5$. The new vortex shedding modes classified, based on the terminology of Williamson and Roshko (1988), are the **14S***, **10S*** and **6S*** modes, where 14, 10 and 6 refer to the total number of vortices shed from the cylinder within the respective periods, T_v, of vortex shedding. It is evident from Table 6.1 that the commonly observed modes are **6S*** and **2S***. It is also evident that irregardless of the cylinder submergence depth, h, the flow is almost periodic over $7T$ and $3T$ for $f/f_0 = 2.25, 2.75$, respectively.

In Figure 6.2 the effect of the free surface inclusion $h(= 0.5)$, and frequency ratio, $f/f_0(= 1.25, 1.75, 2.25, 2.75)$, on the mechanical energy transfer is summarized. It is immediately evident that E is negative for all cases, with the exception of $f/f_0 = 1.25$, at the cylinder submergence depth $h = 0.5$. This is indicative of the transfer of mechanical energy for $f/f_0 = 2.25, 2.75$ at $h = \infty, 0.5$, but not so for $f/f_0 = 1.25, 1.75$ at $h = \infty, 0.5$. From the Lissajous patterns of $f/f_0 = 1.25, 1.75$ at $h = \infty, 0.5$ (see Figures 6.1-6.12), it is evident that changes in direction of the patterns takes place

	$h = \infty$		$h = 0.5$	
f/f_0	Mode	T_v	Mode	T_v
1.25	**14S***	$9T$	non-locked	-
1.75	**10S***	$9T$	non-locked	-
2.25	**6S***	$7T$	**C(6S)***	$7T$
2.75	**2S***	$3T$	**2S***	$3T$

Table 6.1: The effect of the free surface inclusion, at $Fr = 0.2, h = 0.5$ and the frequency ratio, f/f_0, compared to the absence of a free surface, $h = \infty$, on vortex shedding modes and their periods, T_v, at $R = 200 : A = 0.13, f/f_0 = 1.25, 1.75, 2.25, 2.75$. The superscript "*" denotes quasi-locked-on modes.

at these frequency ratios, hence the transfer of mechanical energy is between the cylinder and fluid. It is concluded that regardless of the value of E the direcion of the Lissajous patterns must be taken into account when establishing the transfer of mechanical energy for any case. As f/f_0 decreases from 1.25 to 2.75 at $h = \infty, 0.5$, the amount of mechanical energy transferred decreases. As the cylinder submergence depth is decreased from ∞ to 0.5, the amount of mechanical energy transferred tends to decrease, with the exception of $f/f_0 = 1.25$ which increases. The transfer of mechanical energy between cylinder and fluid is represented by '$\leftrightarrow$,' from cylinder to fluid by '$\rightarrow$' and finally, from fluid to cylinder by '$\leftarrow$.' For $f/f_0 = 1.25, 1.75$, at $h = \infty, 0.5$, the transfer of mechanical energy occurs between the fluid and cylinder and for $f/f_0 = 2.25, 2.75$ from the cylinder to fluid. Hence, the decrease of cylinder submergence depth of the transversely oscillating cylinder does not affect the transfer of mechanical energy for each f/f_0.

	Mechanical Energy Transfer (=E)		Direction of $C_L(y)$
f/f_0	$h=\infty$	$h=0.5$	
1.25	2.460	-0.583	cylinder $\leftrightarrow$ fluid
1.75	-2.369	-2.272	cylinder $\leftrightarrow$ fluid
2.25	-11.475	-5.224	cylinder $\rightarrow$ fluid
2.75	-30.159	-9.792	cylinder $\rightarrow$ fluid

Table 6.2: The effect of the free surface inclusion, $h(=0.5)$, and frequency ratio, $f/f_0(=1.25, 1.75, 2.25, 2.75)$, on the mechanical energy transfer, E, for the cases $Fr=0.2$ when $h=0.5,\infty$ at $R=200: A=0.13, f/f_0=1.25, 1.75, 2.25, 2.75$.

Table 6.3 summarizes the effect of f/f_0 and h on the mean lift coefficient, $\widehat{C_L}$, and mean drag coefficient, $\widehat{C_D}$. This table suggests that $\widehat{C_L}$ values are affected by the presence of a free surface at $h=0.5$ for $1.25 \leq f/f_0 \leq 2.75$. The $\widehat{C_L}$ values of $f/f_0=1.25, 1.75$, in the presence of a free surface at $h=0.5$, are larger then the nearly zero $\widehat{C_L}$ values in the absence of a free surface at $h=\infty$. As f/f_0 increases from 1.25 to 2.75, the $\widehat{C_L}$ values at $h=\infty$ tend to increase, and the $\widehat{C_L}$ values at $h=0.5$ decrease, with the exception of $f/f_0=2.75$ for both cases. The $\widehat{C_D}$ values at $h=0.5$ are larger then the $\widehat{C_D}$ values at $h=\infty$, which are ≈ 1.3 for each f/f_0. It is evident that as f/f_0 is increased from 1.25 to 2.75, the $\widehat{C_D}$ values at $h=\infty, 0.5$ tend to increase, with the exception of $f/f_0=2.75$ at $h=0.5$.

In Table 6.4 the values of the root mean square (rms) lift and drag coeffients, $C_{L,rms}$ and $C_{D,rms}$, are displayed. It is evident that with the inclusion of a free surface at $h=0.5$ that the $C_{L,rms}$ values increase. The maximum increased observed for $C_{L,rms}$

values is by a factor of 1.39. As f/f_0 increase from 1.25 to 2.75, it is evident that the $C_{L,rms}$ values at $h = \infty, 0.5$ increase. Similarly to the $C_{L,rms}$ values, the $C_{D,rms}$ values increase with the inclusion of the free surface at $h = 0.5$. The maximum increase is by a factor of 1.38. A value 0.01 lower then the maximum increase of the $C_{L,rms}$ values. As well, as f/f_0 is increased, the $C_{D,rms}$ values increase.

The effect of cylinder submergence depth, $h(= 0.5)$, and the frequency ratio, $f/f_0(= 1.25, 1.75, 2.25, 2.75)$, on the equivorticity patterns in the near wake region of the cylinder is summarized in Figure 6.20. The snapshots are taken at $x(t) = A$. For periodic/quasi-periodic cases the snapshots are taken within the time intervals the flow reaches a periodic/quasi-periodic state. For the non periodic cases, the snapshots are taken with $0 < t \leq 100$. It is evident that with the inclusion of the free surface at $h = 0.5$, that deformation of the free surface is more pronounced as f/f_0 increases from 1.25 to 2.75. Only moderate changes in the near wake stuctures are observed at $h = 0.5$ when compared to the reference case, $h = \infty$. It can be seen that the negative vortex is lifted up toward the free surface, for each f/f_0, by the propogation of a positive vortex into the upper vortex shedding layer. In addition, the negative vorticity becomes weaker as it approaches the free surface. The presence of opposite signed vorticity is observed, at $h = 0.5$, near the free surface. As h decreases from ∞ to 0.5, it is evident that the vortex formation length remains relatively the same. This is also the case as f/f_0 increases from 1.25 to 2.75.

	$\widehat{C_L}$		$\widehat{C_D}$	
f/f_0	$h=\infty$	$h=0.5$	$h=\infty$	$h=0.5$
1.25	0.001547	0.03367	1.329	1.6209
1.75	0.004122	0.02259	1.335	1.6509
2.25	0.007328	0.002126	1.353	1.7241
2.75	0.01372	0.006427	1.3689	1.7100

Table 6.3: The effect of the free surface inclusion on the mean lift, $\widehat{C_L}$, and drag coefficient, $\widehat{C_D}$, for the cases $Fr = 0.2$ when $h = 0.5, \infty$ at $R = 200 : A = 0.13, f/f_0 = 1.25, 1.75, 2.25, 2.75$.

	$C_{L,rms}$		$C_{D,rms}$	
f/f_0	$h=\infty$	$h=0.5$	$h=\infty$	$h=0.5$
1.25	0.7306	0.9090	1.3340	1.6709
1.75	1.0550	1.3533	1.3391	1.7188
2.25	1.558	2.1609	1.3585	1.8190
2.75	2.1910	2.1878	1.3621	1.8748

Table 6.4: The effect of the free surface inclusion on the rms lift, $C_{L,rms}$, and drag coefficient, $C_{D,rms}$ for the case $Fr = 0.2$ when $h = 0.5, \infty$ at $R = 200 : A = 0.13, f/f_0 = 1.25, 1.75, 2.25, 2.75$.

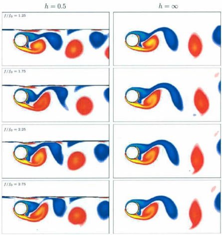

Figure 6.20: The effect of the cylinder submergence depth, h (=0.5), and the frequency ratio, f/f_0(=1.25, 1.75, 2.25, 2.75), on the equivorticity patterns at $R = 200$: $A = 0.13$, $Fr = 0.2$ from transverse motion.

7. Flow past a circular cylinder under combined streamwise and transverse oscillations

This Chapter analyzes the results for flow past a circular cylinder under combined forced streamwise and transverse ocillations, both in the absence ($h = \infty$) and presence of a free surface at $h = 0.5$. Combined streamwise and trasverse motions are studied in this thesis because they are thought to be more natural than transverse or streamwise only motions. The numerical simulations are carried out at a Reynolds number of $R = 200$, in the frequency range of $1.25 \leq f/f_0 \leq 2.75$, where f/f_0 increases by increments of 0.50. Similarly to the previous two cases, the results are obtained by analyzing the fluid forces acting on the cylinder and by means of the equivorticity patterns in the near wake of the cylinder. Based on the above equation for total mechanical energy, the Lissajous patterns $C_L(y)$ and $C_D(x)$, are the only Lissajous patterns presented in this chapter. It should be noted that the results obtained will be compared to those obtained for flow past an streamwise and transversely oscillating cylinder, in the presence of a free surface at a cylinder submergence depth of $h = 0.5$. The goal is to understand the effect the motion, and free-surface inclusion has on vortex shedding modes and fluid forces acting on the cylinder for the cylinder undergoing the figure-eight type motion.

7.1 Flow past a circular cylinder under combined oscillations in the absence of a free surface

7.1.1 Fluid Forces ($h = \infty$) :

Figure 7.1 displays the time history of the fluctuating lift coefficient, C_L, and the PSD of C_L for $f/f_0 = 1.25, 1.75, 2.25, 2.75$. It is evident, that similarly to the streamwise case when $h = \infty$, the C_L trace of $f/f_0 = 1.75$ displays a periodic signature every two cycles of cylinder oscillation, $2T$. This periodic behaviour is observed within $7T \leq t \leq 34T$. The periodic nature of C_L for this frequency ratio is also suggested by the corresponding Lissajous pattern, which is highly congruent from cycle to cycle of cylinder oscillation. The C_L traces for $f/f_0 = 1.25, 2.75$ display quasi-periodic signatures every three periods of cylinder oscillation, $3T$, within $5T \leq t \leq 24T$ and $5T \leq t \leq 54T$, respectively. The C_L trace for $f/f_0 = 2.25$ displays a quasi-periodic signature every seven periods of cylinder oscillation, $7T$, within $8T \leq t \leq 44T$. The quasi-periodic behaviour of each C_L trace, for $f/f_0 = 1.25, 2.25, 2.75$, is also suggested by the corresponding $C_L(y)$ patterns which display congruent behaviour. It is evident, however, that the congruency of the Lissajous patterns increase as f/f_0 increases from 1.25 to 2.75. It can be seen that the hysteresis loops of C_L, for each f/f_0, are mainly confined to both the upper and lower half-planes. As f/f_0 increases, there is a slight shift of the $C_L(y)$ patterns into the lower half-plane. It is evident that for each frequency ratio, f/f_0, the corresponding spectra display peaks at f_0 and f, with the dominant peak occuring at f. An additional peak at $f + 2f/3$ is also observed in the spectrum for $f/f_0 = 2.75$, indicative of the weakened effect of f on C_L as f/f_0 increases.

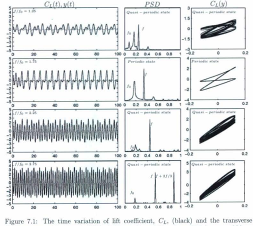

Figure 7.1: The time variation of lift coefficient, C_L, (black) and the transverse displacement, $y(t)$, (gray); PSD of C_L; at $R = 200 : A = 0.13, h = \infty, f/f_0 = 1.25, 1.75, 2.25, 2.75$. The Lissajous and PSD plots for $f/f_0 = 1.25, 1.75, 2.25, 2.75$ are obtained for quasi-periodic states in the following time intervals $5T \leq t \leq 24T, 7T \leq t \leq 34T, 8T \leq t \leq 44T, 5T \leq t \leq 54T$, respectively. The corresponding flow states are also indicated for each f/f_0.

In Figure 7.2, the time history of the fluctuating drag coefficient, C_D, and the PSD of C_D for $f/f_0 = 1.25, 1.75, 2.25, 2.75$ is displayed. The behaviour of the C_D traces and

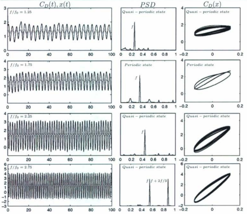

Figure 7.2: The time variation of drag coefficient, C_D, (black) and the streamwise displacement, $x(t)$, (gray); PSD of C_D at $R = 200$: $A = 0.13$, $h = \infty, f/f_0 = 1.25, 1.75, 2.25, 2.75$. The Lissajous and PSD plots for $f/f_0 = 1.25, 1.75, 2.25, 2.75$ are obtained for quasi-periodic states in the following time intervals $5T \leq t \leq 24T, 7T \leq t \leq 34T, 8T \leq t \leq 44T, 5T \leq t \leq 54T$, respectively. The corresponding flow states are also indicated for each f/f_0.

the spectra for each f/f_0 display similar behaviour to the traces and spectra associated with C_L in Figure 7.1. Similarly to the traces of C_L, the C_D traces display almost repeatable signatures every $3T$ for $f/f_0 = 1.25, 2.75$, and $7T$ for $f/f_0 = 2.25$. The C_D trace of $f/f_0 = 1.75$, displays a repeatable signature every $2T$. It is seen that the

	$h = \infty$		
f/f_0	E	Direction of	Direction of
	(Numerical value)	$C_L(y)$	$C_D(x)$
1.25	−3.911	$\leftrightarrow$	$\rightarrow$
1.75	−5.800	$\leftrightarrow$	$\leftrightarrow$
2.25	−12.435	$\leftrightarrow$	$\rightarrow$
2.75	−23.527	$\rightarrow$	$\rightarrow$

Table 7.1: The mechanical energy numerical values, E, and direction of Lissajous patterns $C_L(y)$ and $C_D(x)$ at $R = 200 : A = 0.13, f/f_0 = 1.25, 1.75, 2.25, 2.75$ when $h = \infty$. The transfer of mechanical energy between cylinder and fluid is represented by '$\leftrightarrow$,' from cylinder to fluid by '$\rightarrow$' and finally, from fluid to cylinder by ' $\leftarrow$.'

Lissajous pattern corresponding to $f/f_0 = 1.75$ displays a highly congruent signature. The Lissajous patterns corresponding to $f/f_0 = 1.25, 2.25, 2.75$ all display congruent behaviour. It is seen that as f/f_0 increases, the congrueny of these Lissajous patterns increase. It can also be seen that the Lissajous patterns shift to the lower half plane as f/f_0 increases from 1.25 to 2.75. The spectra corresponding to the C_D traces of $f/f_0 = 1.25, 1.75, 2.25, 2.75$, all display a dominant peak at f. It can be seen that an additional peak occurs at $f + 2f/3$ in the spectrum corresponding to $f/f_0 = 2.75$. It is noted, however, that unlike the PSD of C_L for each f/f_0, the spectra of C_D do not display discernable peaks at f_0.

It is noted that Lissajous patterns $C_L(y)$ and $C_D(x)$ are presented in Figures 7.1 and 7.2, respectively, in accordance with the equation of mechanical energy transfer

1.13. Equation 1.13 describes the total dimensionless mechanical energy transfer of a cylinder undergoing orbital motion in terms of $C_L(y)$ and $C_D(x)$. Table 7.1 summarizes the total mechanical energy values, E, and the direction of energy transfer for $f/f_0 = 1.25, 1.75, 2.25, 2.75$ at $h = \infty$. It is seen from this table that the total mechanical energy values, E, are negative and thereby the transfer of mechanical energy is from the cylinder to fluid , for each f/f_0. However, it is evident that there are changes in the direction of $C_L(y)$ when $f/f_0 = 1.25, 1.75, 2.25$, and of $C_D(x)$ when $f/f_0 = 1.75$. Otherwise, the direction of the Lissajous patterns are counterclockwise (for $C_L(y)$ at $f/f_0 = 2.75$, and for $C_D(x)$ at $f/f_0 = 1.25, 2.25, 2.75$).

7.1.2 Vortex formation modes ($h = \infty$) :

Figures 7.3-7.10, display the equivorticity, streamline patterns and the pressure contours in the near wake of the cylinder when $f/f_0 = 1.25, 1.75, 2.25, 2.75$. The observed flow behaviour is (*i*) periodic, per $2T$, for $f/f_0 = 1.75$ and (*ii*) quasi-periodic per $3T$ for $f/f_0 = 1.25, 2.75$ and per $7T$ for $f/f_0 = 2.25$, respectively.

In Figure 7.3 the equivorticity patterns are displayed over three periods of cylinder oscillation, $3T$, for $f/f_0 = 1.25$. The observed lock-on mode is the quasi-locked-on $\mathbf{C(2S)^* + 2S^*}$ mode, per $3T$, within $5T \leq t \leq 24T$. This is consistent with the behaviour of C_L and C_D at this frequency ratio. This mode describes the alternate shedding of a positive and negative vortex (formed from coalescence), followed by the alternate shedding of a positive and negative vortex. A negative vortex formed during the previous vortex shedding cycle continues to develop over $0 \leq t \leq 7T/6$,

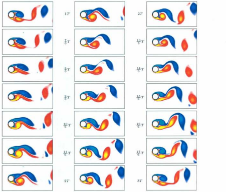

Figure 7.3: The equivorticity patterns over three periods of cylinder oscillation, $3T$, at $R = 200 : A = 0.13, f/f_0 = 1.25$ when $h = \infty$ $[T \approx 4.04, 60.61 \leq t \leq 72.73 : (15T, 18T)]$. The quasi-locked-on $\mathbf{C(2S)}^* + \mathbf{2S}^*$ mode, per $3T$, is observed.

and then sheds downstream of the cylinder at $t \approx 8T/6$. A negative vortex formed from coalescence at $t = 9T/6$ develops ver $10T/6 \leq t \leq 16T/6$. The negative vortex is shed downstream of the cylinder at $t = 17T/6$. In the lower vortex shedding region, a positive vortex developed from the previous vortex shedding cycle sheds downstream of the cylinder at $t = T/6$. A positive vortex formed from coalescence at $t = 4T/6$, develops over $5T/6 \leq t \leq 10T/6$, and then sheds downstream of the cylinder at $t = 11T/6$.

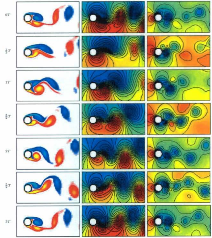

Figure 7.4: The equivorticity patterns (left), streamline patterns (middle) and the pressure contours (right) in the near wake region of the cylinder over three periods of cylinder oscillation, $3T$, at $R = 200$: A=0.13, $f/f_0 = 1.25$ when $h = \infty$ [$T \approx 4.04, 60.61 \leq t \leq 72.73$: $(15T, 18T)$]. The quasi-locked-on $\mathbf{C(2S)}^* + \mathbf{2S}^*$ mode, per $3T$, is observed.

The pressure contours for $f/f_0 = 1.25$ are displayed in the last column of Figure 7.4. At $t = 0T$, it can be seen that the high pressure region develops in the stagnation region of the cylinder, and that the low pressure region mostly develops behind the cylinder (near wake region). It is evident over $3T$, that the high pressure remains predominently in the stagnation region of the cylinder except at $t = T/2, 3T/2, 5T/2$ when it also extends above and below the low pressure regions in the downstream of the cylinder. Synonomous with the development of a positive vortex at $t = T/2$, the region of low pressure resides mostly in the lower side of the cylinder. On the other hand, at $t = 5T/2$, as a new negative vortex develops in the near wake region of the cylinder it can be seen that the low pressure region resides in the upper side of the cylinder and also behind the cylinder (near wake region). It can be seen that the low pressure structures at $t = 0T$ and $t = 3T$ are nearly identical. Hence, the quasi-periodicity of the flow field is reproduced in this figure.

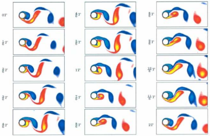

Figure 7.5: The equivorticity patterns over two periods of cylinder oscillation, $2T$, at $R = 200$: A=0.13, $f/f_0 = 1.75$ when $h = \infty$ [$T \approx 2.886, 66.38 \leq t \leq 72.15$: $(23T, 25T)$]. The locked-on $\mathbf{C}(\mathbf{P}+\mathbf{S})$ mode, per $2T$, is observed.

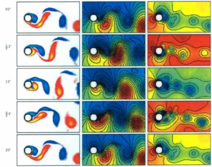

Figure 7.6: The equivorticity patterns (left), streamline patterns (middle) and the pressure contours (right) in the near wake region of the cylinder over two periods of cylinder oscillation, $2T$, at $R = 200$: A=0.13, $f/f_0 = 1.75$ when $h = \infty$ [$T \approx 2.886, 66.38 \leq t \leq 72.15$: $(23T, 25T)$]. The locked-on $\mathbf{C(P+S)}$ mode, per $2T$, is observed.

In Figure 7.5 the equivorticity patterns over two periods of cylinder oscillation, $2T$, are displayed for $f/f_0 = 1.75$. The vortex shedding mode is the quasi-locked-on $\mathbf{C(P+S)}$ mode, per $2T$, within $7T \leq t \leq 34T$. This is consistent with the behaviour of C_L and C_D at this frequency ratio. In this mode the shedding of a positive vortex followed by the shedding of a negative vortex pair occurs within three periods of cylinder oscillation, $3T$. A negative vortex in the upper side of the cylinder develops over $0 \leq t \leq 3T/6$, and the development of a second negative vortex occurs at $t = 4T/6$. Over $4T/6 \leq t \leq T$, these negative vortices co-rotate and at $t = 2T$ this negative vortex pair sheds into the downstream of the cylinder. It is evident that this vortex pair decays rapidly as it flows downstream. Meanwhile, a positive vortex formed during the previous vortex shedding cycle continues to develop over $0 \leq t \leq 3T/6$, and then sheds into the downstream of the cylinder at $t = 4T/6$.

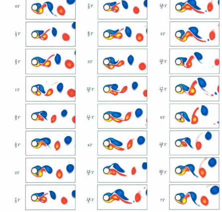

Figure 7.7: The equivorticity patterns over seven periods of cylinder oscillation, $7T$, at $R = 200$: A=0.13, $f/f_0 = 2.25$ when $h = \infty$ $[T \approx 2.245, 33.67 \leq t \leq 49.38 : (15T, 22T)]$. The quasi-locked-on $\mathbf{C(6S)}^*$ mode, per $7T$, is observed.

The pressure contours are displayed in the last column of Figure 7.6 for $f/f_0 = 1.75$, over two periods of cylinder oscillation, $2T$. At $t = 0T$, it is evident that the low pressure region develops in the upper side and downstream of the cylinder. The high pressure develops in the stagnation region of the cylinder. Over $0 \leq t \leq T/2$, as the positive vortex develops in the lower region of the cylinder, the low pressure region shifts predominently to the lower side of the cylinder. The high pressure region shifts above the cylinder in the near wake region and above and below the low pressure regions in the downstream of the cylinder. On the other hand, as a negative vortex develops in the near wake of the cylinder, and the shedding of the negative vortex pair of vortices from the upper vortex shedding region occurs, at $t = 2T$, the low pressure region shifts mostly to the upper side of the cylinder. The high pressure region shift mostly to the stagnation region. In general, at $t = nT/2$ $(n = 1, 3)$, the high pressure region is confined above the cylinder in the near wake region, and above and below the low pressure regions in the downstream of the cylinder. It is evident at $t = 0T$ and $t = 2T$, that the high and low pressure structures in the near wake of the cylinder are identical for this frequency ratio. Hence, the periodic nature of the flow is reproduced by the pressure contours.

Figure 7.7 displays the equivorticity patterns for $f/f_0 = 2.25$ over seven periods of cylinder oscillation, $7T$. The observed mode for this frequency ratio is the quasi-locked-on $\mathbf{C(6S)}^*$ mode, per $7T$, within $8T \leq t \leq 44T$. This is consistent with the behaviour of C_L and C_D at this frequency ratio. In this mode, three vortices develop on each side of the cylinder and are alternately shed over $7T$. In the upper vortex shedding layer, a negative vortex develops over $0 \leq t \leq T/3$, and then coalesces with a second negative vortex at $t = 2T/3$. The resulting negative vortex develops over

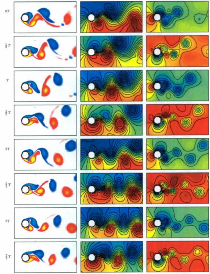

Figure 7.8: The figure caption is given on page 225

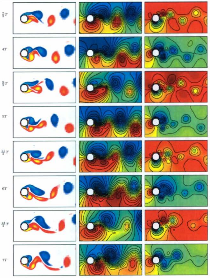

Figure 7.8: The equivorticity patterns (left), streamline patterns (middle) and the pressure contours (right) in the near wake region of the cylinder over seven periods of cylinder oscillation, $7T$, at $R = 200$: A=0.13, $f/f_0 = 2.25$ when $h = \infty$ [$T \approx 2.245, 44.89 \leq t \leq 60.61$: $(20T, 27T)$). The quasi-locked-on $\mathbf{C(6S)}^*$ mode, per $7T$, is observed.

$T \le t \le 2T$, and then sheds downstream of the cylinder at $t = 7T/3$. A negative vortex formed from the coalescence of two negative vortices at $t = 8T/3$, develops over $3T \le t \le 4T$ and then coaleces with a third negative vortex at $t = 13T/2$. This large negative vortex sheds downstream of the cylinder at $t = 5T$. A negative vortex develops over $5T \le t \le 16T/3$, and then coalesces with a newly formed megative vortex in the near wake of the cylinder at $t = 17T/3$. This vortex develops over $17T/3 \le t \le 20T/3$, and then sheds downstream of the cylinder at $t \approx 7T$. Meanwhile, in the lower vortex shedding region, a positive vortex developed from the previous vortex shedding cycle continues to develop over $0 \le t \le 2T/3$. This vortex then sheds into the near wake of the cylinder at $t = T$. A positive vortex develops over $T \le t \le 5T/3$, and coalesces with a second positive vortex at $t = 2T$. This newly formed positive vortex develops over $2T \le t \le 11T/3$, and then sheds into the near wake of the cylinder at $t = 4T$. Two unshed positive vortices in the near wake of the cylinder coalesce at $t = 13T/3$. The newly formed vortex develops over $13T \le t \le 5T$, and then coalesces with a third positive vortex at $t = 16T/3$. This newly formed positive vortex develops over $16T/3 \le t \le 17T/3$, and then sheds into the downstream of the cylinder at $t = 6T$.

Figure 7.8 displays the pressure contours for the frequency ratio $f/f_0 = 2.25$ over seven periods of cylinder oscillation, $7T$. At $t = 0T$, the high pressure region develops in the stagnation region, and the low pressure region develops in the upper side and downstream of the cylinder. As a result of the multiple shedding of single vortices from the upper and lower regions of the cylinder, the concentrations of high and low pressure regions in the vicinity of the near wake of the cylinder fluctuate dramatically. At $t = nT/2$ $(n = 1, 3, 5, 7, 9, 11, 13, 15, 17)$, the high pressure region shift to the upper

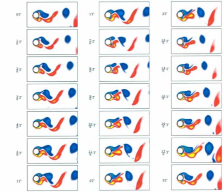

Figure 7.9: The equivorticity patterns over three periods of cylinder oscillation, $3T$, at $R = 200 : A = 0.13, f/f_0 = 2.75$ when $h = \infty$ [$T \approx 1.837, 60.61 \leq t \leq 66.12$: $(33T, 36T)$]. The quasi-locked-on $\mathbf{C}(\mathbf{P}+\mathbf{S})^*$ mode, per $3T$, is observed.

side of the cylinder, and above and below the low pressure regions in the downstream of the cylinder. On the other hand for example, at $t = 2T$, as a negative vortex in the upper vortex shedding region of the cylinder begins to detach, it can be seen that the low pressure region shifts substantially behind, and to the upper side of the cylinder. The area of high pressure shifts mostly to the stagnation region. As a negative vortex propogates downstream, and the development of a positive vortex in the lower vortex shedding region of the cylinder occurs, it is evident at $t = 5T/2$ that

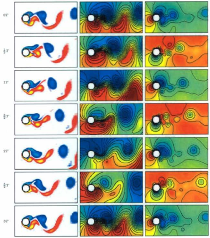

Figure 7.10: The equivorticity patterns (left), streamline patterns (middle) and the pressure contours (right) in the near wake region of the cylinder over three periods of cylinder oscillation, $3T$, at R = 200: A=0.13, $f/f_0 = 2.75$ when $h = \infty$ [$T \approx 1.837, 40.40 \leq t \leq 45.91$: $(22T, 25T)$]. The quasi-locked-on $\mathbf{C(P+S)}^*$ mode, per $3T$, is observed.

the concentration of the low pressure is quite high in the near wake of the cylinder. The high pressure region, at this time, shifts above and below the low pressure regions in the downstream of the cylinder. The snapshots at $t = 0T$ and $t = 7T$ are nearly identical, thus the quasi-periodic nature of the flow field is reproduced in this figure.

In Figure 7.9 the equivorticity patterns for $f/f_0 = 2.75$ are displayed over three periods of cylinder oscillations, $3T$. The vortex shedding mode is the quasi-locked-on $\mathbf{C(P+S)}^*$ mode, per $3T$, within $5T \leq t \leq 54T$. This is consistent with the behaviour of C_L and C_D at this frequency ratio. This mode describes the alternate shedding of a pair of positive vortices followed by the shedding of a negative vortex within three periods of cylinder oscillation. In the upper vortex shedding region a negative vortex formed from the coalescence of two negative vortices at $t = 2T/6$ develops over $3T \leq t \leq T$, and then sheds downstream of the cylinder at $t = 7T/6$. Meanwhile, in the lower vortex shedding layer, a pair of positive vortices formed during the previous vortex shedding cycle, sheds downstream of the cylinder at $t = T/6$.

The pressure contours for $f/f_0 = 2.75$ are displayed in the last column of Figure 7.10. Initially, the high pressure region develops in the stagnation region of the cylinder. The low pressure region develops behind, and in the upper side of the cylinder. At $t = nT/2$ $(n = 2, 4, 6)$, the low pressure region is confined mostly behind and in the upper side of the cylinder. The high pressure region is positioned in the lower left side of the cylinder. At $t = nT/2$ $(n = 1, 3, 5)$, the low pressure region mostly to the lower side of the cylinder, and the high pressure region is mostly confined to the upper side of the cylinder in the near wake, and above and below the low pressure regions downstream of the cylinder. The instantaneous snapshots at $t = 0T$ and $t = 3T$ are nearly identical, hence the quasi-periodic nature of the flow field is reproduced in this figure.

7.2 Free surface flow past a cylinder under combined oscillations at $Fr = 0.2$

7.2.1 Fluid forces at $Fr = 0.2 : \ h = 0.5$

The time history of the fluctuating lift coefficient, C_L, the PSD of C_L and the Lissajous patterns, $C_L(y)$, are displayed in Figure 7.11. The C_L trace of $f/f_0 = 1.75$ displays a quasi-periodic signature per $2T$ within $6T \leq t \leq 34T$. The C_L trace of $f/f_0 = 2.75$ displays a quasi-periodic signature per $3T$ within $5T \leq t \leq 54T$. On the other hand, the C_L traces of $f/f_0 = 1.25, 2.25$ display both quasi-periodic and non-periodic signatures. The C_L trace of $f/f_0 = 1.25$ displays a quasi-periodic signature per $4T$ within $9T \leq t \leq 20T$, followed by non-periodic signature within $21T \leq t \leq 24T$. For $f/f_0 = 2.25$, the C_L trace displays a quasi-periodic signature per $2T$ within $3T \leq t \leq 9T$, and per $5T$ within $14T \leq t \leq 32T$. The trace displays non-periodic signatures within $10T \leq t \leq 13T$ and $33T \leq t44T$, respectively. It is evident that the Lissajous patterns associated with $f/f_0 = 1.75, 2.75$ display more congruent behaviour than the Lissajous patterns associated with $f/f_0 = 1.25, 2.25$. As f/f_0 increases from 1.25 to 2.75, the $C_L(y)$ patterns shift further into the lower half plane. The spectra of Figure 7.11 all display a dominant peak at the forcing frequency f. It is noted, however, that a very large peak at $7f_0/4 + f$ in the spectrum of $f/f_0 = 2.75$. This is indicative of the weakened effect of f on C_D as f/f_0 increases.

In Figure 7.12, the time history of the drag coefficient, C_D, the PSD of C_D and the corresponding Lissajous patterns, $C_D(x)$, of C_D are displayed. It is evident that the

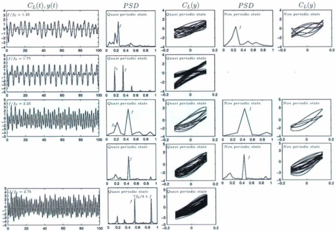

Figure 7.11: The time variation of lift coefficient, C_L, (black) and the transverse displacement, $y(t)$, (gray); PSD of C_L; at $R = 200 : A = 0.13, h = \infty, f/f_0 = 1.25, 1.75, 2.25, 2.75$. The Lissajous and PSD plots for $f/f_0 = 1.25, 1.75, 2.25, 2.75$ are obtained for quasi-periodic states in the following time intervals $9T \leq t \leq 20T, 6T \leq t \leq 34T, 3T \leq t \leq 9T$ $(14T \leq t \leq 32T), 5T \leq t \leq 54T$, respectively. The corresponding flow states are also indicated for each f/f_0.

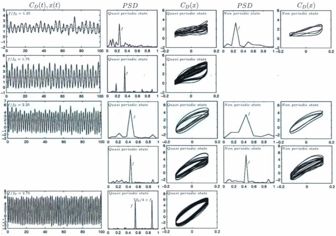

Figure 7.12: The time variation of drag coefficient, C_D, (black) and the inline displacement, $x(t)$, (gray); PSD of C_D at $R = 200 : A = 0.13,\ h = \infty, f/f_0 = 1.25, 1.75, 2.25, 2.75$. The Lissajous and PSD plots for $f/f_0 = 1.25, 1.75, 2.25, 2.75$ are obtained for quasi-periodic states in the following time intervals $9T \leq t \leq 20T, 6T \leq t \leq 34T, 3T \leq t \leq 9T$ $(14T \leq t \leq 32T), 5T \leq t \leq 54T$, respectively. The corresponding flow states are also indicated for each f/f_0.

	$h = \infty$		
f/f_0	E (Numerical value)	Direction of $C_L(y)$	Direction of $C_D(x)$
1.25	-0.7364	$\leftrightarrow$	$\rightarrow$
1.75	-11.32	$\leftrightarrow$	$\rightarrow$
2.25	-4.210 (-12.43)	$\leftrightarrow$	$\rightarrow$
2.75	-47.46	$\leftrightarrow$	$\rightarrow$

Table 7.2: The mechanical energy numerical values, E, and direction of Lissajous patterns $C_L(y)$ and $C_D(x)$ at $R = 200 : A = 0.13, f/f_0 = 1.25, 1.75, 2.25, 2.75$ when $h = 0.5, Fr = 0.2$. The transfer of mechanical energy between cylinder and fluid is represented by '$\leftrightarrow$,' from cylinder to fluid by '$\rightarrow$' and finally, from fluid to cylinder by '$\leftarrow$.'

C_D traces of $f/f_0 = 1.25, 1.75, 2.75$ display quasi-periodic signatures every $4T, 2T$, and $3T$, respectively. The C_D trace for $f/f_0 = 2.25$, similarly to the C_L trace, displays a quasi-periodic signature per $2T$ until $t \approx 9T$, followed by a quasi-periodic signature per $5T$ within $14T \leq t \leq 32T$. It is observed that the Lissajous patterns increase in congrueny as f/f_0 increases from 1.25 to 2.75. As well, the Lissajous patterns shift moreso into the bottom half-plane. The corresponding spectra of $f/f_0 = 1.25, 1.75, 2.25, 2.75$ all display a dominant peak at f, whereas the spectrum of $f/f_0 = 2.75$ displays an additional peak at $7f_0/4 + f$. This is indicative of the weakened effect of f on C_D as f/f_0 increases.

In table 7.2, the total mechanical energy values, E, and the direction of energy transfer for $f/f_0 = 1.25, 1.75, 2.25, 2.75$ at $h = 0.5$, when $Fr = 0.2$ are summarized. It is seen from this table that the total mechanical energy values, E, are negative and thereby the transfer of mechanical energy is from the cylinder to fluid , for each f/f_0. As f/f_0 increases from 1.25 to 2.75 the values of E increase substantially. It is evident that there are changes in the direction of $C_L(y)$ when $f/f_0 = 1.25, 1.75, 2.25, 2.75$ and of $C_D(x)$ when $f/f_0 = 1.25$ (switching from counterclockwise to clockwise). Otherwise, the direction of the Lissajous patterns are strictly counterclockwise (for $C_D(x)$ at $f/f_0 = 1.75, 2.25, 2.75$).

7.2.2 Vortex shedding modes at $Fr = 0.2: \; h = 0.5$

Figures 7.13-7.22 display the equivorticity and streamline patterns, and pressure contours in the near wake of the cylinder when $f/f_0 = 1.25, 1.75, 2.25$, and 2.75. The observed flow behaviour is (i) quasi-periodic per $4T, 2T, 2T\ (5T), 3T$ for $f/f_0 = 1.25, 1.75, 2.25, 2.75$, respectively.

Figure 7.13 displays the equivorticity patterns for $f/f_0 = 1.25$ over four periods of cylinder oscillation, $4T$, within $15T \le t \le 19T$. The vortex shedding mode is the quasi-locked-on $[\mathbf{C(2S)+4S}]^*$, per $4T$, within $9T \le t \le 20T$. This is consistent with C_L behaviour at this frequency ratio, but not C_D. In this mode, three single vortices are alternately shed from the upper and lower vortex shedding region of the cylinder, one of which is formed from coalescence, within $4T$. In the upper vortex shedding region, a negative vortex formed during the previous vortex shedding region completely detaches from the primary vortex, into the upper vortex shedding layer at $t = 2T/3$. A negative vortex develops over $2T/3 \le t \le 4T/3$, and due to the interaction of with a positive vortex in the lower vortex shedding layer at $t = 5T/3$ the negative vortex is forced up towards the free surface. This negative vortex sheds completely into the upper layer of the cylinder at $t = 2T$. A negative vortex forms over $2T \leq t \leq 8T/3$, and is then sheds downstream of the cylinder at $t = 3T$. In the lower vortex shedding region, a positive vortex formed during the previous vortex shedding cycle begins to co-rotate with a second positive vortex at $t = 2T/3$. This positive vortex subsequently seperates from the primary positive vortex in the near wake of the cylinder at $t = T$. A positive vortex develops over $T \leq t \leq 4T/3$, and at $t = 5T/3$ coalesces with a second positive vortex. The resulting positive vortex sheds downstream of the cylinder at $t = 7T/3$. Over $8T/3 \leq t \leq 3T$, a positive vortex develops and at $t = 10T/3$ it begins to co-rotate with a newly formed positive vortex in the near wake of the cylinder. The secondary positive vortex then detaches downstream of the cylinder at $t = 11T/3$. To summarize, a negative and positive single are shed within $0 \leq t \leq T$ (**2S**). Within $4T/3 \leq t \leq 7T/3$ a negative vortex and a positive vortex formed from coalescence are both shed downstream of the cylinder ($\mathbf{C(2S)^*}$). Finally, the shedding of a negative and positive vortex occurs within $8T/3 \leq t \leq 4T$. (**2S**). Therefore, the mode is described as $[\mathbf{C(2S)} + \mathbf{4S}]^*$.

In Figure 7.14, the pressure contours for $f/f_0 = 1.25$ are displayed for over four periods of cylinder oscillation, $4T$. Initially, the high pressure region develops in the stagnation region of the cylinder and the low pressure region develops behind, and in the upper side of the cylinder. At $t = T/2$, synonmous with the development of a new positive vortex, the low pressure region shifts to the lower sie of the cylinder, and downstream. The high pressure region remains in the stagnation region. With the shedding of a positive vortex at $t = T$, the high pressure region has shifted clockwise

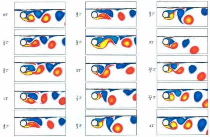

Figure 7.13: The equivorticity patterns over four periods of cylinder oscillation, $4T$, at $R = 200$: $A = 0.13, f/f_0 = 1.25, Fr = 0.2$ when $h = 0.5$ [$T \approx 4.04, 76.768 \leq t \leq 92.929$: $(19T, 23T)$]. The quasi-locked-on $[\mathbf{C(2S)} + \mathbf{4S}]^*$ mode, per $4T$, is observed.

to the upper left side of the cylinder, and the low pressure region has shifted behind, and in the upper side of the cylinder (similarly to the position at $t = 0T$). At $t = 3T/2$, it can be seen that the concentration of low pressure has dramatically increased, and that there is no discernable presence of the high pressure region in the near wake or downstream of the cylinder. It is known that the distribution of low pressure in the near wake of a cylinder is highly dependent on the formation of new vortices. For example, at $t = 5T/2$ synonmous with the formation of a positive vortex, the low pressure region shifts mostly to the lower side of the cylinder and downstream (near wake region). On the other hand, at $t = 3T$ as a negative vortex develops in the upper side of the cylinder, the low pressure shifts mostly to the upper side of the cylinder and also downstream (near wake region). At $t = 3T/2, 7T/2$, the concentration of

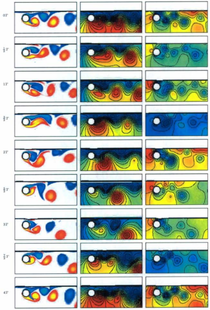

Figure 7.14: The equivorticity patterns (left), streamline patterns (middle) and the pressure contours (right) in the near wake region of the cylinder over four periods of cylinder oscillation, $4T$, at $R = 200$: A=0.13, $f/f_0 = 1.25, Fr = 0.2$ when $h = 0.5$ $[T \approx 4.04, 76.768 \leq t \leq 92.929 : (19T, 23T)]$. The quasi-locked-on $\mathbf{C(6S)}^*$ mode, per $2T$, is observed.

low pressure in the near wake of the cylinder and downstream is very high. It can be seen that low pressure completely encloses the cylinder in the near wake. There is no discernable presence of high pressure in the near wake or downstream of the cylinder at these time instances. Conversely, at $t = 0T, 2T, 4T$, the high pressure region is confined mostly to the stagnation region of the cylinder, and above and below the low pressure regions in the downstream of the cylinder. The low pressure is confined mostly to the upper side of the cylinder and downstream (near wake), at these time instances. The structure of low pressure at $t = 0T$ and $t = 4T$ are somewhat alike, and hence the quasi-periodic nature of the flow field is reproduced in this figure.

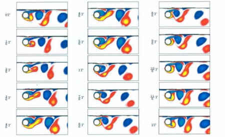

Figure 7.15: The equivorticity patterns over two periods of cylinder oscillation, $2T$, at $R = 200$: A=0.13, $f/f_0 = 1.75, Fr = 0.2$ when $h = 0.5$ [$T \approx 2.886, 66.38 \leq t \leq 72.15$: $(23T, 25T)$]. The quasi-locked-on $(\mathbf{P}+\mathbf{S})^*$ mode, per $2T$, is observed.

Figure 7.15 displays the equivorticity patterns for $f/f_0 = 1.75$ for over two periods of cylinder oscillation, $2T$, within $23T \leq t \leq 25T$. The vortex shedding mode is the quasi-locked-on $(\mathbf{P}+\mathbf{S})^*$ mode, per $2T$, within $6T \leq t \leq 34T$. In the upper vortex shedding layer, a negative vortex developed from the previous vortex shedding cycle sheds downstream of the cylinder at $t = 2T/6$. In the lower vortex shedding region, a positive vortex develops over $0 \leq t \leq 3T/6$, and begins to co-rotate with a second positive vortex located in the near wake of the cylinder at $t = 4T/6$. These vortices co-rotate over $4T/6 \leq t \leq 8T/6$, and the positive vortex pair is shed completely into the downstream of the cylinder at $t = 9T/6$. The coalescence phenomenom was not observed in this case.

The pressure contours for $f/f_0 = 1.75$ are displayed in the last column of Figure 7.16. At $t = 0T$, it is evident that the high pressure region is developing in the upper stagnation region of the cylinder, and the low pressure region in the upper side and downstream of the cylinder. At $t = T/2$, it is evident that the low pressure region has shifted below and above the cylinder in the near wake region, and that the high pressure region hsa shifted mostly above and below the low pressure regions in the downstream of the cylinder. As a negative vortex sheds and a positive vortex pair has developed, it is evident that at $t = T$, that the low pressure region has shifted predominently to the upper right side of the cylinder and behind the cylinder in the near wake. The high pressure region has shifted mostly to the stagnation region. Synonomous with the shedding of a positive pair, and the development of a new positive vortex at $t = 3T/2$, the low pressure region has shifted mostly to the lower side of the cylinder, stagnation region and downstream of the cylinder. The high pressure region has shifted directly above the cylinder. It is evident that the concentration of high pressure has dramatically decreased at this time. Finally, at $t = 2T$ it can be seen that the low pressure region has shifted to the upper side of the

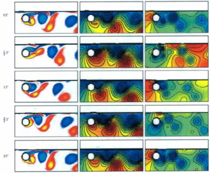

Figure 7.16: The equivorticity patterns (left), streamline patterns (middle) and the pressure contours (right) in the near wake region of the cylinder over two periods of cylinder oscillation, $2T$, at $R = 200$: A=0.13, $f/f_0 = 1.75, Fr = 0.2$ when $h = 0.5$ $[T \approx 2.886, 66.38 \leq t \leq 72.15 : (23T, 25T)]$. The quasi-locked-on $\mathbf{C(P+S)}^*$ mode, per $2T$, is observed.

cylinder, but mostly downstream of the cylinder. The high pressure region has shifted to the stagnation region of the cylinder. It is the case that the quasi-periodic nature of the flow field has been reproduced in this figure since the snapshots at $t = 0T$ and $t = 2T$ are nearly identical.

For frequency ratio $f/f_0 = 2.25$, the flow displays quasi-periodic behaviour every two periods of cylinder oscillation, $2T$, within $3T \leq t \leq 9T$ and every five periods of cylinder oscillation, $5T$, within $14T \leq t \leq 32T$. Within $10T \leq t \leq 13T$ and $t > 32T$ the flow behaviour is non-periodic. Figure 5 displays the vortex shedding mode of $f/f_0 = 2.25$ within $4T \leq t \leq 6T$. The vortex shedding mode is the quasi-locked-on $\mathbf{C(2S)}^*$ mode, per $2T$, within $3T \leq t \leq 9T$. In this mode two vortices of opposite rotation are alternately shed from the bottom and top of the cylinder, respectively. In the upper vortex shedding layer, it is evident that a negative vortex has developed in the previous vortex shedding cycle. This vortex continues to develop over $T/6 \leq t \leq 2T/6$, and coalesces with a second negative vortex at $t = 3T/6$. The resulting negative vortex develops over $4T/5 \leq t \leq 7T/6$, and is shed downstream of the cylinder at $t = 8T/6$. In the lower vortex shedding region, a positive vortex formed during the previous vortex shedding cycle detaches from the primary vortex in the near wake of the cylinder at $t \approx 2T/6$. Positive vortices developed in the remainder of the period, remain attached to the cylinder. In Figure 7.19, the equivorticity patterns for $f/f_0 = 2.25$ are displayed for over five periods of cylinder oscillation, $5T$, within $27T \leq t \leq 32T$. The vortex shedding mode is the quasi-locked-on $[\mathbf{C(P+S)} + \mathbf{C(2S)}]^*$ mode, per $5T$, within $14T \leq t \leq 32T$. In this mode a pair of positive vortices and a single negative vortex are alternately shed, from the top and bottom of the cylinder, followed by the alternate shedding of two single vortices of opposite rotation. In the upper vortex shedding region, a negative vortex formed from the coalescence of two negative vortices at $t = 2T/3$, continues to develop over $T \leq t \leq 8T/3$. The interaction of the newly formed negative vortex with the free-surface, ultimately leads to detachment from the primary negative vortex in the near wake of the cylinder at $t = 3T$. Furthermore, a negative vortex develops over $3T \leq t \leq 10T/3$, and then coalesces with a second negative vortex at $t = 11T/3$. The resulting negative vortex sheds into the upper vortex shedding layer of the cylinder at $t \approx 13T/3$. In the lower vortex shedding region, a positive vortex formed during the previous vortex shedding cycle begins to co-rotate with a second negative vortex at $t = 2T/3$. This pair of co-rotating positive vortices develop over $T \leq t \leq 4T/3$ and begin to co-rotate with a third positive vortex at $t = 5T/3$. The three positive vortices co-rotate over $5T/3 \leq t \leq 2T$ and then the positive vortex pair sheds downstream of the cylinder at $t = 7T/3$. A positive vortex formed from the coalescence of two positive vortices at $t = 10T/3$, is then shed downstream of the cylinder at $t = 11T/3$. The sequence of vortex shedding is as follows: a positive vortex pair is shed at $t = 7T/3$ followed by a negative vortex at $t = 3T$, which gives the $\mathbf{C(P+S)}^*$ mode. Then the shedding of a positive vortex occurs at $t = 11T/3$, followed by the shedding of a negative vortex at $t = 5T$, giving the $\mathbf{C(2S)}^*$ mode.

The pressure contours of $f/f_0 = 2.25$ are displayed for over two periods of cylinder oscillation, $2T$, in Figure 7.18. At $t = 0T$, the high pressure region is developing in the stagnation region of the cylinder, and the low pressure region is mainly developing in the upper side of the cylinder and downstream. As negative and positive vortices develop in the near wake of the cylinder at $t = T/2, 3T/2$, it is evident that the low pressure region completely encloses the cylinder at these times. That is the low pressure region resides mostly in the front, upper and lower sides of the cylinder and also downstream. The concentration of high pressure is very low at both time instances. On the other hand, at $t = 0T, T, 2T$ the high pressure region resides mostly in the stagnation region of the cylinder and the low pressure region resides mostly in the upper side of the cylinder and downstream. It is evident that the low pressure structures in the near wake of the cylinder are nearly identical at $t = 0T$ and $t = 2T$,

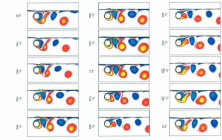

Figure 7.17: The equivorticity patterns over two periods of cylinder oscillation, $2T$, at $R = 200$: A=0.13, $f/f_0 = 2.25, Fr = 0.2$ when $h = 0.5$ [$T \approx 2.245, 8.979 \leq t \leq 13.468$: $(4T, 6T)$]. The quasi-locked-on $\mathbf{C(2S)}^*$ mode, per $2T$, is observed.

hence the quasi-periodic nature of the flow field is reproduced in this figure.

In figure 7.20, the pressure contours for $f/f_0 = 2.25$ are displayed for over five periods of cylinder oscillation, $5T$. At $t = 0$, the high pressure region develops in the stagnation region and the low pressure region develops downstream, and in the upper side of the cylinder. At $t = nT/2$ ($n = 1, 3, 5, 7, 9$), the region of low pressure is highly concentrated in the near wake of the cylinder. It is confined mostly to the front, upper and lower side of the cylinder, as well as downstream. The high pressure region at these time instances are located mostly in the upper right side of the cylinder and above and below the low pressure regions in the downstream of the cylinder. However, the concentration of low pressure is very low at these times. Else, at $t = nT/2$ ($n =$

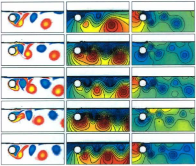

Figure 7.18: The equivorticity patterns (left), streamline patterns (middle) and the pressure contours (right) in the near wake region of the cylinder over two periods of cylinder oscillation, $2T$, at R = 200: A=0.13, f/f_0 = 2.25, Fr = 0.2 when h = 0.5 [$T \approx 2.245, 8.979 \leq t \leq 13.468$: $(4T, 6T)$]. The quasi-locked-on $\mathbf{C(2S)}^*$ mode, per $2T$, is observed.

$0, 2, 4, 6, 8, 10)$, the high pressure region is mainly confined to the stagnation region of the cylinder, and downstream of the cylinder (near wake region). For example, as a positive vortex is shed at $t = 7T/3$ (see Figure 7.19), and the development of a new positive and negative vortex occurs at $t = 5T/2$, is can be seen that the low pressure region resides mostly in the lower side of the cylinder. The high pressure region resides above and below the low pressure contours in the downstream of the cylinder. It is evident that the low pressure structures in the near wake of the cylinder

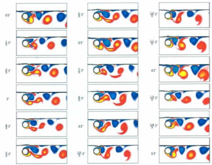

Figure 7.19: The equivorticity patterns over four periods of cylinder oscillation, $5T$, at $R = 200$: A=0.13, $f/f_0 = 2.25, Fr = 0.2$ when $h = 0.5$ [$T \approx 2.245, 60.606 \leq t \leq 71.829$: $(27T, 32T)$]. The quasi-locked-on $[\mathbf{C(P+S)} + \mathbf{C(2S)}]^*$ mode, per $5T$, is observed.

are nearly identical at $t = 0T$ and $t = 5T$, hence the quasi-periodic nature of the flow field is reproduced in this figure.

In Figure 7.21 the equivorticity patterns for $f/f_0 = 2.75$ are displayed for over three periods of cylinder oscillations, $3T$, within $25T \leq t \leq 28T$. The vortex shedding mode is the quasi-locked-on $\mathbf{C(2S)}^*$, per $3T$, within $5T \leq t \leq 54T$. At $t = 0T$, the negative vortex in the near wake of the cylinder continues to develop until $t = 5T/6$ when at this time it coalesces with a second negative vortex. The negative vortex formed from the coalescence develops over $T \leq t \leq 11T/6$ and at $t = 2T$ begins to co-rotate

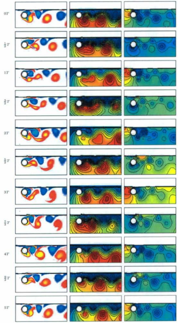

Figure 7.20: The equivorticity patterns (left), streamline patterns (middle) and the pressure contours (right) in the near wake region of the cylinder over five periods of cylinder oscillation, $5T$, at $R = 200$: A=0.13, $f/f_0 = 2.25, Fr = 0.2$ when $h = 0.5$ [$T \approx 2.245, 60.606 \le t \le 71.829$: $(27T, 32T)$]. The quasi-locked-on $[\mathbf{C(P+S)+C(2S)}]^*$ mode, per $5T$, is observed.

with a second negative vortex, only to detach from this negative vortex at $t = 13T/6$. Meanwhile, in the lower vortex shedding region, it is evident at $t = 0T$ that a pair of co-rotating vortices has been developed in the previous vortex shedding cycle. This pair continues to develop until $t = 4T/6$ when at this time it detaches from the positive vortex in the near wake. At $t = 5T/6$ the positive vortex pair reattaches to the positive vortex in the near wake. After the reattachment to the positive vortex in the near wake, the positive pair of vortices coalesce to form a single positive vortex. This positive vortex is shed downstream of the cylinder at $t = 7T/6$.

In Figure 7.21, the equivorticity patterns of $f/f_0 = 2.75$ over three periods of cylinder oscillation, $3T$, are displayed. A negative vortex develops over $0 \leq t \leq 4T/6$ and then coalesces with a second negative vortex at $t = 5T/6$. The resulting negative vortex develops over $T \leq t \leq 2T$, and then sheds downstream of the cylinder at $t = 13T/6$. A positive vortex pair formed during the previous vortex shedding cycle continues to develop over $0 \leq t \leq 4T/6$, and then two vortices of this pair coalesces at $t = 7T/6$.

Figure 7.22, displays the pressure contours for $f/f_0 = 2.75$, over three periods of cylinder oscillation, $3T$. Initially, this figure displays the development of the high pressure in the stagnation region of the cylinder and the low pressure region in the upper side, and downstream of the cylinder. It can be seen that with the development of new negative and positive vortices at $t = T/2$, that the high pressure region shifts mostly downstream of the cylinder. The low pressure region, in return, moves mostly to the front, upper and lower side of the cylinder. In general, it is evident that at $t = nT/2$ $(n = 0, 2, 4, 6)$, that the low pressure region is mostly confined to the upper side, and downstream, of the cylinder and the high pressure region is mostly

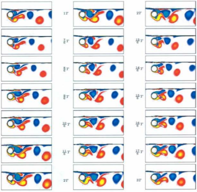

Figure 7.21: The equivorticity patterns over three periods of cylinder oscillation, $3T$, at $R = 200 : A = 0.13, f/f_0 = 2.75, Fr = 0.2$ when $h = 0.5$ $[T \approx 1.837, 45.914 \leq t \leq 51.423 : (25T, 28T)]$. The quasi-locked-on $\mathbf{C(2S)}^*$ mode, per $3T$, is observed.

confined to the stagnation region. On the other hand, at $t = nT/2$ $(n = 1, 3, 5)$, the low pressure region is confined mostly to the front, upper and lower side of the cylinder, dominating the near wake at these times. The high pressure moves farther downstream. It is evident that the concentration of high pressure in the downstream of the cylinder, is highest at $t = T/2$ as opposed to $t = 3T/2.5T/2$. The low pressure structures of the snapshots at $t = 0T$ and $t = 3T$ are almost identical, and hence the quasi-periodic nature of the flow field is reproduced in this figure.

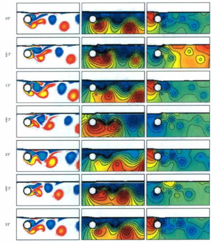

Figure 7.22: The equivorticity patterns (left), streamline patterns (middle) and the pressure contours (right) in the near wake region of the cylinder over three periods of cylinder oscillation, $3T$, at $R = 200$: $A = 0.13, f/f_0 = 2.75, Fr = 0.2$ when $h = 0.5$ $[T \approx 1.837, 45.914 \leq t \leq 51.423$: $(25T, 28T)]$. The quasi-locked-on $\mathbf{C(2S)}^*$ mode, per $3T$, is observed.

7.3 Summary and Discussion

Table 7.3 displays the effect the free surface presence at $h = 0.5$, when $f/f_0 = 1.25, 1.75, 2.25, 2.75$, has on vortex shedding modes of a cylinder undergoing transverse-streamwise motion, and their periods, T_v. For $f/f_0 = 1.25, 1.75, 2.25, 2.75$, lock-on modes were found every $3T, 2T, 7T, 3T$, respectively. It is interesting to note that regardless of the cylinder submergence depth, h, the vortex shedding periods for $f/f_0 = 1.75, 2.75$ are $2T$ and $3T$, respectively. Also interesting to note is that the sum of the vortex shedding periods $T_v = 2T + 5T$, for $f/f_0 = 2.25$ at $h = 0.5$, is equal to the vortex shedding period, $T_v = 7T$, for $f/f_0 = 2.25$ at $h = \infty$. The newly classified vortex shedding modes are the $[\mathbf{C(2S) + 2S}]^*$, for $f/f_0 = 1.25$, and $[\mathbf{C(P+S) + C(2S)}]^*$, for $f/f_0 = 2.25$. These modes are combinations of the most commonly observed modes near the fundamental lock-on region found by Williamson and Roshko in the 1988 study of a transversely oscillating cylinder in the absence of a free surface.

Table 7.4 summarizes the effect cylinder submergence depth, h, and f/f_0 has on the mean lift coefficent, $\widehat{C_L}$, and the mean drag coefficient, $\widehat{C_D}$. This table suggests that the values of $\widehat{C_L}$ are affected by the inclusion of the free surface at $h = 0.5$ for $1.25 \leq f/f_0 \leq 2.75$. The $\widehat{C_L}$ values are negative, and within the range $-0.1919 \leq \widehat{C_L} \leq -0.1012$ at $h = \infty$ and within $-0.4610 \leq \widehat{C_L} \leq -0.1259$. On average, the $\widehat{C_L}$ values at $h = \infty$ are greater than those at $h = 0.5$. As f/f_0 increases from 1.25 to 2.75, the $\widehat{C_L}$ values decreases for $h = 0.5, \infty$. The magnitude of the $\widehat{C_L}$ values for $h = \infty$ are less than the magnitude of the $\widehat{C_L}$ values at $h = 0.5$. In contrast, the inclusion of the free surface at $h = 0.5$ has only a slight effect on $\widehat{C_D}$ values. In fact,

	$h=\infty$		$h=0.5$	
f/f_0	Mode	T_v	Mode	T_v
1.25	$\mathbf{C(2S)}^{*}+\mathbf{2S}^{*}$	$3T$	$\mathbf{C(6S)}^{*}$	$4T$
1.75	$\mathbf{C(P+S)}$	$2T$	$\mathbf{(P+S)}^{*}$	$2T$
2.25	$\mathbf{C(6S)}^{*}$	$7T$	$\mathbf{C(2S)}^{*}$	$2T$
			$[\mathbf{C(P+S)}+\mathbf{C(2S)}]^{*}$	$5T$
2.75	$\mathbf{C(P+S)}^{*}$	$3T$	$\mathbf{C(2S)}^{*}$	$3T$

Table 7.3: The effect of the free surface inclusion, at $Fr=0.2, h=0.5$ and the frequency ratio, f/f_0, compared to the absence of a free surface when $h=\infty$, on vortex shedding modes and their periods, T_v, at $R=200 : A=0.13, f/f_0=1.25, 1.75, 2.25, 2.75$. The superscript "*" denotes quasi-locked-on modes.

the values of $\widehat{C_D}$ do no increase by more than a factor of 1.30 for all f/f_0. Each $\widehat{C_D}$ value is positive, and vary within the range $1.326 \leq \widehat{C_D} \leq 1.852$. As f/f_0 increases from 1.25 to 2.75, the $\widehat{C_D}$ values tend to decrease for $h=\infty$, with the exception of $f/f_0=1.25$. On the other hand, the $\widehat{C_D}$ values at $h=0.5$, tend to decrease as f/f_0 increases from 1.25 to 2.75, with the exception of $f/f_0=1.25$.

Table 7.5 displays the root mean square (rms) values of the lift coefficient, $C_{L,rms}$, and the drag coefficient, $C_{D,rms}$, at $h=\infty$ and $h=0.5$. The inclusion of the free surface at $h=0.5$ seems to increase the $C_{L,rms}$ and $C_{D,rms}$ values, except the $C_{L,rms}$ value for $f/f_0=2.75$ at $h=0.5$. The maximum increase observed for the $C_{L,rms}$ values is by a factor of 1.293, and by a factor of 1.510 for the $C_{D,rms}$ values. It is evident that as f/f_0 increases, the $C_{L,rms}$ and $C_{D,rms}$ values increase at both $h=\infty, 0.5$. In general, the magnitude of the $C_{L,rms}$ values at $h = 0.5, \infty$ are lower than the $C_{D,rms}$ values at $h = 0.5, \infty$.

In Figure 7.23, the effect of cylinder submergence depth, $h(= 0.5)$, and the frequency ratio, $f/f_0(= 1.25, 1.75, 2.25, 2.75)$, on the equivorticity patterns in the near wake region of the cylinder is summarized. The snapshots are taken at $x(t) = A$. For periodic/quasi-periodic cases the snapshots are taken within the time intervals the flow reaches a periodic/quasi-periodic state. For the non periodic cases, the snapshots are taken with $0 < t \leq 100$. The reference case is also displayed in this figure. It is seen at $h = 0.5$, that the free surface deformations are pronounced. Only moderate changes in the near wake stuctures are observed at $h = 0.5$ at $f/f_0 = 2.25, 2.75$ when compared to the reference case, $h = \infty$. The negative vortex structures associated with $f/f_0 = 1.25, 1.75$ differ more dramtically than those of $h = \infty$, whereas the positive vortex structures differ slightly. It is evident from this figure that there is presence of opposite signed vorticity near the free surface. It is evident from this figure that the vortex structures as f/f_0 increases from 1.25 to 2.75 vary highly as opposed to the vortex structures of the tranverse case as f/f_0 increases from 1.25 to 2.75. Hence, the increase in f/f_0 for this case results greatly affect the formation of the vortex structures. As h decreases from ∞ to 0.5, it is evident that the vortex formation length of the positive and negative vortex structures remain relatively the same, with the exception of $f/f_0 = 1.25, 1.75$ whose positive vortex structures seem to decrease in length (maximum by 22.9%). When $h = 0.5, \infty$ the negative vortex formation length tends to decrease as f/f_0 increases from 1.25 to 2.25 (maximum by $\approx 73.5\%$).

	$\widehat{C_L}$		$\widehat{C_D}$	
f/f_0	$h=\infty$	$h=0.5$	$h=\infty$	$h=0.5$
1.25	−0.1012	−0.1259	1.326	1.6394
1.75	−0.1495	−0.2509	1.6168	1.852
2.25	−0.1919	−0.4610	1.4428	1.7477
2.75	−0.1816	−0.3580	1.4248	1.8340

Table 7.4: The effect of the free surface inclusion on the mean lift, $\widehat{C_L}$, and drag coefficient, $\widehat{C_D}$, for the cases $Fr = 0.2$ when $h = 0.5, \infty$ at $R = 200 : A = 0.13, f/f_0 = 1.25, 1.75, 2.25, 2.75$.

	$C_{L,rms}$		$C_{D,rms}$	
f/f_0	$h=\infty$	$h=0.5$	$h=\infty$	$h=0.5$
1.25	0.7659	0.9903	1.3812	1.7819
1.75	1.2190	1.5107	1.7836	2.3172
2.25	1.5697	1.7060	1.8865	2.6593
2.75	2.1928	1.7707	2.3758	3.5837

Table 7.5: The effect of the free surface inclusion on the rms lift, $C_{L,rms}$, and drag coefficient, $C_{D,rms}$ for the case $Fr = 0.2$ when $h = 0.5, \infty$ at $R = 200 : A = 0.13, f/f_0 = 1.25, 1.75, 2.25, 2.75$.

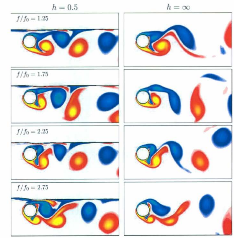

Figure 7.23: The effect of the cylinder submergence depth, $h(= 0.5)$, and the frequency ratio, $f/f_0(=1.25, 1.75, 2.25, 2.75)$, on the equivorticity patterns at $R = 200$: $A = 0.13$, $Fr = 0.2$ for a cylinder subjected to two-degrees of freedom.

References

Al-Mdallal, Q. M. (2004). *Analysis and computation of the cross-flow past an oscillating cylinder with two degrees of freedom.* Unpublished doctoral dissertation, Memorial University of Newfoundland.

Al-Mdallal, Q. M., Lawrence, K. P. and & Kocabiyik, S. (2007). Forced streamwise oscillations of a circular cylinder: Locked-on modes and resulting fluid forces. *Journal of Fluids and Structures*, 23(5):681-701.

Anagnostopoulos, P. (2000). Numerical study of the flow past a cylinder excited transversely to the incident stream. Part 1: Lock-in zone, hydrodynamic forces and wake geometry. *Journal of Fluids and Structures*, 14:819-851.

Aulisa, E., Manservisi, S., Scardovelli, R. and & Zaleski, S. (2003b). A geometrical area-preserving volume-of-fluid advection method. *Journal of Computational Physics*, 192(1):355-364.

Baranayi, L. (2008). Numerical simulation of flow around an orbiting cylinder at different ellipticity values. *Journal of Fluid and Structures*, 24:883-906.

Batchelor, G. (1967). *An Introduction to Fluid Dynamics.* Cambridge University Press, United Kingdom.

Bishop, R. and & Hassan, A. (1964). The lift and drag forces on a circular cylinder oscillating in a flowing fluid. *Proceedings of the Royal Society of London. Series A, Mathematical and Physical Sciences*, 277:51-75.

Blackburn, H. M. and & Henderson, R. D. (1999). A study of two-dimensional flow past an oscillating cylinder. *Journal of Fluid Mechanics*, 385:255-286.

Cetiner, O. and & Rockwell, D. (2001a). Streamwise oscillations of a cylinder in a steady current. Part 1. Locked-on states of vortex formation and loading.

Journal of Fluid Mechanics, 427:1-28.

Cetiner, O. and & Rockwell, D. (2001b). Streamwise oscillations of a cylinder in steady current. Part 2. Free-surface effects on vortex formation and loading. *Journal of Fluid Mechanics*, 427:29-59.

Choi, H., Jeon, W. and & Kim, J. (2008). *Control of Flow over a Bluff Body.* Annual Review of Fluid Mechanics, 40:113-139.

Coutanceau, M. and & Pineau, G. (1997). Some typical mechanisms in the early phase of the vortex-shedding process from particle-streak visualization in Atlas of visualization III edited by The visualization society of Japan. *CRC Press.*

Dahl, J., Hover, F. and & Triantafyllou, M. (2006). Two-degree-of-freedom vortex induced vibrations using a force assisted apparatus. *Journal of Fluids and Structures*, 22:807-818.

Gad-El-Hak, M. (2000). *Flow Control.* Passive, Active, and Reactive Flow Management. Cambridge University Press, UK.

Gerrits, J. (2001). *Dynamics of liquid-filled spacecraft.* Unpublished doctoral dissertation, University of Groningen.

Gresho, P. M. and & Sani, R. L. (1998). *Incompressible Flow and the Finite Element Method.* John Wiley and Sons, Inc., New York.

Gubanov, O. (2006). *Design of CFD code using high level programming paradigms: Free surface flows with arbitrarily moving rigid bodies.* Unpublished master's thesis, Memorial University of Newfoundland.

Hirt, C. W. and & Nichols, B. D. (1981). Volume of fluid (VOF) method for the dynamics of free boundaries. *Journal of Computational Physics*, 39:201-225.

Hirt, C. W. and & Sicilian, J. M. (1985). *A porosity technique for the definition* *of obstacles in rectangular cell meshes.* Flow Science, Inc., Los Alamos, New Mexico.

Jauvtis, N. and & Williamson, C. (2004). The effect of two degrees of freedom on vortex-induced vibration at low mass damping. *Journal of Fluid Mechanics*, 509:23-62.

Jeon, D. and & Gharib, M. (2001). On circular cylinders undergoing two-degree-of-freedom forced motions. *Journal of Fluids and Structures*, 15:533-541.

Kim, S. H., Park, J., Park, N., J.H., B. and & Yoo, J. (2009). Direct numerical simulation of vortex synchronization due to small pertubations. *Journal of Fluid Mechanics*, 634:61-90.

Leong, C. and & Wei, T. (2008). Two-degree-of-freedom vortex-induced vibration of a pivoted cylinder below critical mass ratio. *Proceedings of the Royal Society of London. Series A: Mathematical and Physical Sciences*, 464:2907-2927.

Li, T., Troch, P. and & De Rouck, J. (2004). *Wave overtopping over a sea dike.* Journal of Computational Physics, 198(2):686-726.

Li, T., Zhang, J., Zhang, W. and & Zhu, M. (2009). Vortex-Induced Vibration Characteristics of an Elastic Circular Cylinder. *World Acamdemy of Science, Engineering and Technology*, 60:56-65.

Li, Y., Shock, R., Zhang, R. and & Chen, H. (2004). Numerical study of flow past an impulsively started cylinder by the lattice-Boltzmann method. *Journal of Fluid Mechanics*, 519:273-300.

Meneghini, J. R. and & Bearman, P. W. (1995). Numerical simulation of high amplitude oscillatory flow about a circular cylinder. *Journal of Fluids and Structures*, 9:435-455.

Mironova, L. (2008). *Accurate computation of free surface flow with an oscillating circular cylinder based on a viscous incompressible two-fluid model.* Unpublished doctoral dissertation, Memorial University of Newfoundland.

Norberg, C. (2003). Fluctuating lift on a circular cylinder: review and new measurements. *Journal of Fluids and Structures*, 17:57-96.

Ongoren, A. and & Rockwell, D. (1988). Flow structure from an oscillating cylinder. Part 1. Mechanisms of phase shift and recovery in the near wake. *Journal of Fluid Mechanics*, 191:197-223.

Pham, A., Lee, C., Seo, J., Chun, H., Kim, H., Yoon, H. and et al. (2010). *Laminar flow past an oscillating cylinder in cross flow.* Journal of Marine Science and Technology, 18:361-368.

Ploumhans, P. and & Winckelmans, G. S. (2000). Vortex methods for high-resolution simulations of viscous flow past bluff bodies of general geometry. *Journal of Computational Physics*, 165(2):354-406.

Reichl, P., Hourigan, K. and & Thompson, M. C. (2005). Flow past a cylinder close to a free surface. *Journal of Fluid Mechanics*, 533:269-296.

Roshko, A. (1955). *On the wake and drag of bluff bodies.* Journal of Aeronautical sciences, 22:124-132.

Sumer, B. M. and & Fredsøe, J. (1997). *Hydrodynamics Around Cylindrical Structures.* Advanced Series on Coastal Engineering, Vol. 12. World Scientific Publishing Company, UK.

Versteeg, H. and & Malalasekera, W. (1995). *An introduction to computational fluid dynamics.* The finite volume method. John Wiley and Sons, Inc., New York.

Williamson, C. H. K. and & Govardhan, R. (2004). Vortex-induced vibrations.

Annual Review of Fluid Mechanics, 36:413-455.

Williamson, C. H. K. and & Roshko, A. (1988). Vortex formation in the wake of an oscillating cylinder. *Journal of Fluids and Structures*, 2:355-381.